Dissertation

submitted to the
Combined Faculties for the Natural Sciences and for Mathematics
of the Ruperto-Carola University of Heidelberg, Germany
for the degree of
Doctor of Natural Sciences

presented by

Zeenna A. Stapper, M.Sc.
Born in: Las Pinas/Manila, Philippines
Oral examination: 08.03.2018

The role of redox homeostasis in *Drosophila* models of Aβ aggregation

Referees: Prof. Dr. Bernd Bukau

PD Dr. Tobias P. Dick

"When things go wrong, as they sometimes will;
When the road you´re trudging seems all uphill;
When the funds are low and the debts are high;
And you want to smile but you have to sign.
When all is pressing you down a bit –
Rest if you must, but don´t you quit.
Success is failure turned inside out;
The silver tint on the clouds of doubt;
And you can never tell how close you are;
It may be near when it seems far.
So stick to the fight when you´re hardest hit –
It´s when things go wrong that you must not quit."

– John Greenleaf Whittier

Abstract

There is accumulating evidence that Alzheimer´s Disease (AD) pathogenesis correlates with increased oxidative stress due to the overproduction of reactive oxygen species (ROS) and decrease in antioxidant defense systems. Several cellular insults increasing oxidative stress in AD include mitochondrial dysfunction, inflammation and the accumulation of oxidative stress markers. Developing genetic *in vivo* models to study the impact of redox homeostasis on amyloid-beta (Aβ) neurotoxicity and to decipher whether changes in redox balance are a cause or consequence of AD pathology is of high importance.

Here, I present 'newly established' *in vivo* models to study the role of redox homeostasis in AD. Therefore, I combine genetically encoded redox sensors with *Drosophila* models of Aβ aggregation. Thereby, I focus on two major regulators of the redox homeostasis. On the one hand, hydrogen peroxide (H_2O_2), a non-radical oxidant and major ROS that possesses cytotoxic effects and is an important signaling molecule. And on the other hand, I focus on glutathione, a low molecular weight thiol, which represents one of the two major Nicotinamide adenine dinucleotide phosphate (NADPH)-dependent reducing systems in the cell that holds protective effects against oxidative damage. In this thesis, I aim to provide new insights into a better characterization and understanding of the impact of changes in redox homeostasis and the involvement of stress responsive pathways in the onset and progression of AD.

The main finding of this study is that changes in glutathione redox potential are linked to $A\beta_{42}$ neurotoxicity. I have found that the common notion of 'oxidative stress' driven neurodegeneration is specifically mediated by changes in the neuronal glutathione redox potential rather than the increasing levels of H_2O_2. Interestingly, neurons respond to the deposition of $A\beta_{42}$ by an increase in glutathione redox potential but glia cells are not susceptible for this insult caused by toxic $A\beta_{42}$. The glutathione redox imbalance already occurs at an early time point of Aβ deposition and is only observable in toxic $A\beta_{42}$-expressing flies but not in flies expressing the less toxic $TandemA\beta_{40}$ variant. Most notably, I show that modifications of glutathione synthesis directly modulate $A\beta_{42}$-mediated neurotoxicity, in parallel to an increase in the c-Jun N-terminal kinase (JNK) stress signaling response. Intriguingly, an increase in glutathione synthesis is not beneficial in this AD disease model, but exacerbates $A\beta_{42}$-mediated toxicity. While recent studies point towards the important role of redox signaling processes being the driving force in many human diseases, main novelty of this thesis is the development of genetic *in vivo* tools to selectively analyze changes in redox homeostasis associated with AD pathomechanisms. To summarize, I hereby provide *in vivo* evidence of the central role of glutathione redox homeostasis in early AD pathogenesis and progression. Furthermore, I examine early events of neuronal dysregulation and disease onset and further offer a screening platform for possible disease modifying therapies. Most importantly, this study proposes additional roles of glutathione beyond the generic neuroprotective antioxidant and being involved in the $A\beta_{42}$-induced neurotoxicity.

Zusammenfassung

Viele Belege weisen darauf hin, dass die Entstehung der Alzheimer Erkrankung mit einem erhöhten Auftreten von oxidativem Stress einhergeht. Oxidativer Stress wird durch eine Überproduktion von reaktiven Sauerstoffspezies oder durch eine Verminderung von anti-oxidativen Abwehrsystemen verursacht. Mehrere zelluläre Prozesse können zu einem erhöhten oxidativen Stress beitragen. Dazu zählen eine Fehlfunktion der Mitochondrien, Entzündungsprozesse und die Anhäufung von oxidativen Stressmarkern. Die Entwicklung von genetischen Modellen im lebenden Organismus ist daher von größter Wichtigkeit um den Einfluss der Redox-Homöostase auf die Neurotoxizität von Amyloid-beta (Aβ) zu untersuchen und zu entschlüsseln, ob Veränderungen des Redox-Gleichgewichtes die Ursache oder Konsequenz der Alzheimer Pathologie sind. Ich präsentiere hier neu etablierte *in vivo* Modelle um die Rolle der Redox-Homöostase in der Alzheimer Erkrankung zu untersuchen. Dafür kombiniere ich genetisch kodierte Redox-Sensoren mit *Drosophila* Modellen der Aβ-Aggregation. Dabei konzentriere ich mich auf zwei Hauptregulatoren der Redox-Homöostase. Einerseits Wasserstoffperoxide (H_2O_2), ein nicht-radikales Oxidans und Haupt-reaktives-Sauerstoffspezies, welches zellschädigende Wirkungen besitzt und ein wichtiges Signalmolekül darstellt. Andererseits konzentriere ich mich auf Glutathion, ein Thiol mit niedrigem Molekulargewicht, welches eines der zwei wesentlichen Nicotinamideadenindinukleotid-phosphat (NADPH)-abhängigen Reduktionssysteme in der Zelle darstellt und gegen oxidative Schäden schützt. Ziel der Studie ist es neue Einblicke in eine bessere Charakterisierung und in ein besseres Verständnis der Auswirkungen von Redox-Homöostase-Veränderungen zu geben. Ein weiteres Ziel ist es neue Erkenntnisse der Beteiligung von Stress-Signalwegen zu Beginn und während des Krankheitsverlaufes der Alzheimer Erkrankung zu gewinnen.

Die Kernaussage der Studie ist, dass Veränderungen des Glutathione-Redoxpotentials mit der Neurotoxizität von $A\beta_{42}$ verknüpft sind. Ich habe herausgefunden, dass die allgemeine Grundauffassung von durch 'oxidativem Stress'-induzierte Neurodegeneration, eher spezifisch durch Veränderungen des Glutathione-Redoxpotentials als durch steigende H_2O_2 Konzentrationen vermittelt wird. Interessanterweise reagieren Neuronen auf die Ablagerungen von toxischem $A\beta_{42}$ durch eine Erhöhung des Glutathione-Redoxpotentials. Jedoch sind Gliazellen durch diesen durch $A\beta_{42}$ verursachten toxischen Schaden nicht anfällig. Bereits zu einem frühen Zeitpunkt der Aβ-Ablagerung tritt ein Glutathion-Redox-Ungleichgewicht auf. Diese ist nur in Fliegen zu beobachten, die eine toxische $A\beta_{42}$-Variante, nicht jedoch eine weniger toxische Tandem$A\beta_{40}$-Variante exprimieren. Insbesondere zeige ich, dass Modifikationen der Glutathion-Synthese die $A\beta_{42}$-vermittelte Neurotoxizität direkt modulieren, und parallel zu einer Zunahme der c-Jun-N-terminale Kinasen (JNK)-Stresssignalantwort führen. Interessanterweise ist eine erhöhte Glutathion-Synthese in diesem Alzheimer-Krankheitsmodell nicht von Vorteil, sondern verschlimmert sogar die $A\beta_{42}$-vermittelte Toxizität. Während jüngste Studien auf die wichtige Rolle von

Redox-Signalprozessen als treibende Kraft bei vielen menschlichen Erkrankungen hindeuten, besteht die Hauptneuheit dieser Arbeit in der Entwicklung genetischer *in-vivo*-Werkzeuge zur selektiven Analyse von Veränderungen der Redox-Homöostase die in Zusammenhang mit AD-Pathomechanismen stehen. Zusammenfassend liefere ich *in vivo* Beweise der zentralen Rolle der Glutathion-Redox-Homöostase in der frühen Krankheitsentstehung und im Krankheitsverlauf der Alzheimer Erkrankung. Darüber hinaus untersuche ich frühe Ereignisse neuronaler Dysregulation und Krankheitsbeginn und biete eine Screening-Plattform für mögliche krankheitsmodifizierende Therapien. Glutathion ist bekannt als neuroprotektives Antioxidans. Diese Studie zeigt auf, dass Glutathione auch zusätzliche Rollen besitzt und an der $A\beta_{42}$-induzierten Neurotoxizität beteiligt ist.

Contents

1. Introduction

1.1 Alzheimer´s disease (AD)

Alzheimer´s disease (AD) is a fatal neurodegenerative disease and the most prevalent type of age-related dementia. Approximately 47 million people are suffering from AD or a related dementia worldwide, with 1.5 million people in Germany alone (Holtzman et al. 2011), (Alzheimer´s Disease International https://www.alz.co.uk/research/statistics). According to the Alzheimer´s Association and Alzheimer´s Disease International the number of people suffering from AD and dementia will dramatically increase within the next decades, with estimated numbers of 131.5 million people in 2050. Clinical symptoms of diagnosed AD patients include gradual memory loss and other cognitive dysfunctions (Aguzzi & O'Connor 2010; De Strooper & Karran 2016). As the disease slowly progresses affected people experience personality and behavioral changes, decline in language, and the loss of the ability to memorize as well as to recall newly learned information. Finally, also long-term memory will be affected. The occurring brain damage due to detrimental loss of neurons mostly affect the hippocampus, the association areas of the cerebral cortex and the subcortical brain regions (Serrano-Pozo et al. 2011; Goedert et al. 1991).
While the typical life expectancy after diagnosis is 4-8 years (Alzheimer´s Association, http://www.alzheimers.net/resources/alzheimers-statistics/), the processes and brain changes initiating the disease pathology are believed to start decades before the occurrence of any clinically detectable symptoms occur (von Bernhardi & Eugenín 2012; Bermejo et al. 2008). The methods for diagnosing AD, e.g. using amyloid PET imaging, improved within the last years (Mallik et al. 2017; de Wilde et al. 2017). This helps building better treatment plans for a more customized individual therapy, compared to earlier days, where a distinct diagnosis of AD could only be secured by post-mortem examinations of the patients brain (McKhann et al. 1984; Rosén et al. 2013). Until now, there is still no cure or therapy available to slowing-down the progressive brain damage and dementia caused by this neurodegenerative disease. Investigating early stages of this disease is therefore important for identifying potential targets and developing new treatments.

1.1.1 Molecular hallmarks of AD

The first person described with symptoms of the disease, which was later called Alzheimer´s Disease, was Auguste Deter in 1907. Emil Kraepelin, who was the director of the Royal Psychatric Clinic in Munic named the disease after Alois Alzheimer, who observed the combined presence of the two stereotypic pathological hallmarks of AD, plaques and tangles, from her examined post-mortem brain, using a reduced silver staining technique (Goedert 2009; Alzheimer 1907). In that same year, another psychiatrist

and neuropathologist Oskar Fischer contributed to the present definition of these hallmarks, when he for the first time described the neuritic plaque by examining 16 cases of senile dementia (Goedert 2009).

As briefly mentioned above, the two pathological hallmarks of AD are the abnormal deposition of intracellular neurofibrillary tangles (NFTs) and extracellular senile plaques, consisting of two distinct aggregated proteins, namely hyperphosphorylated tau (Goedert et al. 1991; Mandelkow 2012) and amyloid beta (Aβ) (John Hardy & Allsop 1991; Holtzman et al. 2011). Tau is a microtubule-binding protein and mainly localized in neuronal axons (Weingarten et al. 1975). Under physiological conditions tau promotes the assembly and stabilization of microtubules. It is rich of serine and threonine residues, making it a target for several kinases including GSK3β and ERK (Aguzzi & O'Connor 2010), which under abnormal conditions are causing its hyperphosphorylation, leading to its vulnerability to aggregate, resulting in its detachment from microtubules and consequently destabilizing the microtubule network (Grundke-Iqbal et al. 1987; Götz & Ittner 2008). The disrupted microtubule network then contributes to neuronal dysfunction including axonal degeneration, disruption of axonal transport and sequestering of proteins and cell death (Aguzzi & O'Connor 2010; Dawson et al. 2010).

The second abnormal depositions that can be found in AD patients are extracellular senile plaques mainly consisting of misfolded and aggregated Aβ. Aβ is produced in the brain throughout life and accumulates during aging in the cerebral cortex, which under pathologic conditions such as in AD, can lead to the excessive deposition of Aβ (John Hardy & Allsop 1991; Aguzzi & O'Connor 2010). A stereotypic spreading of Aβ pathology throughout the brain has been observed in AD patients, where senile plaques first occur in the neocortex, next in the allocortex and eventually progress to subcortical regions (Thal et al. 2002; Jucker & Walker 2013). Its amyloid precursor protein (APP) is an integral membrane protein and is expressed in several tissues, but much higher in the brain (Nalivaeva & Turner 2013). APP has been linked to synapse formation and activity (Priller et al. 2006), iron export (Duce et al. 2010) and neuronal plasticity (Turner et al. 2003). A number of physiological functions of Aβ have been described, including the maintenance of the structural integrity of the blood brain barrier (BBB) (Atwood et al. 2003), the involvement in Ca^{2+} signaling (Smith et al. 2004; Pearson & Peers 2006) and its antioxidant properties at low concentrations due to its metal binding sites and its ability to act as metal chelator capturing metals, such as Fe, Cu and Zn which prevents this potentially redox active species from participation in oxidative reactions (Pearson & Peers 2006; Atwood et al. 2003).

Aβ is generated through the amyloidogenic pathway and is derived from proteolytic cleavage of the APP by distinct secretases. This processing of the integral membrane protein APP, which takes place in the endosome (Rajendran & Annaert 2012), includes its initial proteolytic cleavage by the β-secretase, followed by the γ-secretase cleavage and resulting in the release of the Aβ peptide. In the initial step, the β-secretase cleaves off the N-terminal part of the APP, giving rise to APPsβ and C99. Then, depending on the position of the γ-secretase cleavage within the C99, the APP intracellular domain (AICD) and

different lengths of Aβ (38-43 amino acids) are formed (Hardy 1997; Aguzzi & O'Connor 2010). The most common forms of the Aβ peptide are the forty and forty-two amino acid long $Aβ_{40}$ and $Aβ_{42}$, which differ in their neurotoxicity levels. $Aβ_{42}$ has been identified as the highly aggregation prone and neurotoxic factor in AD, and because of its higher rate of fibrillization and insolubility, $Aβ_{42}$ is much more abundant within senile plaques than $Aβ_{40}$. In contrast, due to its low aggregation susceptibility, lacking the two additional unpolar amino acids (C-terminal Isoleucin and Alanin) $Aβ_{40}$ possesses a high turnover rate. In healthy condition the ratio of $Aβ_{40}$:$Aβ_{42}$ is 9:1 (Ramona Quelle 35, 36), whereas in malignant situation this ratio shifts towards more $Aβ_{42}$ (Kuperstein et al. 2010). It is known that mutations in the γ-secretase or APP (Chartier-Harlin et al. 1991; Goate 2006; Selkoe & Wolfe 2007) lead to the production of more toxic $Aβ_{42}$ and a less efficient or impaired clearance of $Aβ_{42}$ (Mawuenyega et al. 2010; Saido & Leissring 2012) contributes to the accumulation of $Aβ_{42}$ in AD. The increase in $Aβ_{42}$ levels results in the formation of soluble oligomeric accumulations and finally the deposition of amyloid plaques found in the AD brain (Bitan et al. 2003; Snyder et al. 1994; Chen & Glabe 2006). The series of events are described in the amyloid cascade hypothesis (Figure 1).

1.1.2 The amyloid cascade hypothesis

The widely supported amyloid cascade hypothesis implies the accumulation of Aβ and the resulting deposition of senile plaques in the brain parenchyma (John Hardy & Allsop 1991; Hardy & Selkoe 2002) as the primary event driving AD pathology, with the hyperphosphorylation of tau and other downstream events (e.g. neuroinflammation) as secondary effects, which eventually cause neuronal dysfunction and neuronal death (Figure 1). Evidence supporting this hypothesis arises from studies of familiar cases of early-onset AD, which is caused by mutations in the genes encoding for APP (*APP*) and for the catalytic centers of the γ-secretase complex, Presenilin (*PSEN1*) 1 and 2 (*PSEN2*) (Chartier-Harlin et al. 1991; Sherrington et al. 1995; Goate 2006; Selkoe & Wolfe 2007). Mutations in these "deterministic genes" were shown to cause Aβ deposition due to increased $Aβ_{42}$ production and self-aggregation (Levy et al. 1990; Van Broeckhoven et al. 1990; Hardy & Selkoe 2002). These familial cases of AD apply for approximately 1-5% of all AD cases (Blennow et al. 2006). Other findings supporting the amyloid cascade hypothesis and supporting Aβ deposition as the initiating step of AD pathology are the following (Hardy 2002): Tau aggregation alone is not sufficient to induce Aβ plaque formation. Mutations in the gene encoding tau are, at worst, causing frontotemporal dementia (FTD) with Parkinsonis (Poorkaj et al. 1998; Hutton et al. 1998; Goedert & Spillantini 2000). Furthermore, changes in Aβ metabolism, APP processing and initial amyloid plaque formation occur rather before tau alterations than after (Hardy et al. 1998; Jada Lewis et al. 2001). This was supported by studies with transgenic mice overexpressing both,

APP and tau. Compared to transgenic mice overexpressing tau alone, the combination of co-expressing mutant human APP and tau showed an increase in tau tangle formation, while the amount of amyloid plaques remained the same. In addition, studies have shown that an imbalance in Aβ clearance also contributes to the risk of developing late onset AD (Kang et al. 2000; Hardy & Selkoe 2002). However, the amyloid cascade hypothesis does not fully explain all the processes occurring in AD pathogenesis and therefore is still under debate. The strongest argument that something is missing in this cascade hypothesis and is still of need of filling in more details, is the fact that the number of Aβ plaques in the brain do not necessarily correlate well with the degree of AD patients symptoms (Perez-Nievas et al. 2013; Sloane et al. 1997). In fact, it has been shown that not the amount of insoluble Aβ aggregates, but rather the total amount of Aβ correlate better with the severity of AD symptoms (Naslund et al. 2000; Haass & Selkoe 2007), which also include soluble Aβ. Recent evidence demonstrate that soluble oligomeric Aβ play a causative role in synaptic dysfunction in AD (Lambert et al. 1998; Walsh et al. 2002) sparking ongoing debates whether soluble oligomers or insoluble fibrils are the neurotoxic species. Still, the exact mechanisms of how Aβ, in any form whatsoever, causes neurotoxicity is not fully understood and gaps need to be filled.

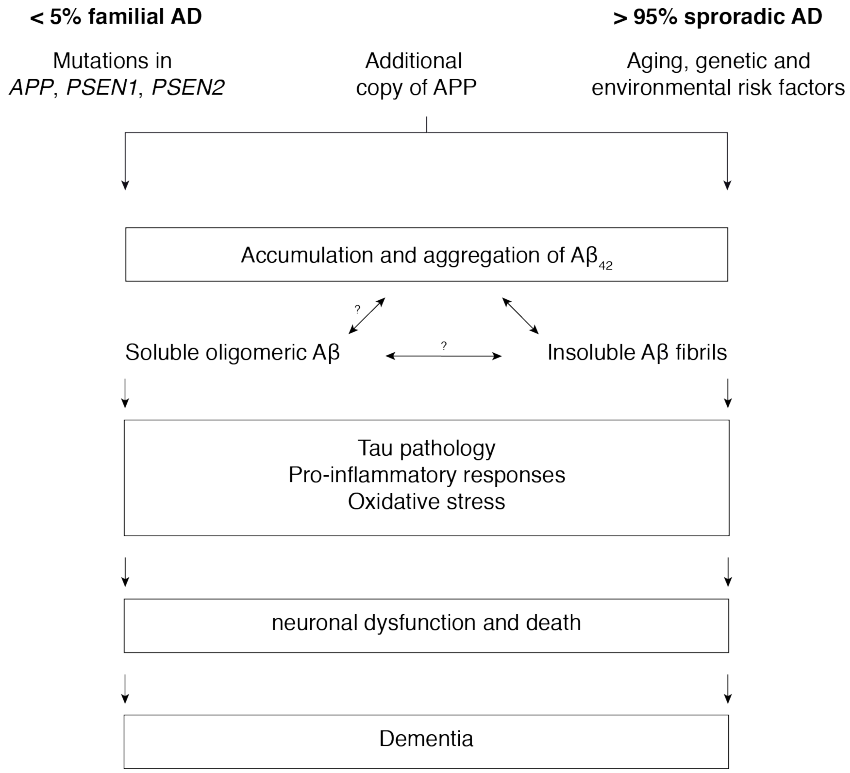

Figure 1: Schematic overview of the amyloid cascade hypothesis. This graph was modified from (Karran et al. 2011) and shows an overview of the series of events occurring in AD of the strong supported hypothesis that the accumulation and aggregation of Aβ is the triggering event leading to neuronal damage and neurotoxicity in AD pathology.

1.2 Disturbed redox homeostasis in AD

1.2.1 The free radical theory of aging

It is still uncertain how the neurotoxicity of Aβ is mediated. Oxidative stress has been proposed to be involved in this. The overall term 'oxidative stress' became increasingly popular and has been used in various diseases. There are several hypotheses of how oxidative stress could contribute to neuronal damage in AD. Some studies have addressed the role of oxidative stress and inflammation in AD, which includes the activation of microglia and a release of numerous inflammatory mediators including pro-inflammatory cytokines (Heneka MT, et al., 2014; Block ML et al., 2007; McGeer R et al., 2001). Other studied have shown that a knock-down of superoxide dismutase (SOD), a major scavenger of ROS generated in mitochondria, leads to an accelerated accumulation of Aβ plaques in an AD mouse model, suggesting that disturbance of free radical metabolism contribute to the amyloid pathology characteristic of AD (Li et al., 2004). This concept of the 'oxidative stress theory' is originated from the 'The free radical theory of aging', which was first introduced in 1956 and a few years later renamed as the 'mitochondrial free radical theory of aging' by Denham Harman (Harman 1956; HARMAN 1972). This theory suggests the accumulation of free radicals, with mitochondria as major source and target of reactive oxygen species (ROS), which over time are causing tissue damage and cell death. In order to also include, for example, hydrogen peroxide (H_2O_2), which is an oxygen species but not a radical, the now common concept 'oxidative stress theory of aging' was introduced by Yu and Yang (Yu & Yang 1996). However, this term is still evolving. Redox homeostasis is currently the most precise description of the balance between various oxidants and antioxidants (Sies 2015). An imbalance on either side is causing a disturbance of the redox homeostasis that may cause redox stress such as oxidative stress or reductive stress that have both been linked to AD (Gella & Durany 2009; Zhao et al. 2013; Lloret et al. 2016).

1.2.2 Oxidants and antioxidants

The group of oxidants includes free radicals and ROS that are unstable and very reactive molecules by themselves or undergo further reactions to generate free radicals. Among them are "superoxide anion radical, hydrogen peroxide, hydroxyl radical, electronically excited states such as singlet molecular oxygen, as well as the nitric oxide radical and peroxynitrite" (Sies 2015). Oxidants are constantly produced, for example during mitochondrial respiration. A certain amount of oxidants are needed for important biological activities such as cell signaling, host defense in phagocytic cells to combat infection and the regulation of proliferation upon stimulation by growth factors (Finkel 1998; Finkel & Holbrook 2000; Hamanaka & Chandel 2010). For maintaining the balance of redox homeostasis, the antioxidant defense system is very important to counterbalance and scavenge the effects of these oxidants. This defense system

is composed of enzymatic and non-enzymatic antioxidants (Finkel & Holbrook 2000; Zhao et al. 2013). ROS detoxification enzymes include for example superoxide dismutase (SOD), catalase (Cat), glutathione reductase (GR), and glutathione peroxidase (GPx) and belong to the enzymatic antioxidants. Vitamin C (ascorbic acid), vitamin E (alpha-tocopherol), carotenoids, polyphenolic compunds and glutathione belong to the non-enzymatic antioxidants and directly scavenge free radicals (Sies 1997; SIES 1993). As mentioned before, an imbalance in oxidants and antioxidants, for example due to low efficiency of the antioxidant defense system or an overproduction of ROS, disturbs the redox homeostasis and is linked to redox stress that implicated in AD. Constructive criticism was mentioned regarding the very general and broad use of the term oxidative stress without identifying the exact species that is affected or disturbed (Sies 2015). Identifying the exact specimen involved in the disturbed redox homeostasis will help deciphering the exact mechanisms behind pathophysiological processes.

In this study, I focused on hydrogen peroxide (H_2O_2), a major ROS, which is a rather stable and non-radical oxidant. When it is converted into more reactive species it may cause oxidative damage. Moreover, H_2O_2 is also a signaling molecule and involved in the regulation of biological processes such as autophagy, proliferation and survival (Gough & Cotter 2011; Veal et al. 2007; Plaine 1955). In context with Aβ, the overproduction of H_2O_2 has been linked to neurotoxicity (Tabner et al. 2005; Behl et al. 1994). Additionally, I focused on glutathione, which is a low-molecular weight scavenger and represents a major antioxidant in the cell and is known for its protective effects against oxidative damage (Dringen 2000). It is a water-soluble, low molecule weight tripeptide, consisting of glutamate, cysteine and glycine. Glutathione is a crucial redox regulator and involved in the regulation of various cellular processes including gene expression, DNA and protein synthesis, cell proliferation and apoptosis (Aquilano et al. 2014; Franco & Cidlowski 2009). Glutathione cycles between a reduced (GSH) and oxidized (GSSG) state and its ratio (GSH/GSSG) and redox potential (E_{GSH}) have been widely used to evaluate perturbations in cellular redox homeostasis (Simone C. Albrecht et al. 2011; Currais & Maher 2013; Rebrin et al. 2004). Alterations in glutathione homeostasis are implicated in various human diseases, including AD (Mandal et al. 2015).

1.2.3 Oxidative stress in AD

There is accumulating evidence that oxidative stress is a characteristic of AD brains next to senile plaques and NFTs (Zhao et al. 2013). Recent studies demonstrate that AD pathogenesis correlates with increased overproduction of ROS and/or a decrease in the anti-oxidative defense system (von Bernhardi & Eugenín 2012; Cai et al. 2011). Several cellular insults that increase ROS in AD pathogenesis are mitochondrial dysfunction (Lin & Beal 2006) and inflammation (Wyss-Coray & Mucke 2002; Liddelow et al. 2017; Heneka et al. 2014; Block et al. 2007). So far, it has been reported that elevated levels of oxidative stress markers can be found in patients with mild cognitive impairment (MCI), an intermediate stage between normal aging and dementia (Yonas E. Geda, MD 2012), and in post mortem AD patients brains (Harris et al. 1995; Gella & Durany 2009). These markers that are all associated with AD pathology include protein carbonylation, lipid peroxidation such as 4-hydroxy-2,3-nonenal (HNE) and malondialdehyde (MDA), advanced glycation endproducts (AEGs) and DNA oxidation such as 8-hydroxy-2-deoxyguanosine (8OHdG) and 8-hydroxyguanosine (8OHD) (Gella & Durany 2009; Sayre et al. 1997; Harris et al. 1995; Sultana, R., Perluigi, M., Allan Butterfield 2013; Butterfield et al. 2001). In addition to the observations of various oxidative damage endproducts, alterations in the activity or expression of ROS detoxification enzymes, such as superoxide dismutase (SOD) and catalase have been observed in dementia and AD patients (Padurariu et al. 2010; Omar et al. 1999; Gsell et al. 1995; Furuta et al. 1995). Moreover, a decrease in glutathione concentration during aging (Chen et al. 1989; Gella & Durany 2009) and low levels of glutathione are observed in patients with MCI and mild AD (Mandal et al. 2015; Ansari & Scheff 2010; Bermejo et al. 2008) that also contribute to the oxidative stress conditions.

Previous studies have pointed out the connection between oxidative stress and Aβ-mediated toxicity (Zhao et al. 2013). It has been shown that dependent on its levels and aggregation state Aβ has a dual role in the relationship to oxidative stress (Zou et al. 2002; Plant et al. 2003; Zhao et al. 2013). On the one hand, abnormal accumulation and aggregation of Aβ can promote oxidative stress (Mohmmad Abdul et al. 2006; Matsuoka et al. 2001; Smith et al. 1998) that enhances neuronal oxidative damage (vice versa), whereas on the other hand low levels of Aβ (picomolar and low nanomolar) can be beneficial for the maintenance of the cellular redox status and can be protective against oxidative stress (Zhao et al. 2013; Nunomura et al. 2006). Several *in vitro* and *in vivo* studies reveal that Aβ can promote oxidative stress. For example, Aβ treatment of clonal CNS cell line B12 (PC12) cells and CNS primary cultures increased H_2O_2 and lipid peroxide levels (Behl et al. 1994) *in vitro*. Additionally, it has been shown that age-linked Aβ accumulation was associated with elevated H_2O_2, nitric oxide production and oxidative modifications of proteins and lipids in AD transgenic mouse models with APP and PS-1 mutations (Smith et al. 1998; Matsuoka et al. 2001; Apelt et al. 2004; Mohmmad Abdul et al. 2006), connecting Aβ with the promotion of oxidative stress. Conversely, it was also shown that oxidative stress could promote Aβ. In AD transgenic mouse models with overexpression of APP mutant (Tg19959 and Tg2576), it has been

reported that manipulating the antioxidant defense system by heterozygous knockout of MnSOD (SOD2) or deletion of Cu-Zn-SOD (SOD1), increased the amyloid plaque burden, Aβ oligomerization and accelerated the loss of spartial learning and memory (Li et al. 2004; Murakami et al. 2011). And on the other hand overexpression of SOD2 decreased amyloid plaque burden and protein oxidation *in vivo* (Dumont et al. 2009). Despite all this research, it is still under debate whether oxidative stress is the primary cause or a secondary effect of this age-related disease and whether changes in the cellular redox balance have a direct impact on the onset and progression of AD. Most importantly, direct *in vivo* evidence showing whether changes in redox balance are directly linked to Aβ neurotoxicity is still missing.

1.3 c-Jun N-terminal Kinase (JNK) stress signaling in AD

Several signaling pathways regulate the cellular response to various stresses and get activated in response to oxidative stress. Among these stress-signaling pathways is the c-Jun N-terminal kinase (JNK) pathway. JNKs, also known as stress-activated protein kinases (SAPKs), belong to the mitogen-activated protein kinase (MAPK) family. The JNK pathway governs a range of biological processes such as brain morphogenesis, synaptic plasticity and memory formation and is an important regulator of stress responses and apoptosis in AD pathology (Coffey 2014; Liu & Lin 2005; Manning & Davis 2003). Not only ROS, but also other stressors including inflammatory cytokines and ultraviolet irradiation can activate the JNK stress pathway (Biteau et al. 2011). Additionally, *in vitro* studies have shown that treatment with Aβ peptides induce JNK activation in primary neuronal cultures (Morishima et al. 2001; Yarza et al. 2016). It has been reported that JNK activation is linked with Aβ accumulation and cell death (Tare et al. 2011; Marques et al. 2003; Jang & Surh 2002; Shoji et al. 2000). Furthermore, a co-localization with Aβ and increased expression of phosphorylated JNK (pJNK) has been observed in post-mortem AD patient brains (Zhu et al. 2001; Ferrer et al. 2001; Coffey 2014). Other studies have presented beneficial effects of JNK signaling. In *Drosophila* it has been shown that JNK activation acts protective against oxidative stress insult due to the transcriptional activation of autophagy (Wu et al. 2009). Also, it has been shown that increased JNK signaling extends life span and is important for oxidative stress tolerance (Wang et al. 2003). Thus, it is of great importance to investigate how changes in redox homeostasis can be translated into a death signal and whether this is promoted via stress-responsive pathways, such as JNK.

1.4 *Drosophila* as a model organism for AD

Numerous *in vitro* and *in vivo* models have been applied to investigate and understand disease-related mechanisms of AD pathology and aiming to find targets for successful therapeutic treatment. Several transgenic mouse models have already been established. They range from overexpression of human tau, APP, or Presenilin 1 with disease-related mutations, triple transgenic mice models expressing all three mutated human genes (J. Lewis et al. 2001; Oddo, Caccamo, Kitazawa, et al. 2003; Oddo, Caccamo, Shepherd, et al. 2003; Stover et al. 2015) to injecting Aβ plaques-containing brain homogenates from AD patients into the hippocampus of APP mice to induce AD-like pathology (Meyer-Luehmann et al. 2008). All these mouse models have provided and will provide valuable insights into various disease-related mechanism of AD. However, non-vertebrate models possess great advantages towards mammalian models and have shown to be equally useful in contributing and adding knowledge to the broad field of AD research. The most obvious advantage of using *Drosophila* models is the easy handling in addition to their time and cost-efficiency compared to mammalian models. The wide availability of genetic tools and the large number of publicly available transgenic stocks *Drosophila* represent an advantageous model organism (Chan & Bonini 2000; Dietzl et al. 2007; del Valle Rodríguez et al. 2011; Venken et al. 2011). Thus, *Drosophila* models provide a favored platform for large-scale screening approaches (Shulman & Feany 2003; Greene et al. 2005; Cao et al. 2008; Rival et al. 2009).

In addition, the various cellular and genetic similarities with humans including 75% of all signaling pathways being conserved and 65% of human-disease-associated genes having a *Drosophila* homolog, *Drosophila* has proven to be a suitable model organism for diverse diseases (Bellen et al. 2010). Particularly, the "complex" neuronal system of the fly has been used to study neuronal dysfunction and neurodegenerative diseases (McGurk et al. 2015; Sang & Jackson 2005). *Drosophila* lacks the β-secretase activity and does not posses APP (McGurk et al. 2015). However, *Drosophila* has all homologs of all components of the γ-secretase complex and an APP homolog, which is called APP-like (APPL) (Boulianne et al. 1997; Hong & Koo 1997; Rosen et al. 1989). To mimic neurodegeneration and generate histopathological hallmarks of AD in *Drosophila* different approaches can be used. On the one hand fly mutants of homologs of disease-associated genes can be studied (Lessing & Bonini 2009) and on the other hand human transgenes, such as APP, β-secretase or different variants of Aβ can be overexpressed in specifically defined tissues to mimic pathological hallmarks of AD and investigate neurotoxic effects (Finelli et al. 2004; Iijima et al. 2004). In this study, I used an Aβ aggregation model, which is based on the expression of the coding sequence of different variants of the human Aβ peptide that are fused to an extracellular secretion signal (Iijima et al. 2004; Crowther et al. 2005; Sowade & Jahn n.d.).

From the identification of the *white* gene by Thomas H. Morgan in 1910 until now the applications and genetic tools for using *Drosophila* as model organism have continuously be evolved (Morgan 1910; Bellen et al. 2010). Favorable methods that I used in the present work were the cell-specific single and dual

expression systems Gal4/UAS (upstream activating sequence) and/or LexA/lexAop (Brand & Dormand 1995; Lai & Lee 2006) to co-express different Aβ variants and/or different redox sensors in different cell types. To monitor the cell stress response in the fly brain I validated specific redox sensors (Simone C. Albrecht et al. 2011) and JNK (Chatterjee & Bohmann 2012) reporters that are explained in more detail in each corresponding results part.

2. Objectives

Recent clinical trials, targeting Aβ initially have been promising to stop and slow down Aβ production (Kennedy et al. 2016), but ultimately failed or were discontinued due to lack of efficacy (Morris et al. 2014). Previous studies have shown that the amount of Aβ plaques does not correlate with the severity of AD symptoms (Perez-Nievas et al. 2013; Chételat et al. 2010; Sloane et al. 1997), which strongly indicates the importance and urgency to investigate other mechanisms that are involved in the early stages of AD progression to find new targets for this still incurable disease. There is growing evidence that AD pathogenesis correlates with increased oxidative stress due to an imbalance in redox homeostasis, either due to overproduction of reactive oxygen species (ROS) and/or a decrease in the anti-oxidative defense system (von Bernhardi & Eugenín 2012; Cai et al. 2011). Several cellular insults elevating oxidative stress have been proposed in AD, such as mitochondrial dysfunction (Lin & Beal 2006) and inflammation (Liddelow et al. 2017; Heneka et al. 2014; Block et al. 2007). However, it is still under discussion whether an imbalance in redox homeostasis has a causative role in AD or is a consequence of neuronal degeneration. It is still to resolve in which scale changes in redox balance impact the onset and progression of AD.

Importantly, providing direct *in vivo* evidence for the connection of redox imbalance with Aβ neurotoxicity is of high importance. The present study aimed to provide new insights into a understanding of the impact of changes in redox homeostasis and the involvement of stress responsive pathways in the onset and progression of AD. The overall aim was to analyze potential connections between changes in the cellular redox homeostasis on the onset of Aβ-induced neurotoxicity. In addition, I was also interested in how redox changes can be translated into a death signal. The involvement of the JNK pathway as an important regulator of stress responses and apoptosis in AD pathology has been previously reported (Coffey 2014; Liu & Lin 2005; Manning & Davis 2003). Moreover, shedding light on the ongoing debate whether JNK activation contributes to cell death in response to oxidative stress (Sclip et al. 2014; Tare et al. 2011; Marques et al. 2003; Jang & Surh 2002; Shoji et al. 2000) or acts as a protection against it (Liu et al. 2015; Wu et al. 2009; Wang et al. 2003) is of high importance. Furthermore, the neuron-glia interactions represent an important and critical aspect in the development of AD pathogenesis and are so far not fully understood. The role of glia cells in AD have been previously described in the context of inflammatory processes, in which Aβ can lead to activated microglia, which in result secret ROS and inflammatory cytokines, contributing to this vicious circle which contribute to neuronal damage (Liddelow et al. 2017; Heneka et al. 2014; Block et al. 2007). But it is still not well characterized which mechanisms mediate the crosstalk between neurons and glia cells and whether changes in redox balance play a crucial role in this. Therefore, in this study, I aimed to specifically monitor neuronal and glial alterations in redox state in an entire organ, the *Drosophila* brain, to explore the role of

neuron-glia communication in this context and associate it directly with changes in neurotoxicity using longevity assays. In this context, the development of qualified tools to analyze the role of redox changes, at early stages, and in more detail is very important.

In this study, I present an *in vivo* model, combining quantitative redox analysis with an *in vivo Drosophila* model of Amyloid-beta (Aβ) aggregation. The major novelty and advance of this system is the combination of two powerful tools: 1) the establishment of dual expression *Drosophila* models allowing the pan-neuronal expression of different Aβ variants (non-toxic/toxic) with the independent expression of the redox sensors in neurons or glia cells and 2) the use of genetically encoded fluorescence-labeled redox sensors (roGFP2s) allowing the quantitative real-time measurement of redox changes in different cellular compartments (cytoplasm or mitochondria), allowing the discrimination of the glutathione redox potential or H_2O_2 levels, respectively (Barata & Dick 2013; Gutscher et al. 2013; Simone C. Albrecht et al. 2011). The aim was to examine early events of neuronal dysregulation and disease onset *in vivo* and further provide a screening platform for possible disease modifying therapies.

3. Materials and Methods

3.1 Materials

3.1.1 Antibodies, Chemicals, Reagents

Table 1: List of Antibodies			
Name	Dilution	Source	Identifier
6E10 for total Aβ detection	1:500 or 1:1000	Covance	Sig-39320-200 Lot: D11LF02498
Actin	1:500	Sigma-Aldrich	A2228
Goat anti-Mouse IgG (H+L), Alexa Fluor® 568	1:2500	Thermo Fisher Scientific	A11004
Goat α-mouse IgG-HRP	1:2000	Thermo Fischer Scientific	62-6520; RRID: AB_88369

Table 2: List of chemicals and reagents		
Name	Source	Identifier
Agar (for standard fly food)	Biomol	A090#4
Agar (for holidic fly food)	Difco	214530
β-mercaptoethanol	Sigma-Aldrich	M6250-250mL
BD Difco™ Granulated Agar	Fisher Scientific	10006334
Biotin	Sigma Aldrich	B4501
Bovine Serum Albumin (BSA)	Sigma-Aldrich	A2153-100G
Brilliant blue	Carl-Roth	3862.1
Calcium chloride	Sigma-Aldrich	C7902
Ca pantothenate	Sigma Aldrich	P2250
Cholesterol	Sigma Aldrich	C8667
Choline chloride	Sigma Aldrich	C1879
ColorPlus™ Prestained Protein Ladder, Broad Range	New England Biolabs (NEB)	P7711 S
Complete™ Protease Inhibitor Cocktail Tablets	Santa Cruz Biotechnology	sc-29130
$CuSO_4.5H_2O$	Sigma Aldrich	C7631
Corn flour	Bäko Süd-West eG	11474
Desoxyribunucleoside triphosphate (dNTPs) mix	Carl Roth	R0182

Dimethyl sulfoxide (DMSO)	Sigma-Aldrich	D8418-100ML
Dream Taq DNA polymerase (5 U/µl)	Thermo Fisher Scientific	EP0701
EDTA-Free Protease Inhibitor mix	Sigma-Aldrich	COEDTAF-RO 11873580001
Ethanol	Sigma-Aldrich	12694
Ethylenediaminetetraacetic acid (EDTA)	Carl Roth	X986.2
Express Five SFM Medium	Life Technologies	10486025
Fetal bovine serum (FBS) Superior	Biochrom	S-0615
$FeSO_4.7H_2O$	Sigma Aldrich	F7002
Formaldehyde, 37%	Sigma-Aldrich	252549-25ML
GenLadder 100 bp	GENAXXON bioscience	M3094.0050
GenLadder 250bp -10kb	GENAXXON bioscience	M3328.0050
Glacial acetic acid	Fisher Scientific	A/0400/PB15
Glucose	Sigma-Aldrich	G7021
Glycerol	Carl Roth	7530.1
Glycine	Sigma Aldrich	G7126
Guanidine hydrochloride	Carl Roth	6069.2
HDGreen^{TM} DNA Stain	Intas Science Imaging	15115390
Hoechst 33342	Thermo Fisher Scientific	631311
Inosine	Sigma Aldrich	I4125
Isopropanol	Sigma-Aldrich	33539-2.5L
KH_2PO_4	Sigma Aldrich	P9791
L-alanine	Sigma Aldrich	A7627
L-arginine	Sigma Aldrich	A5131
L-asparagine	Sigma Aldrich	A0884
L-aspartic acid	Sigma Aldrich	A6683
L-cysteine (HCl)	Sigma Aldrich	C1276
L-glutamine	Sigma Aldrich	G3126
L-histidine	Sigma Aldrich	H8000
L-isoleucine	Sigma Aldrich	I2752
L-leucine	Sigma Aldrich	L8912
L-lysine (HCl)	Sigma Aldrich	L5626
L-methionine	Sigma Aldrich	M9625
L-phenylalanine	Sigma Aldrich	P2126

L-proline	Sigma Aldrich	P0380
L-serine	Sigma Aldrich	S4500
L-threonine	Sigma Aldrich	T8625
L-tryptophan	Sigma Aldrich	T0254
L-tyrosine	Sigma Aldrich	T3754
L-valine	Sigma Aldrich	V0500
Magnesium chloride hexahydrate	Carl Roth	A537.4
Malt extract	BakeMark Germany	728985
$MgSO_4$ (anhydrous)	Sigma Aldrich	M7506
$MnCl_2.4H_2O$	Sigma Aldrich	M3634
Myo-inositol	Sigma Aldrich	I7508
Nicotinic acid	Sigma Aldrich	N4126
Nipagin (Methyl-4-Hydroxybenzoat)	VWR International	1.06757.5000
Nonfat dried milk powder	Panreac AppliChem	A0830.1000
PeqGOLD Universal Agarose	Peqlab Biotechnology GmbH	732-2790
Phosphate-buffered saline (PBS) tablets	Panreac AppliChem	A9191.0100
Phosphoric acid	Sigma-Adrich	N/A
PhosSTOP Phosphatase Inhibitor mix	Sigma-Aldrich	PHOSS-RO
Propionic acid (for standard fly food)	VWR International	8.00605.2500
Propionic acid (for holidic fly food)	Sigma Aldrich	P5561
Proteinase K	Panreac AppliChem GmbH	A4392
Pyridoxine (HCl)	Sigma Aldrich	P9755
Quick Start Bradford 1x Dye Reagent	Bio-Rad	5000205
Riboflavin	Sigma Aldrich	R4500
Sarkosyl/N-Lauroylsarcosine sodium	Sigma-Aldrich	137-16-16
Sodium chloride	Sigma-Aldrich	31434-1KG-R
Sodium dodecyl sulfate (SDS) pellets	Carl Roth	CN30.1
Sodium folate	Sigma Aldrich	F7876
Sodium fluoride	Panreac AppliChem	A3904.0025
Sodium glutamate	Sigma Aldrich	G5889
Sodium hydrogen carbonate	Sigma-Adrich	S5761
Sodium orthovanadate	Sigma-Aldrich	S6508

Sodium phosphate monobasic monohydrate	Sigma-Aldrich	S9638
Soybean meal	Amorebio GmbH	895
Spectra^{TM} Multicolor Low Range Protein Ladder	Thermo Fisher Scientific	26628
Sugar beet syrup	Grafschafter Krautfabrik	01901
Sucrose	Sigma Aldrich	S1888
SuperSignal West Pico Chemiluminescent Substrate	Thermo Fisher Scientific	34080
SuperSignal West Femto Chemiluminescent Substrate	Thermo Fisher Scientific	34095
Thiamine (aneurin)	Sigma Aldrich	T4625
Thioflavin S	Sigma-Aldrich	T1892
Trizma® base	Sigma-Aldrich	T1503-1KG
Trizma® hydrochloride	Sigma-Aldrich	T3038
Triton X-100	Sigma-Aldrich	T8787
Tween-20	Sigma-Aldrich	P1379-1L
Uridine	Sigma Aldrich	U3750
VECTASHIELD® Mounting Medium	Vector Laboratories	VEC-H-1000
Yeast	Heierler Cenovis GmbH	98206
$ZnSO_4.7H_2O$	Sigma Aldrich	Z0251

3.1.2 Buffers

Table 3: List of buffers	
Name	Components
AlphaLISA buffer I (4 M Guanidine buffer)	50 mM Trizma base 1x protease inhibitor 1 mM EDTA 4 M guanidine hydrochloride pH 7.4 (stored at 4 °C, shortly before use at RT)
AlphaLISA buffer II (400 mM Guanidine buffer)	50 mM Trizma base 1x protease inhibitor 1 mM EDTA 400 mM guanidine hydrochloride pH 7.4 (stored at 4 °C, shortly before use at RT)
AlphaLISA buffer III (without Guanidine)	50 mM Trizma base 1x protease inhibitor 1 mM EDTA pH 7.4 (stored at 4 °C, shortly before use at RT)
Genomic DNA extraction buffer	10 mM Trizma hydrochloride (pH 8.0) 1 mM EDTA 25 mM sodium chloride 1 % (v/v) proteinase K (200 µg/ml) Aliquoted and stored at -20°C (without Proteinase K). Proteinase K was always added freshly directly before use.
Lämmli	60mM Trizma base (pH 6.8) 2 % (w/v) SDS 10% glycerol 5 % (v/v) β-mercaptoethanol 0.01 % (w/v) brilliant blue

Protein extraction buffer	50 mM Trizma base (pH 7.5) 2 mM sodium orthovanadate 50 mM sodium fluoride 50 mM β-Glycerophosphate disodium salt hydrate 1 x phosphatase inhibitor 1 x protease inhibitor 150 mM sodium chloride 2 mM magnesium chloride 1 % (w/v) N-Lauroylsarcosine 1 % (v/v) Triton X-100 1 % (w/v) SDS
NuPAGE MES SDS Running Buffer	Composition see specifications from Life Technologies
Rinaldini solution (for live-imaging) (Harzer et al. 2013)	8mg/ml NaCl 0.2mg/ml KCl 0.05mg/ml NaH_2PO_4 1mg/ml $NaHCO_3$ 1mg/ml Glucose
Rotiphorese® NF 10x TBE-Buffer (0.5x)	Composition see specifications from Carl Roth GmbH

3.1.3 Consumables, Equipment and Kits

Table 4: List of consumables	
Name	Source
Amersham™ Protran™ 0.1 µm nitrocellulose blotting membrane	GE Healthcare
Centrifuge tubes (Polypropylen tubes 15 ml and 50 ml)	Greiner Bio-One
Corning® 96-well microplates (Product #3642)	Corning
Corning® Costar® Stripette® serological pipettes (5 ml, 10 ml and 25 ml)	Sigma-Aldrich
Eppendorf Safe-Lock tubes (1.5 ml)	Eppendorf
Forceps, Dumont No. 5	neoLab
Hard-Shell® 96-well PCR Plate (Product #HSP9601)	Bio-Rad
Microscope slides	Thermo Fisher Scientific

Microseal® B Adhesive Sealer	Bio-Rad
NuPAGE™ Novex™ 4-12 % Bis-Tris gels	Thermo Fischer Scientific
PCR tubes (0.2 ml, RNase-free)	nerbe plus
Pipette tips (200 µl, 1000µl)	Greiner Bio-One
Pipette tips TipOne® (10 µl)	STARLAB Group
Precellys mashing tubes (CK14 – 0.5 ml)	Bertin Instruments
Premium surface pipet tips (100 µl, 1250 µl)	nerbe plus
RNase-free microfuge tubes (0.5 and 1.5 ml)	Thermo Fisher Scientific
Siliconized microcentrifuge tubes (1.5 ml)	Sigma-Aldrich

Table 5: List of equipment

Name	Source
8-well Chambered Coverglass System (Nunc™ Lab-Tek™)	Thermo Fischer Scientific #155411
24-well plates, 662160	Greiner Bio-One #2511
AccuBlock™ Digital Dry Bath	Labnet International
Benchtop Flowbuddy with a blowgun	Genesee Scientific
C-Digit® Blot Scanner	Li-COR®
Centrifuge 5430 R	Eppendorf
E-BOX VX2 gel analysis chamber	Vilber Lourmat
Eppendorf Research® plus pipettes	Eppendorf
FLUOstar Omega microplate reader	BMG LABTECH
Laser Scanning Microscope (LSM) 780 and 880 with Airyscan	Zeiss
Leica SP5	Leica Microsystems
Minilys personal homogenizer	Bertin Corp.
MiniSpin® table centrifuge	Eppendorf
Mini-Sub® Cell GT Systems	Bio-Rad
NanoDropTM Lite Spectrophotometer	Thermo Fisher Scientific
PIPETBOY acu 2 pipet aid	INTEGRA Biosciences
PowerPac™ Basic Power Supply	Bio-Rad
Reax top test tube shaker	Heidolph Instruments
Rotamax 120 orbital platform shaker	Heidolph Instruments
RUMED® fly incubator 3201	Rubarth Apparate GmbH

Sonorex RK 102 Transistor	BANDELIN
Stemi 2000 stereomicroscope	Zeiss
T100 Thermal Cycler for PCR	Bio-Rad
ThermoCell Mixing Block MB-102	Bioer
Trans-Blot® Turbo™ Transfer System	Bio-Rad
Ultimate Flypad	Genesee Scientific
Wide Mini-Sub® Cell GT Horizontal Electrophoresis System	Bio-Rad
XCell SureLoc™ Mini-Cell Electrophoresis System	Invitrogen

Table 6: List of Kits

Name	Source	Identifier
Amyloid β 1-x (human) AlphaLISA Detection Kit	PerkinElmer	AL288C
Effectene Transfection Reagent Kit	Qiagen	301427
DC™ Protein assay (Lowry)	Bio-Rad	500-0113
Trans-Blot® Turbo™ RTA Transfer Kit	Bio-Rad	1704270

3.1.4 Drugs and Antioxidants

Table 7: List of Antioxidants and Drugs for feeding experiments

Name	End concentration for feeding experiment	Source	Identifier
Ascorbat (L-ascorbic acid)	0.36mM	Sigma Aldrich	A0278-25G
α-tocopherol (Vitamin E, Trolox)	1.1mM 6.7mM 13.3mM	Sigma Aldrich	T3251-5G
Buthionine Sulfoximine (BSO)	1mM	Cayman Chemical Company	Cay14484-1
Buthionine Sulfoximine (BSO)	1mM	Sigma Aldrich	B2515-500MG
DMSO control	0.2% v/v	Sigma Aldrich	D8418-100ML
Ethanol controls	0.75% v/v 0.026% v/v 0.7% v/v 2% v/v	Sigma Aldrich	12694

Hydrogen peroxide, 30% (H_2O_2)	88mM	Carl Roth	8070.2
NAC (N-acetyl-L-cysteine)	10mg/ml	Sigma Aldrich	A7250-25G
NDGA (Nordihydroguaiaretic acid)	16.536mM	Sigma Aldrich	74540-1G
Paraquat dichlorid hydrat pestanal (Paraquat)	1mM	Sigma Aldrich	36541-100MG
Propyl gallate	0.1mM	Sigma Aldrich	48710-100G-F
Reduced GSH	0.22mM	Sigma Aldrich	G4251-5G
Rotenone	100µM	Sigma Aldrich	R8875-1G
Stearic acid (C18)	10% w/v	Santa Cruz Biotechnology	sc-484614A
TCA (L-4-Thiazolidinecarboxylic acid)	0.5% w/v	Sigma Aldrich	T27502-10G
tert-Butylhydroquinone (tBHQ, Nrf2 inducer)	0.1% w/v 0.15% w/v	Sigma Aldrich	112941-100G

3.1.5 Fly lines

Table 8: List of *Drosophila melanogaster* lines		
Name	Source or FlyBase Genotype	Identifier, BDSC[1] or VDRC[2] number
Driver lines:		
elav-Gal4	*P{GawB}elav^{C155}*	458
nSyb-Gal4::*nSyb*-LexA	*w*;+;nSyb*-Gal4::*nSyb*-LexA	T.R. Jahn Lab
repo-Gal4	*repo*-Gal4;+;+	M. Freeman lab (Sepp et al. 2001)
w;+;repo*-Gal4::*nSyb*-LexA	*w*;+;repo*-Gal4::*nSyb*-LexA	T.R. Jahn
Target lines:		
lexA.op-TAβ$_{40}$	*w*;+;lexA.op-TAβ$_{40}$*	T.R. Jahn
lexA.op-Aβ$_{42}$	*w*;+;lexA.op-Aβ$_{42}$*	T.R. Jahn
UAS-Aβ$_{42}$	w*;pJFRC7-Aβ$_{42}$;+ (attP40)	T.R. Jahn

[1] Bloomington *Drosophila* Stock Center (BDSC)
[2] Vienna *Drosophila* Resource Center (VDRC)

cyto-Grx1-roGFP2	*w*;pUAST-cyto-Grx1-roGFP2;+*	T. P. Dick Lab (Simone C Albrecht et al. 2011)
mito-Grx1-roGFP2	*w*;pUAST-mito-roGFP2-Grx1;+*	T. P. Dick Lab (Simone C Albrecht et al. 2011)
cyto-roGFP2-Orp1	*w*;pUAST-cyto-roGFP2-Orp1;+*	T. P. Dick Lab (Simone C Albrecht et al. 2011)
mito-roGFP2-Orp1	*w*;pUAST-mito-roGFP2-Orp1;+*	T. P. Dick Lab (Simone C Albrecht et al. 2011)
Others:		
w^{1118}	w^{1118};+;+	BDSC 5905
TRE-DsRed	*w;TRE-DsRed-2R;* +	D. Bohman Lab (Chatterjee & Bohmann 2012)

Table 9: List of *Drosophila melanogaster* lines for genetic screening (ordered from BDSC or VDRC)		
Name	Source or FlyBase Genotype	Identifier, BDSC or VDRC number
Overexpression lines		
cat-OE	w^3; P{UAS-Cat.A}2	24621
dPRX5-OE_1	*UAS-dPRX5_2nd*	W.C. Orr Lab
dPRX5-OE_2	*UAS-dPRX5_3rd*	W.C. Orr Lab
Eaat1-OE_WT	y1 w1118; P{UAS-Eaat1.Exel}3/TM6B, Tb1	8202
G6PD5c-OE_1	*UAS-G6PD5c_2nd*	W.C. Orr Lab
G6PD5c-OE_2	*UAS-G6PD5c_3rd*	W.C. Orr Lab
Gclc-OE	*w; pP[UAST]-Gclc6;* +	W.C. Orr Lab
GST^{s14}*-OE*	*UAS-*GST^{s14}*_3rd*	A.J. Whitworth lab
Prx4-OE	w1118; PBac{WH}Jafrac2f01922	18489

SOD1-OE_1	w^1; P{UAS-Sod1.A}B36	24754
SOD1-OE_2	w^1; P{UAS-Sod1.A}B37	24750
SOD2-OE	w^1; P{UAS-Sod2.M}UM83	24494
Downregulation lines		
Cat_TRiP_1	y^1 sc^* v^1; P{TRiP.GL01541}attP40	43197
Cat_TRiP_2	y^1 v^1; P{TRiP.JF02173}attP2	31894
cnc_TRiP_1	y^1 v^1; P{TRiP.JF02006}attP2	25984
cnc_TRiP_2	y^1 v^1; P{TRiP.HMS02021}attP40	40854
dhd_TRiP	y^1 v^1; P{TRiP.GL01285}attP2	41857
Eaat1_TRiP	y^1 sc* v^1; P{TRiP.HMS02659}attP40/CyO	43287
Eaat2_TRiP	y^1 v^1; P{TRiP.HMS01998}attP40/CyO	40832
GclcRNAi	P{KK101607}VIE-260B	M. Boutros Lab VDRC v108022
GstD1_TRiP	y^1 sc^* v^1; P{TRiP.GL01039}attP2/TM3, Sb^1	36818
Keap1_TRiP	y^1 v^1; P{TRiP.HMJ21798}attP40	57801
MafS_TRiP_1	y^1 v^1; P{TRiP.HMS02020}attP40	40853
MafS_TRiP_2	y^1 v^1; P{TRiP.JF02008}attP2	25986
PHGPx_TRiP	y^1 sc^* v^1; P{TRiP.GL01312}attP40	41879
SOD1_RNAi_1	w^*; P{UAS-Sod1.IR}F103/SM5	24493
SOD1_RNAi_2	w^*; P{UAS-Sod1.IR}4	24491
SOD2_dsRNA	w^1; P{UAS-Sod2.dsRNA.K}15/SM5	24489
TrxR_TRip_1	y^1 sc* v^1; P{TRiP.GL01017}attP40	36805
Trxr-1_TRiP_2	y^1 v^1; P{TRiP.HMJ21198}attP40	53883
Trxr-1_TRiP_3	y1 sc* v1; P{TRiP.HMS00784}attP2/TM3, Sb1	32984

3.1.6 Holidic fly food

Table 10: Protocol for preparing holidic fly food (Piper et al. 2014)			
Ingredients	Ingredients	Stock solution	Amount [Per liter]
Step 1: Prepare solution with following ingredients:			
Gelling agent	Agar		20g
Base	10x Buffer	Glacial acetic acid (30ml/l)	100ml
		KH_2PO_4 (30 g/l)	
		$NaHCO_3$ (10 g/l)	
Sugar	Sucrose		17.12g
Amino acids	L-isoleucine		1.82g
	L-leucine		1.21g
	L-tyrosine		0.42g
Metal ions	$CaCl_2.6H_2O$	1000x: 250 g/l	1 ml
	$CuSO_4.5H_2O$	1000x: 2.5 g/l	1 ml
	$FeSO_4.7H_2O$	1000x: 25 g/l	1 ml
	$MgSO_4$ (anhydrous)	1000x: 250 g/l	1 ml
	$MnCl_2.4H_2O$	1000x: 1 g/l	1 ml
	$ZnSO_4.7H_2O$	1000x: 25 g/l	1 ml
Cholesterol	Cholesterol	in EtOH (20 mg/ml)	5ml
Water	Water		add to 1l
Step 2: Autoclave for 15min at 120°C and cool down to 65°C on a stirrer and add the following:			
Amino acids	Essential Stock	L-arginine (8 g/l)	60.51ml
		L-histidine (10 g/l)	
		L-lysine(HCl) (19 g/l)	
		L-methionine (8 g/l)	
		L-phenylalanine (13 g/l)	
		L-threonine (20 g/l)	
		L-tryptophan (5 g/l)	
		L-valine (28 g/l)	
	Non-essential Stock	L-alanine (35 g/l)	60.51ml
		L-asparagine (17 g/l)	
		L-aspartic acid (17 g/l)	
		L-cysteine HCl (1 g/l)	

		L-glutamine (25 g/l)	
		glycine (32 g/l)	
		L-proline (15 g/l)	
		L-serine (19 g/l)	
	Sodium glutamate	100 g/l	15.13ml
Vitamins	Vitamin Stock (125x)	Thiamine (aneurin) (0.1 g/l)	14ml
		Tiboflavin (0.05 g/l)	
		Nicotinic acid (0.6 g/l)	
		Ca pantothenate (0.775 g/l)	
		Pyridoxine (HCl) (0.125 g/l)	
		Biotin (0.01 g/l)	
	Sodium Folate (1000x)	0.5 g/l	1ml
Other nutrients	Stock solution (125x)	Choline chloride (6.25 g/l)	8ml
		Myo-inositol (0.63 g/l)	
		Inosine (8.13 g/l)	
		Uridine (7.5 g/l)	
Preservatives	Propionic acid		6ml
	Nipagin	Methyl 4-hydroxybenzoate in 95% EtOH (100 g/l)	15 ml
Step 3: Keep warm at 65°C in water bath and decant it in small 50ml vials.			
All Stock solutions were steril filtered through a 0.22µl filter. CuSO4.5H2O, HeSO4.7H2O, Vitamin solution (125x) and Folic acid (0.5g/l) were stored at -20°C and the other stock solutions were stored at -4°C.			

3.1.7 Primers and DNA sequences

Table 11: List of primers and DNA sequences		
Primer used for genotyping flies		
Target	Sequence of forward and reverse primers (5`-3`)	Annealing temperature
Gal4	Forward: GATGCCGTCACAGATAGAT Reverse: TTTAAAGCCAATAGATCGA	52 °C
LexA	Forward: CCTGCCACTGGTGGGACGCG Reverse: CGGCGAGGAGGTCACCATCC	70 °C
lexAop	Forward: CATCCATACAGTAAGCGGAG Reverse: ACAGAAGTAAGGTTCCTTCA	55 °C
UAS-transgene	Forward: TACTGTCCTCCGAGCGGAG or CTGCAACTACTGAAATCTGCC Reverse: GGCATTCCACCACTGCTC	59 °C
TRE-DsRed.T4	Forward: GATTTCTTATGAGTCATCGTGATTTC or: GAGCGCCGGAGTATAAATAGAG Reverse: GATACATTGATGAGTTTGGACAAACC	52°C
DNA sequences Dr. R.F. Sowade cloned in the pJFRC7 or pJFRC19 vectors		
Name	Sequence (5`- 3`)	
TAβ_{40}	GATGCGGAATTTCGCCATGACAGCGGCTACGAAGTGCATCATC AAAAATTGGTGTTTTTTGCGGAAGACGTGGGCTCGAACAAAGG CGCGATTATTGGCTTGATGGTGGGCGGCgtggtgggcggcggcggcagcggc ggcggcggcagcggcggcGATGCGGAATTTCGCCATGACAGCGGCTACGA AGTGCATCATCAAAAATTGGTGTTTTTTGCGGAAGACGTGGGC TCGAACAAAGGCGCGATTATTGGCTTGATGGTGGGCGGCGTG GTGTAA	
Aβ_{42}	GATGCGGAATTTCGCCATGACAGCGGCTACGAAGTGCATCATC AAAAATTGGTGTTTTTTGCGGAAGACGTGGGCTCGAACAAAGG CGCGATTATTGGCTTGATGGTGGGCGGCGTGGTGATTGCGTA A	
Signal Peptide	ATGGCGAGCAAAGTCTCGATCCTTCTCCTGCTAACCGTCCATC TTCTGGCTGCTCAGACCTTCGCCCAG	

3.1.8 Softwares

Table 12: List of softwares		
Name	Source	Identifier
MS Office	Microsoft Cooperation	2011
Adobe Illustrator CS6	Adobe Systems	Version 16.0.0
GraphPad Prism	GraphPad Software Inc.	Version 7.0a
Fiji (ImageJ)	NIH, Schindelin et al., 2012	Version 2.0.0-rc-49/1.51a
Image Studio Lite	LI-COR Biosciences	Version 5.2.5

3.2 Methods

3.2.1 Transgenic *Drosophila melanogaster* lines

All used Aβ fly lines were generated in our laboratory. To allow the secretion of Aβ by neurons upon pan-neuronal expression, the human sequences of $A\beta_{42}$ and $TandemA\beta_{40}$ were cloned downstream of a secretory signal peptide (Crowther et al. 2005). I used $A\beta_{42}$ as the neurotoxic variant and $TandemA\beta_{40}$, a dimer of two $A\beta_{40}$ monomers linked via a twelve amino acid linker (Speretta et al. 2012), served as a negative control for non-toxic cellular effects based on protein accumulation. In most experiments, Aβ was expressed under the control of the LexA/LexAop expression system. In the experiments shown in Figure 4 C, D, F and G, I used the Gal4/UAS expression system with the pJFRC7 vector (Addgene #26224, (Pfeiffer et al. 2010)) for pan-neuronal Aβ expression. The pJFRC19 vector (Addgene #26224) was used for both *w; +; lexA.op-*$A\beta_{42}$ and *w; +; lexA.op-*$TA\beta_{40}$ (Pfeiffer et al. 2010). Transgenic flies were generated by phiC31 integrase-mediated transgenesis (Bischof et al. 2007) using attP landing sites 25C7 (attP40 for 2nd chromosome) and 68A4 (attP2 for 3rd chromosome). The PD Dr. T.P. Dick laboratory provided all used redox sensor flies *(pUAST-cytoGrx1-roGFP2, pUAST-cyto-roGFP2-Orp1, pUAST-mito-roGFP2-Orp1)* (Simone C. Albrecht et al. 2011). Prof. Dr. W.C. Orr (Southern Methodist University, Dallas, USA) kindly provided the *UAS-Gclc*-OE fly line (*w; pP[UAST]-Gclc6;* +) as published in (Orr et al. 2005). The Gclc-RNAi fly line (VDRC v108022) was obtained from the Prof. Dr. Michael Boutros laboratory (DKFZ Heidelberg, Germany). The JNK reporter flies (*w; TRE-DsRed-2R;* +) were kindly given by the Dr. D. Bohmann laboratory (University of Rochester Medical Center, USA), as published in (Chatterjee & Bohmann 2012). The Dr. M. Freeman laboratory (University of British Columbia, Canada) provided the *repo*-Gal4 driver line (Sepp et al. 2001) for pan-glial expression. For expression of Aβ in all neurons I used the *nSyb*-LexA, *nSyb*-Gal4 or the *elav*-Gal4 driver line, which was acquired from the Bloomington *Drosophila* Stock Center. An overview of all fly lines with their genotype and exact

sources can be found in Table 8 and Table 9.

3.2.2 Fly Husbandry and feeding experiments

All fly stocks were kept at 25°C on a 12h light / 12h dark cycle at 60% relative humidity and were raised on standard *Drosophila* food, containing 0,8% (w/v) agar (Biomol), 8% (w/v) corn flour (Bäko Süd-West eG), 8% (v/v) malt extract (BakeMark), 0,24% (w/v) nipagin (VWR International), 0,0625% (v/v) phosphoric acid (Sigma-Adrich), 0,625% (v/v) propionic acid (VWR International), 1% (w/v) soybean meal (Amorebio GmbH), 1,8% (w/v) 2,2% (v/v) sugar beet syrup (Grafschafter Krautfabrik), yeast (Heierler GmbH) and water. The composition of the holidic fly food for drug and antioxidant feeding experiments are shown in Table 10. All Crosses were reared in 200ml bottles. For all experiments the crosses were incubated at 25°C for 3 days and then kept at 29°C during aging before freezing at -80°C at the stated time points or for aging. Enclosing adult flies were collected within a 12h time period and were mated for 24h. In all experiments only female flies were used. For drug and antioxidant feeding experiments, the components were solubilized as required either in water, DMSO or EtOH and added to the according fly food. All final concentrations can be taken from Table 7. For the feeding experiments, during development the larvae were first maintained on standard *Drosophila* food. After hatching and mating for 24h the flies were transferred to the drug food, which was prepared in standard *Drosophila* or holidic fly food.

3.2.3 Preparing of drug and antioxidant fly food

Stock solutions for each compound were prepared freshly before use, subsequently mixed with the respective drug or antioxidant (Table 7) and added to the standard *Drosophila* (see 3.2.2) or holidic fly food Table 10, (Piper et al. 2014). Then the drug food (3-5ml) was decanted into small 50ml vials. To prevent the food from getting solid too fast, each bottle was kept at 65°) in a water bath during the decanting process. The fly food was dried for a few hours or over night, covered with paper towels to avoid contamination, before finally the vials were plugged with anti-mite-plugs. The drug food was always prepared freshly once every 1 to 1.5 weeks.

3.2.4 Longevity assays

All longevity assays were performed at 29°C. Flies were maintained at a density of 9-11 flies per vial. They were transferred to new fly food every 2 to 3 days. For the drug and genetic screening approximately sixty mated females were used. For the core experiments for each genotype and condition, approximately hundred mated females were used. The number of deceased flies was counted on every flipping day and documented in flytracker.gen.cam.ac.uk/. The overall lifespan is depicted in Kaplan-Meier curves and the median survival per vial (9-11 flies) is visualized as dot plots. Data analysis was conducted with GraphPad Prism 7.0a.

3.2.5 Genotyping of transgenic flies

To verify the presence of transgenes in newly generated double- or triple-transgenic fly lines, genomic DNA was extracted from adult flies and subsequently PCR analysis was performed in a 3-step protocol using DreamTaq DNA polymerase (Thermo Fisher Scientific) according to manufacturer´s instructions. For genomic DNA extraction, one fly per genotype was anesthetized with CO_2 and transferred into a 1.5ml Eppendorf tube on ice. Then, 50µl of genomic DNA extraction buffer (Table 3) was added to each vial. After squashing the fly with a pipette tip, the samples were incubated at 37°C for 30min, shaking, followed by a 2min incubation at 95°C for Proteinase K inactivation. Either 1 to 2µl per sample was used per PCR reaction (Table 13), either directly after genomic DNA extraction or after storing the sample at -20°C. The composition of the PCR reaction mix is depicted in Table 13. The PCR analysis was performed as described in Figure 14. PCR products were separated using agarose gel electrophoresis (1.2% agarose in 0.5x TBE buffer including HDGreen^{TM} DNA Stain (Intas Science Imaging)). The GeneLadder (100pb and/or 250bp-10kb, GENAXXON bioscience) was used to determine the DNA fragment size under ultraviolet light in the E-BOX VX2 gel analysis chamber.

Table 13: PCR reaction mix per sample (25µl or 50µl):		
Volume for 25µl reaction (µl)	Volume for 50µl reaction (µl)	Name
2,5	5	DreamTaq^{TM} Green Buffer (10x)
0.5	1	dNTP mix (10mM)
0.5	1	Forward Primer (10µM)
0.5	1	Reverse Primer (10µM)
0.2	0.3	DreamTaq DNA polymerase
1	2	DNA template
to 25µl	to 50µl	water

Table 14: PCR program	
Temperature	Time
95°C	3 min
95°C	30 s
x°C *	30 s
72°C	1:30 min → 34 cycles
72°C	10 min
4°C	∞
*Annealing temperature adjusted for each primer pair as described in Table 11.	

3.2.6 Immunohistochemical stainings

Fly brains were dissected in PBS and afterwards incubated in 1 x PBS + 0.5% (v/v) Triton X-100 (PBST). This was followed by a fixation step in always freshly prepared 3.7% (w/v) formaldehyde solution (Sigma) in PBST for 30min. To wash out the fixation solution and for permeabilization, the fly brains were washed with PBST for 10min at RT for four times. For blocking, the brains were incubated in 5% (v/v) FBS in PBST for 30min at RT or over night at 4°C. To stain for total Aβ, the brains were incubated in the primary α-6E10 antibody (1:1000, Covance, Sig-39320-200 Lot: D11LF02498) for 2-3 days at 4°C, shaking. The antibody was removed by a 5-10min washing step in PBST which was repeated four times. This was followed by a two day incubation of the brains in the goat anti-mouse IgG (H+L) secondary antibody, Alexa Fluor® 568 conjugate (1:2500, Thermo Fischer Scientific) at 4°C, shaking. Thioflavin S (ThS, Sigma-Aldrich) was additionally added at this point in a final concentration of 5µM and co-incubated with the secondary antibody. More detailed descriptions of amyloids/β-sheet plaque staining

with ThS can be taken from (Berg et al. 2010). After the final washing steps (4x10min, RT), the fly brains were mounted in VECTASHIELD® Mounting Medium without DAPI (Vector Laboratories) for 30min at RT. Translucent nail polish was used to seal the cover slips. Imaging of the fly brains was performed with the laser scanning confocal microscope LSM 780 (Zeiss). All shown images were processed using Fiji (Schindelin et al. 2012) and Adobe Illustrator CS6.

3.2.7 Redox Analysis of fixed and freshly dissected adult fly brains

The redox sensors (cytoGrx1-roGFP2, cyto-roGFP2-Orp1, mito-roGFP2-Orp1) were expressed in the fly brain using the Gal4/UAS expression system. The *nSyb*-Gal4 and *elav*-Gal4 or *repo*-Gal4 driver lines were used to drive expression of the redox sensors in all neurons or glia cells, respectively. Fly brains were dissected following the instructions from (Wu & Luo 2006). Briefly, the adult flies were anesthetized shorty, rinsed in 70% Ethanol (Sigma-Aldrich), transferred onto a dissection pad and fixed with a needle. To determine the responsiveness and the maximal attainable redox changes of the redox sensors to reducing and oxidizing conditions, I dissected fly brains in 1 x PBS and immediately transferred them into 8-well Chambered Coverglass Systems (Thermo Fischer Scientific) containing 200µl 1x PBS + 0,1% Tween 20. The chambers with the brains were kept on ice. To fully reduce or to fully oxidize the probe, 2-5mM (final concentration) of the reductant DTT (Carl Roth) or 2-5mM of the oxidant DA (Sigma-Aldrich), was added to the brains for at least 30min on ice and 5-15min at RT (Figure 2). The fly brains were either imaged directly or fixed in 3.7% freshly prepared formaldehyde solution (Sigma) for 30min at RT, washed four times with 0.1% PBST, followed by 30min 20mM N-ethyl maleimide (NEM) treatment and finally embedding the brains in VECTASHIELD® Mounting Medium without DAPI (Vector Laboratories). To conserve the redox state of the redox sensors during the dissection process, I dissected the fly brains in NEM (Sigma-Aldrich) (Guan & Kaback 2007; Barata & Dick 2013; Fujikawa et al. 2016). This alkylating agent binds to all reduced cysteins and therefore protects the sample from further oxidation by e.g. atmospheric oxygen. For live imaging of freshly dissected samples, I dissected the fly brains directly in Rinaldini´s solution (8mg/ml NaCl, 0.2mg/ml KCl, 0.05mg/ml NaH_2PO_4, 1mg/ml $NaHCO_3$, 1mg/ml Glucose diluted in distilled water and sterile filtered, all components were obtained from Sigma-Aldrich, (Harzer et al. 2013)) containing 25mM NEM. I let the brains incubate for maximal 1h on ice, while dissecting the other fly brains, and then directly imaged them. DTT, DA and NEM solutions were always prepared freshly and kept on ice. Live imaging of the fly brains was performed in the 8-well Chambered Coverglass plates using the confocal microscope LSM 780 or LSM 880 (ZEN 2010 B SP1 or ZEN 2.1 Software). I used a Plan-Apochromat 20x/0.6 M27 objective and a T-PMT detector. The probe fluorescence was excited at 405nm and 488nm, sequentially, line by line and the detector range

detected from 499-534nm or 499-536nm. I used an averaging of 4, a bit depth of 16bit, a zoom of 0.6, a pinhole size (section thickness) of 3.5-4.0 µm, a gain of 790-910V and a digital offset of 0. The frame size was 512 x 512 pixels, and the scanning frequency "8-9" 1.52-1.58 µs. For each experiment all imaging setups were kept unchanged.

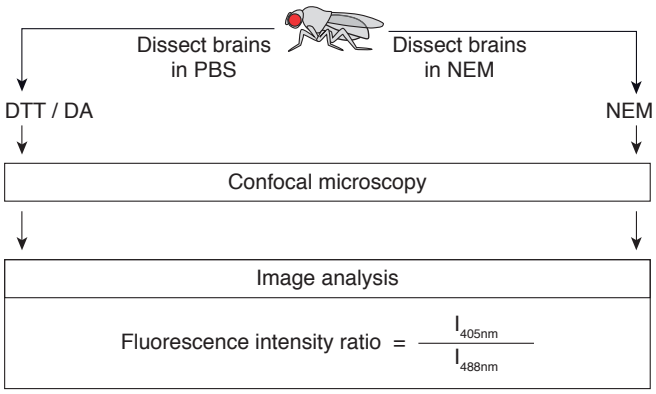

Figure 2: Schematic overview of the workflow for redox analysis in fly brains. Imaging of freshly dissected fly brains, which were fully reduced or oxidized with DTT or DA, or treated with NEM, was performed with confocal microscopy. This was followed by image analysis, calculating the fluorescence intensity ratio 405nm/488nm with ImageJ.

3.2.8 Cell line and validation of the redox analysis *in vitro*

For the validation of the redox sensors *in vitro,* I used *Drosophila* Schneider *Drosophila* Line 2 (S2) cells adapted in serum-free medium, which were maintained in Express Five SFM Medium (Life Technologies). Cells were grown at 25°C without CO_2 in presence of 10% L-Glutamine (Sigma-Aldrich), 100IU/ml penicillin and 100µg/ml streptomycin. One day before transfection $1x10^6$ cells were seeded on 0.5mg/ml Concanavaln A (Carl Roth)-coated glass cover slips in 24-well plates (Greiner Bio-One). Transfection was performed using the Effectene Transfection Reagent (Qiagen) according to manufacturer´s instructions, by applying 200ng plasmid of interest per well. The cells were transfected with each redox sensor (pCaSper4 cyto-Grx1-roGFP2, pCaSper4 mitoCOX8-roGFP2-Grx1, pCaSper4 cyto-roGFP2-Orp1, pCaSper4 mitoCOX8-roGFP2-Orp1), kindly provided by the T.P. Dick laboratory. Three days after transfection, I treated the samples with 2-5mM DTT (Carl Roth) or 2-5mM oxidant DA (Sigma-Aldrich), which was followed by 20mM NEM treatment. The cells were fixed with 3.7% PFA, each for 10min at RT, followed by four washing steps with 1xPBS for 5min. The glass cover slips were mounted in VECTASHIELD® Mounting Medium without DAPI (Vector Laboratories). The fixed samples were imaged with a Zeiss LSM 780 confocal microscope using a Plan-Apochromat 63x/1.40 Oil

DIC M27 objective and a 1,5 x zoom (image size 89,8µm x 89,8µm). The detailed image processing and data analysis can be taken from 3.2.9.

3.2.9 Image processing and data analysis for redox analysis

For image processing ImageJ (Version 2.0.0-rc-49/1.51a) was used. First, the obtained confocal pictures were converted to 32-bit format. A threshold was set for the fluorescence intensities of the 405nm and 488nm images and values below were set to "not a number" (NaN). To calculate the 405nm/488nm fluorescent intensity ratios, I divided the 405nm image by the 488nm image pixel by pixel. For comparison between different experiments I normalized the values to the fully reduced DTT sample = 0.2. The maximal attainable redox changes, also called dynamic range (DR), were calculated by dividing the 405nm/488nm ratio from the fully oxidized DA sample by the fully reduced DTT sample. To calculate the degree of oxidation (OxD) of roGFP2, which gives information about the percentage of the pool of the redox sensor molecules that are in an oxidized state, I used the Nernst equation, as described previously (Meyer & Dick 2010):

$$\mathrm{OxDroGFP2} = \frac{\mathrm{R} - \mathrm{Rred}}{\frac{\mathrm{I488red}}{\mathrm{I488ox}}(\mathrm{Rox} - \mathrm{R}) + (\mathrm{R} - \mathrm{Rred})}$$

The corresponding intracellular glutathione redox potential (E_{GSH}), which is dependent on the OxD, was also calculated using the Nernst equation, with adaptations to the roGFP2 redox sensor and my recording conditions. $E^{\circ\prime}{}_{roGFP2}$ has been determined as –280 mV (Dooley et al. 2004):

$$EGSH = EroGFP2 = E^{\circ\prime}roGFP2 - \frac{RT}{2F}\ln\frac{1-OxDroGFP2}{OxDroGFP2}$$

For the fluorescent ratio images shown in this study, I applied multiplicative Random J Gamma 3-7 and false colored the images using lookup table "Fire" to illustrate the redox changes in a more discernible way.

3.2.10 Imaging and quantification of JNK activation of whole fly brains

To monitor the JNK activation in response to Aβ in the fly brain I used the JNK reporter flies, kindly provided by the D. Bohmann´s laboratory (Chatterjee & Bohmann 2012). These reporter flies contain a stress-inducible promoter element (TRE) fused to the fluorescent reporter DsRed. For imaging of the JNK activation, I dissected the fly brains in Rinaldini´s solution and directly transferred them into an 8-well

plate filled with 200µl Rinaldini´s solution. The DsRed signal of the freshly dissected fly brains was directly imaged with the laser scanning confocal microscope LSM 780 (Zeiss) or Leica SP5. To ensure the comparability between the different data sets, I performed a time course analysis (Figure 13), where I dissected fly brains of different time points all on one day in four different imaging cycles. Per genotype 3-5 brains were imaged and analyzed. For quantification, the DsRed fluorescent intensity of the whole image was measured, using Fiji (Schindelin et al. 2012). To monitor also minor differences in JNK activation in $A\beta_{42}$ +/- Gclc-OE or Gclc-RNAi flies (Figure 13), I quantified the DsRed fluorescent intensity divided by the brain size. The plugin for Fiji, which I used to process the images in Figure 14, is depicted here:

```
run("Rotate... ")
wait(500);
run("Subtract Background...", "rolling=100");
roiManager("Reset");
run("Select None");
run("Set Measurements...", "area integrated limit display redirect=None decimal=3");
run("Threshold...");
setAutoThreshold("Default dark");
setThreshold(209, 4095);
waitForUser("Please check the Thr.");
run("Measure");

run("Duplicate...", "");
run("Gaussian Blur...", "sigma=20");
wait(500);
setAutoThreshold("Default dark");
setThreshold(32, 4095);
waitForUser("Please check the Thr.");
run("Analyze Particles...", "size=10000-Infinity pixel circularity=0.00-1.00 show=Nothing include summarize add");
run("Close");
roiManager("Select", 0);
run("Enlarge...", "enlarge=-20 pixel");
run("Add to Manager");
resetThreshold();
run("Measure");
```

3.2.11 Extraction of soluble and insoluble Aβ from fly brain homogenates

The mated female flies I used for protein extration were previously kept at -80°C. To decapitate the flies, the frozen whole flies were first transferred into a 15ml falcon tube. Afterwards, the falcon tubes were

immersed in liquid nitrogen, then vortexed and strongly tapped on the table. This was repeatedly executed four times. To get a yield of approximately 180-250µg total protein were used. The 20 or 30 decapitated fly heads were transferred into a mashing tube (CK14 – 0,5ml) and mashed in protein extraction buffer (Table 3) (1-1,3µl per fly head) using a Minilys personal homogenizer (Peqlab). Then the samples were sonicated for 5min on ice and mashed again. To avoid the formation of foam, the detergents 1% (w/v) N-lauroylsarcosine, 1% (w/v) SDS and 1% (v/v) Triton X-100 were added to protein extraction buffer after the homogenization step. For lysing, the samples were sonicated and incubated on ice for 15min for each step. To remove the tissue debris, the samples were centrifuged for 5min, at 3800 x g at 4°C and the supernatant was subsequently transferred to a new tube. The amount of total protein in the samples was determined by Lowry protein assay (DC™ Protein Assay, BioRad), then concentrations were equalized and the desired amount of total protein was transferred into a new tube. To reduce disulfide bridges, I performed a 1h incubation step in 1% (v/v) β-Mercaptoethanol on ice and separated soluble (supernatant) and insoluble (pellet) protein fractions by centrifugation at 21000 x g at 4°C for 1h.

3.2.12 Western Blot Analysis

The soluble protein fraction was transferred into a fresh tube and was diluted 1:6 in Lämmli (5% β-Mercaptoethanol, 0.01% bromophenol blue, 10% Glycerol, 2% SDS 60mM, Tris-HCl pH 6.8) and boiled at 95°C for 5min. The samples were then either stored at -20°C or directly loaded on a gel. The remaining insoluble protein fraction, as pellet, was furthermore resuspended and washed in 400µl protein extraction buffer (Table 3) including all detergents, followed by sonication for 15min on ice and centrifugation for 30min, 21000 x g at 4°C. This was repeated 3 times. Then, the pellet was solubilized in 7,5µl 100% DMSO and incubated at 25°C for 1h, shaking, without pipetting up and down. Finally, I added 7,5µl of protein extraction buffer and 1:6 Lämmli, boiled the sample at 95°C for 5min and stored it at -20°C or directly loaded the samples on a gel. For gel electrophoresis the NuPAGE Novex 4-12 % Bis-Tris gels and NuPAGE MES SDS Running Buffer (Thermo Fischer Scientific) and for semi-dry transfer the Amersham Protran 0.1 µm Nitrocellulose membranes (GE Healthcare) and the Trans-Blot® Turbo™ Transfer System (BioRad) were used. For antigen retrieval after the transfer, I boiled the membrane in PBS in a microwave for 1,5min and subsequently blocked the membrane in 5% (w/v) milk powder in 1x PBS + 0,1% Tween-20 for at least 1h at RT. For Aβ staining, I used the primary α-6E10 antibody (1:500 or 1:1000, Covance, Sig-39320-200 Lot: D11LF02498). As loading control I used the primary α-Actin antibody (1:500, Sigma-Aldrich, A2228). The incubation of the membrane in the primary antibody was performed for least 2h at RT or overnight at 4°C. After the washing steps for 6 x 5min at RT, the secondary antibody (goat α-mouse IgG-HRP 1:2000 or goat α-rabbit IgG-HRP 1:3000, Thermo Fischer

Scientific) was added for 1h at RT. For visualization of the signal, the membranes were incubated in SuperSignal West pico or femto Chemiluminescent Substrate and imaged using a C-DiGit® Blot Scanner (LI-COR®). For quantification, the Aβ levels were normalized to Actin as loading control using the Image Studio Lite Software (LI-COR®).

3.2.13 Enzyme-linked immunosorbent assay (ELISA)

For ELISA measurements, the soluble protein fraction was transferred into a new tube, diluted 1:1 with AlphaLISA Buffer I (pH = 7,4), containing 4M GdnHCl (Carl Roth), 50mM Tris (pH = 7,4), 1mM EDTA (Carl Roth), 1x protease inhibitor (Santa Cruz Biotechnology Inc.) and incubated for 1h at 25°C, shaking. To prevent interference of too high concentrations of GdnHCl with the ELISA detection kit, I further diluted the samples 1:1 in AlphaLISA Buffer III (pH = 7,4) without GdnHCl (Table 3), to achieve a final GdnHCl concentration of 2M. Then, I incubated the samples for 30min at 25°C, shaking, sonicated them for 5°C on ice and finally stored them at -20°C. For ELISA measurements, the insoluble protein fraction was prepared according to the Western Blot analysis protocol, with following modifications: after the centrifugation and washing steps, the pellet was incubated in 8µl AlphaLISA Buffer I for 1h at RT, shaking. The samples were further diluted 1:1 in AlphaLISA Buffer III to achieve a final GdnHCl concentration of 2M. At the end, the samples were incubated for 30min at 25°C, shaking, sonicated for 5°C on ice and finally stored at -20°C. Before using the AlphaLISA Detection Kit (PerkinElmer), I diluted all freshly thawed samples in 2M GdnHCl, in AlphaLISA Buffer III to a desired concentration of 400mM GdnHCl. Soluble and insoluble $A\beta_{42}$ levels were measured in triplicates with the Aβ 1-x (human) AlphaLISA Detection Kit (PerkinElmer) according to the manufacturer´s instructions in triplicates. For this, I used the Corning 96-well microplates (#3642, Corning) and a FLUOstar Omega microplate reader (BMG LABTECH). For all ELISA measurements I used triplicates of each 5µl sample volume and a final end concentration of 200mM GdnHCl per well. The values were normalized to references values of AlphaLISA Buffer II (pH = 7,4), containing 400mM GdnHCl, 50mM Tris (pH = 7,4), 1mM EDTA, 1x protease inhibitor, which was diluted in the well to a final concentration of 200mM GdnHCl. To calculate total $A\beta_{42}$ levels, soluble and insoluble $A\beta_{42}$ levels were added to each other.

3.2.14 Statistical Analysis

All presented data are shown as mean ± standard error of the mean (s.e.m.). Statistical analysis was performed with Excel and GraphPad Prism 7.0a software. The statistical significance was carried out using one-way ANOVA and Dunnett´s multiple comparisons test. All results were considered as statistically significant when $p < 0.05$ *, $p < 0.01$ **, $p < 0.001$ *** and $p < 0.0001$ ****.

4. Results

4.1 Establishment of redox analysis in *Drosophila* Aβ aggregation models

4.1.1 Validation of the redox sensors *in vitro*

To monitor perturbations in redox homeostasis in the fly system, I made use of four genetically encoded redox sensors (Barata & Dick 2013; Gutscher et al. 2013; Simone C Albrecht et al. 2011) and first validated them *in vitro* in *Drosophila* S2 cells. These sensors allow specific measurement of glutathione redox potential and hydrogen peroxide (H_2O_2) levels, either in the cytosol or mitochondria. This is enabled by the direct fusion of roGFP2 to either glutaredoxin 1 (Grx1) or oxidant receptor peroxidase 1 (Orp1), redox proteins which specifically and reversibly mediate roGFP2 oxidation by oxidized glutathione (GSSG) or H_2O_2, respectively (Simone C. Albrecht et al. 2011). First, I transfected the cells with each sensor (cyto-Grx1-roGFP2, mito-roGFP2-Grx1, cyto-roGFP2-Orp1, mito-roGFP2-Orp1). To determine their responsiveness to reduction or oxidation, the samples were treated with the reductant Dithiothreitol (DTT, Carl Roth) or the oxidant Diamide (DA, Sigma-Aldrich) three days after transfection. The alkylating agent N-ethyl maleimide (NEM, Sigma-Aldrich) was administered immediately afterwards to prevent them from further oxidation. To monitor the changes in the fluorescent intensity ratios, as they are an indicator of changes in the H_2O_2 concentration or glutathione redox potential (E_{GSH}) (Meyer & Dick 2010), the fixed samples were imaged with confocal microscopy (Zeiss LSM 780). The samples were excited sequentially at 405 nm and 488 nm and detected from 500-530nm, processed and analyzed as previously described (Simone C Albrecht et al. 2011). As depicted for the cytosolic H_2O_2 and E_{GSH} sensor (Figure 3A and B), treatment with the oxidant DA resulted in an increase of the fluorescent intensity at 405nm and a decrease at 488nm, and reversed under reducing conditions. The increase in fluorescence intensity ratio 405nm/488nm indicates an increase in oxidation of the sensor. The degree of oxidation (OxD) can be calculated using the Nernst equation as described in (Meyer & Dick 2010), and ultimately gives information about the E_{GSH} or H_2O_2 concentration. The maximal attainable redox changes (dynamic range, DR), which represents the rate of maximal oxidation and maximal reduction of the probe, was calculated by dividing the 405/488nm ratio from the fully oxidized DA by the fully reduced DTT sample and are depicted in Figure 3A` and B`. The sensitivity of the sensors to reducing and oxidizing conditions confirmed the suitability of the system for *Drosophila* cell culture experiments.

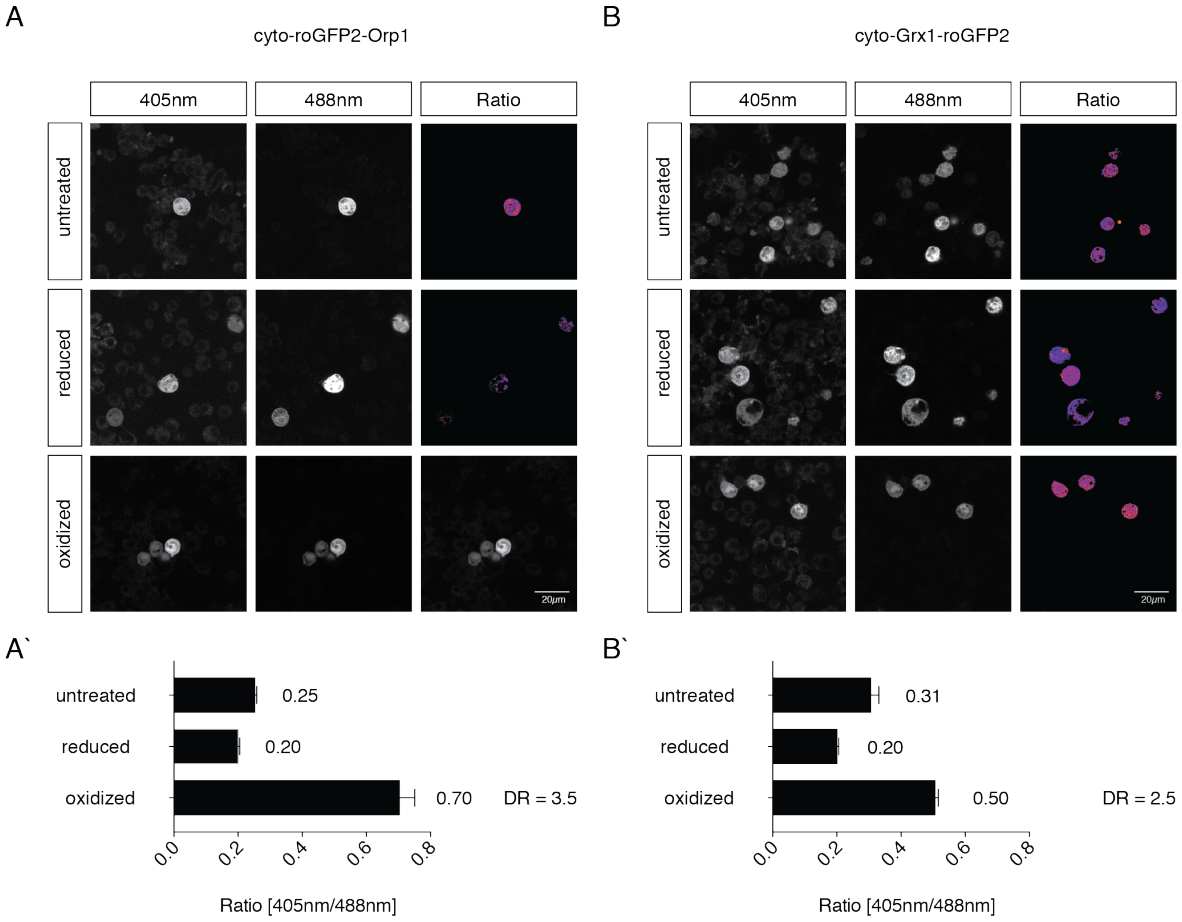

Figure 3: Validation of the cytosolic H_2O_2 (cyto-roGFP2-Orp1) and E_{GSH} (cyto-Grx1-roGFP2) redox sensor *in vitro* in fixed samples. (A-B) S2 cells transfected with the H_2O_2 (A) and E_{GSH} sensor (B). Single stack images are shown taken with a 63x/1.40 Oil DIC M27 objective and a 1,5 x zoom (image size 89.8µm x 89.8µm). Here are shown the 405nm/488nm fluorescent intensity ratios of the probes normalized to DTT = 0.2. DTT treatment decreased and DA treatment increased the 405nm/488nm ratio. The corresponding maximal attainable redox changes (dynamic range, DR) are depicted in A` and B` with the dynamic range of 2.5 – 3.5. Scale bars: 20µm.

4.1.2 Validation of the redox sensors *in vivo* in fly brains

To test the suitability of the redox sensors in our *Drosophila in vivo* system, the Gal4/UAS system (Brand & Dormand 1995) was used to express the redox sensors in all glia cells of the fly brain (Figure 4C-D) under the control of the *repo*-Gal4 promoter. Glia cells play an important role in the maintenance of neuronal glutathione levels (Sagara et al. 1993; Dringen, Pfeiffer, et al. 1999) and in pro-inflammatory processes contributing to oxidative stress conditions in AD (Liddelow et al. 2017; Heneka et al. 2014; Block et al. 2007). Investigating the role of glia cells in the context of AD and disturbed redox homeostasis is therefore of great importance. After dissecting the brains and treating them with the reductant, oxidant and alkylating agent as described above, fly brains were fixed and imaged using a confocal microscope. Afterwards, the 405nm/488nm fluorescent intensity ratios were determined. Figure 4C shows fly brains expressing the cytosolic H_2O_2 sensor and Figure 4D depicts fly brains expressing the cytosolic E_{GSH} sensor in all glia cells. The corresponding DRs are shown in Figure 4C` and D`. The responsiveness of the redox sensors to reduction and oxidation in fixed fly brains confirmed the validity and the sensitivity in our *Drosophila in vivo* system. The complete protocol for DTT, DA, NEM treatment and imaging setups can be found in the Material and Methods section 3.2.7.

To investigate redox changes on a cell-type specific level in neuronal and glial cells of the fly brain), these redox sensors were selectively expressed in either all neurons (using the *nSyb*-Gal4 promoter) or in all glia cells (using the *Repo*-Gal4 promoter). Although initial experiments validated our experimental setup *in vivo*, tissue sections showed a high variability of the redox states in different layers and differentiation between neurons and glia cells was insufficient. To better discriminate between neurons and glia cells, improve the different variability of previous redox analysis and furthermore to overall represent the whole fly brain with several combined z-stacks and not just as a single stack like performed in fixed tissue, the redox analysis was tested with freshly dissected fly brains instead of fixed samples. After dissecting, the unfixed and freshly dissected fly brains were oxidized with Diamide (2-5mM) and a reduced with DTT (2-5mM) and subsequently imaged by confocal microscopy. As illustrated for cyto-Grx1-roGFP2 expressed in all glia cells (Figure 5A) and neurons (Figure 5B), treatment with the reducing agent DTT resulted in the expected increase in fluorescence intensity at 488nm and a decrease at 405nm, vice versa under oxidizing conditions. The maximal attainable redox changes are illustrated in Figure 5A` and B`, ranging from DR = 1.9 in neurons to DR = 2.9 in glia cells. The responsiveness of the redox sensor to reduction and oxidation confirmed the validity and the sensitivity of redox analysis in freshly dissected fly brains. Furthermore, by comparing redox analysis of the freshly dissected fly brains (Figure 5) with fixed tissue (Figure 4), no overall increase in the dynamic range was observed, however discrimination between neurons from glia cells was improved. Moreover, several z-stack pictures represent the whole brain without differences in the redox state in different layers of the fly brain. All redox analyses from now on were performed with freshly dissected fly brains.

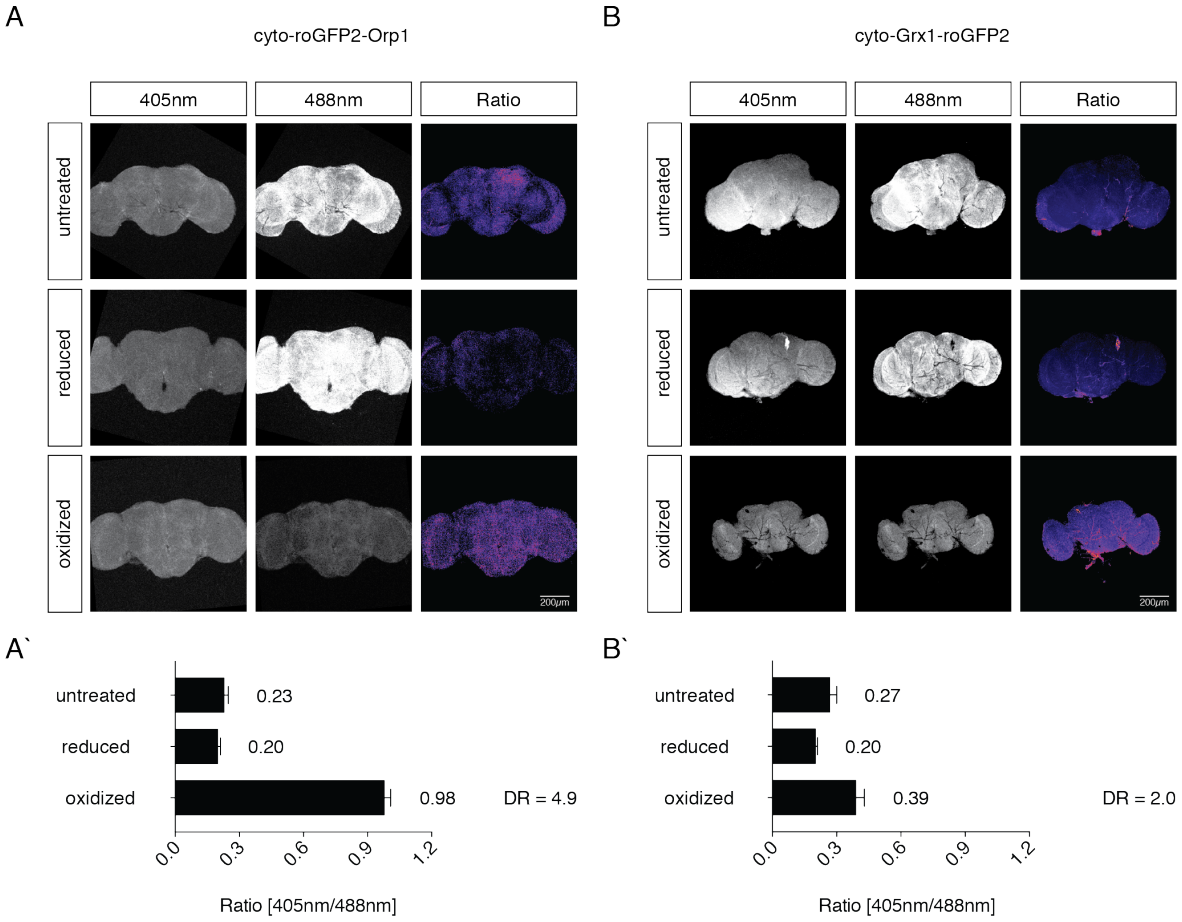

Figure 4: Validation of the cytosolic H_2O_2 (cyto-roGFP2-Orp1) and E_{GSH} (cyto-Grx1-roGFP2) redox sensor *in vivo* of fixed samples. (A-B) Under the control of the *repo*-Gal4 promoter the redox sensors were expressed in all glia cells of the fly brain. Single stack images are shown taken with a 10x/0.30 M27 objective and a 0.8 x zoom (image size 1060.7µm x 1060.7µm). Shown are the 405nm/488nm fluorescent intensity ratios of the probes normalized to DTT = 0.2. The dynamic range between fully reduced samples (realized with DTT treatment) and fully oxidized samples (realized with DA-treatment) varies from 2.0 using the cytosolic E_{GSH} (A`), and 4.9, using the cytosolic $H_2O_2$ sensor (B`). False color scale (fire) was applied to all presented 405/488nm ratio images. Scale bars: 200µm.

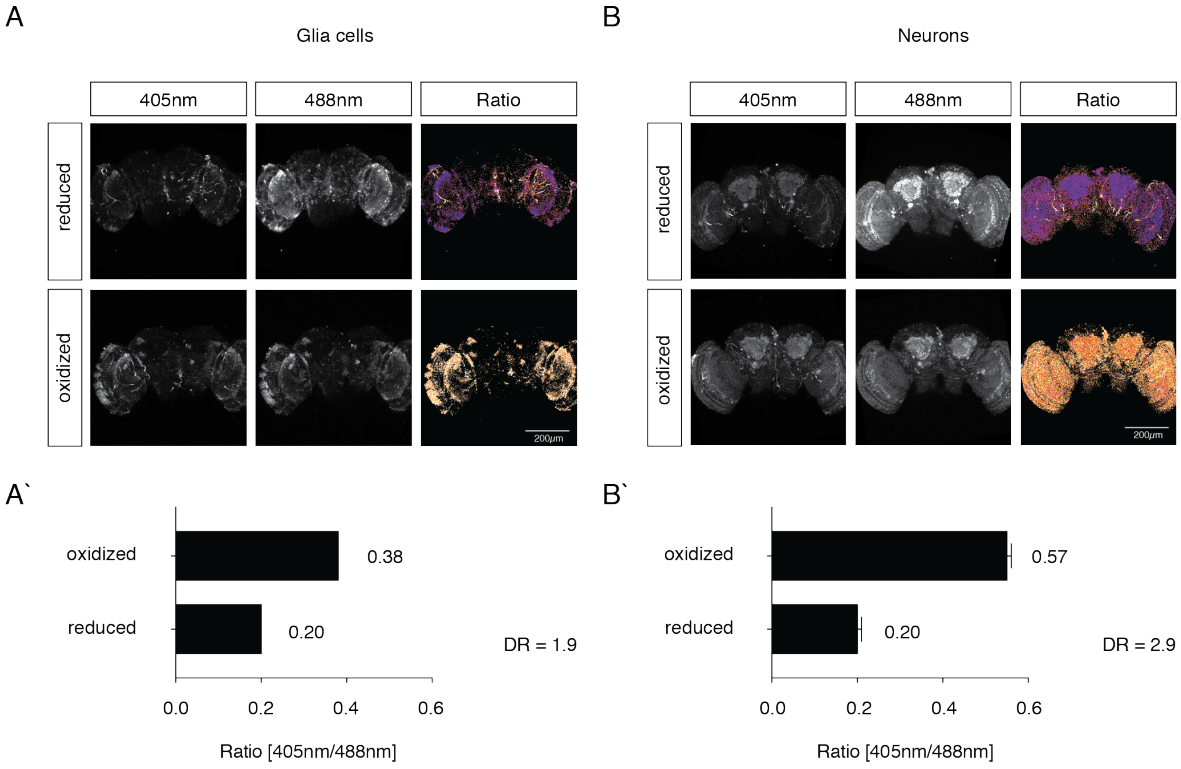

Figure 5: Validation of the redox sensors in neurons and glia cells of freshly dissected adult fly brains. Under the control of the pan-glial *repo*-Gal4 or pan-neuronal *nsyb*-Gal4 promoter, the cyto-Grx1-roGFP2 redox sensor was expressed in all glia cells (A) or all neurons (B). The redox sensor responded to exogenously applied DTT and DA. Depicted are the 405nm/488nm fluorescent intensity ratios of the probes normalized to DTT = 0.2. To illustrate the redox changes in a more discernible way I applied multiplicative Random J Gamma 13 and used false color scale (fire) to all shown 405/488nm ratio images. The maximal attainable redox changes (dynamic range) are depicted in A` and B`. All confocal microscopy images are maximum intensity projections (MIPs). Scale bars: 200µm.

4.1.3 Combining redox sensors with *Drosophila* Aβ aggregation models

To investigate cell-specific redox changes in the onset and progression of AD, I introduced the genetically encoded fluorescence proteins (Barata & Dick 2013; Gutscher et al. 2013; Simone C. Albrecht et al. 2011) into our *in vivo Drosophila* Aβ aggregation models, to induce neurodegeneration. I used a tissue-specific dual expression system to express different transgenes in neurons or glia cells, independently from each other. Aβ variants were expressed pan-neuronally (with the LexA/LexAop system) and redox sensors were co-express in neurons or glia cells (with the Gal4/UAS system) without crosstalk (Figure 6).

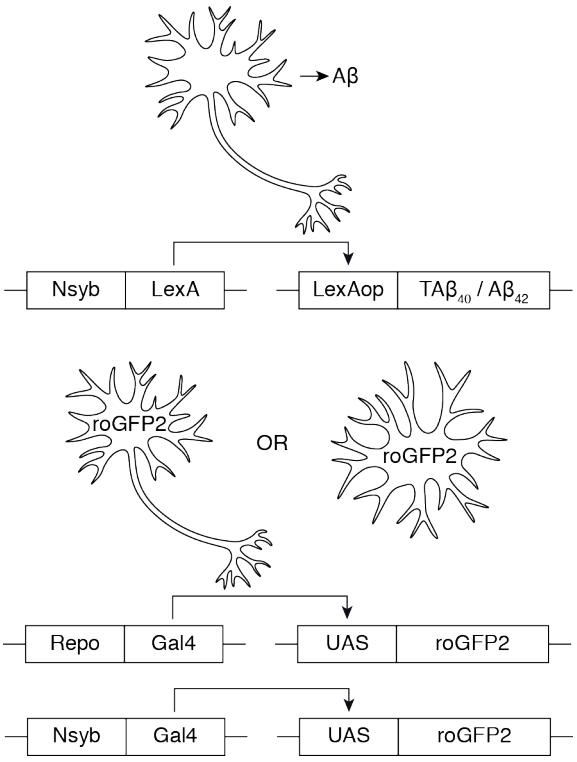

Figure 6: Schematic overview to perform redox analysis with redox protein coupled roGFP2s in adult fly brains combined with our *in vivo Drosophila* Aβ aggregation models. Using the tissue-specific dual expression system (Gal4/UAS and LexA/LexAop), we independently expressed toxic $A\beta_{42}$ and less-toxic $TA\beta_{40}$ peptide under the control of the *nSyb*-LexA promoter in all neurons and co-expressed the redox sensor under the control of *nSyb*-Gal4 or *repo*-Gal4 promoter pan-neuronal or pan-glial, respectively.

The fast aggregating human $A\beta_{42}$ peptide causes toxicity in the fly nervous system (Iijima et al. 2004; Speretta et al. 2012) and was used as a neurotoxic agent for this study (J Hardy & Allsop 1991; Karran et al. 2011). To exclude that protein accumulation per se is causing any redox stress, the Tandem$A\beta_{40}$ ($TA\beta_{40}$) variant was used as a direct negative control (Speretta et al. 2012). $TA\beta_{40}$ is a fast aggregating dimeric construct, consisting of two $A\beta_{40}$ monomers linked via a twelve amino acid linker (Speretta et al. 2012). While the monomeric $A\beta_{40}$ variant is rapidly cleared due to its high turnover rate (Iijima et al. 2004), the $TA\beta_{40}$ construct leads to the accelerated aggregation and consequent accumulation of $A\beta_{40}$, but is not expected to cause strong toxicity (Speretta et al. 2012). Both $A\beta_{42}$ and $TA\beta_{40}$ peptides are fused to a secretory signal peptide, leading to their secretion from neurons into the extracellular space, thereby mimicking the physiological situation in the human brain (Crowther et al. 2005). To confirm the aggregation properties of these two Aβ constructs, I quantified the levels of soluble Aβ and insoluble Aβ aggregates in fly head extracts (Figure 7A and Figure 7B). Western blot analysis showed that soluble levels of Aβ remained rather low in flies expressing the $A\beta_{42}$ variant, while seven times higher levels were observed in $TA\beta_{40}$ expressing flies. However, increasing levels of insoluble $A\beta_{42}$ were observed over time, with similar amounts of insoluble aggregates in $TA\beta_{40}$ flies and $A\beta_{42}$ expressing flies at two weeks of age.

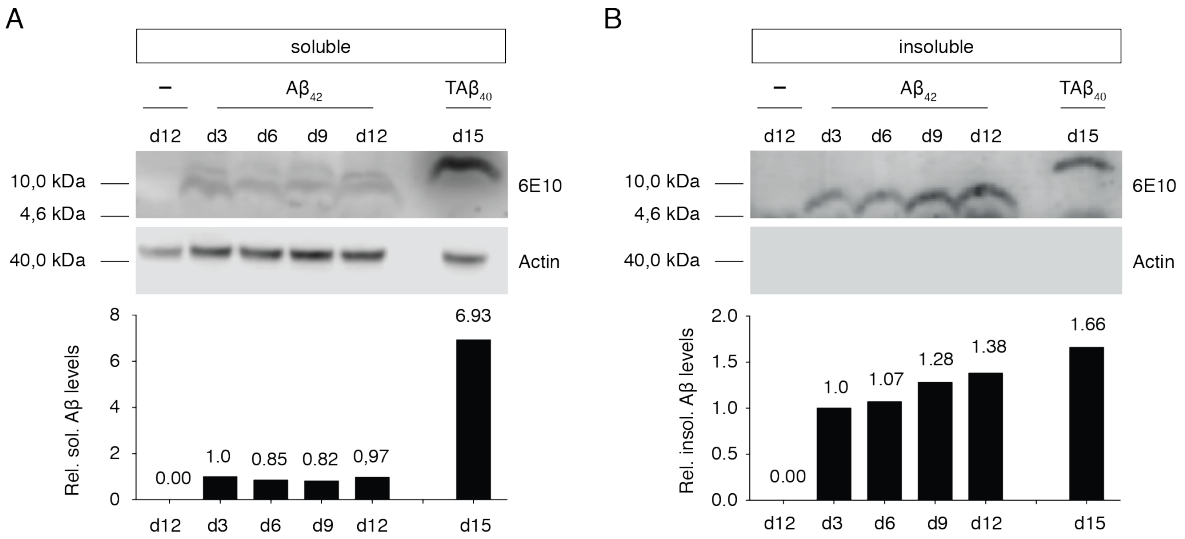

Figure 7: Confirmation of the aggregation properties of $A\beta_{42}$ and $TA\beta_{40}$ in our *Drosophila* model. Soluble and insoluble Aβ levels are depicted in (A) and (B), respectively. Western Blot analysis revealed an accumulation of Sarkosyl- and SDS insoluble aggregated $A\beta_{42}$ over time in $A\beta_{42}$ flies (in days, B), while soluble Aβ levels nearly stay the same (A). The monoclonal 6E10 antibody was used for total Aβ detection and actin as loading control.

To characterize the neurotoxic properties of accumulations consisting of these two Aβ variants, well-established longevity assays were performed as a readout of the neurological integrity and an indirect readout for neurotoxicity of these flies (Burnouf et al. 2015; Luheshi et al. 2007; Iijima et al. 2004). Consistent with previous studies (Speretta et al. 2012), a dramatic decrease in the survival rate of flies pan-neuronal expressing $A\beta_{42}$ was observed (median survival = 14.9 +/- 0.4 days, Figure 8, black). In contrast, the pan-neuronal expression of $TA\beta_{40}$ only led to a slightly reduced survival rate (median survival = 36.2 +/- 0.9 days, Figure 8, pink) compared to control flies (median survival of 44.5 +/- 0.5 days). To verify that the genetic background of the redox sensors does not severely alter the Aβ-mediated toxicity, the different Aβ variants were expressed in neurons and the redox sensors was co-expressed in either neurons or glia cells. Overall, co-expression of the cyto-Grx1-roGFP2 redox sensor in neurons Figure 8A) or glia cells (Figure 8B) does not strongly alter the survival of Aβ-expressing flies.

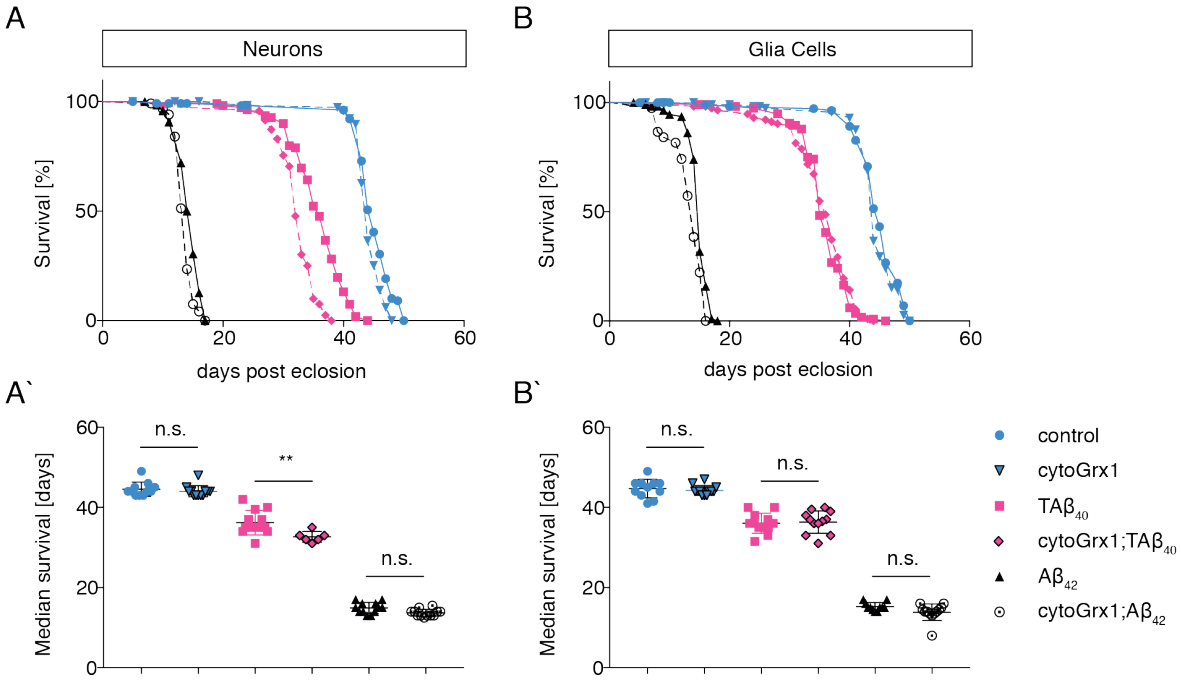

Figure 8: $TA\beta_{40}$ and $A\beta_{42}$ variants differ in their neurotoxicity levels. Longevity assays show a strong neurotoxicity due to a decrease in life span of $A\beta_{42}$ flies (black) and lower neurotoxicity in $TA\beta_{40}$ flies (pink) compared to control flies (blue). The genetic background of the redox sensors in neurons (A) or glia cells (B) does not strongly alter the life span of Aβ flies. Survival curves are depicted (n=60-120 flies per genotype). All error bars indicate s.e.m. Statistical analysis was performed with one-way ANOVA, *p ≤ 0,05, **p ≤ 0,01, ***p ≤ 0,001.

To get further insights into the observed functional differences between these Aβ accumulations, immunohistochemical analysis of dissected fly brains was performed at day 12, shortly before $A\beta_{42}$ expressing flies start to die (Figure 8A). Confirming our biochemical analysis, staining for Aβ using the 6E10 antibody revealed higher overall Aβ accumulation in $TA\beta_{40}$ over $A\beta_{42}$. To specifically look at the deposition of β-sheet rich amyloid plaques, the amyloid specific dye Thioflavin S (ThS) was used (Berg et al. 2010). Importantly, almost no ThS positive staining was detectable in $TA\beta_{40}$ fly brains, whereas $A\beta_{42}$ fly brains showed overall very strong ThS positive staining (Figure 9). These data indicate that despite the comparable deposition of insoluble aggregates from both Aβ variants (Figure 7B), the structural features of these deposits have a differential impact on cellular viability (Figure 8A). Taken together, these data suggest the suitability of these *Drosophila* models of Aβ aggregation to investigate the impact of neurotoxic protein aggregates on the cellular redox homeostasis in a quantitative manner.

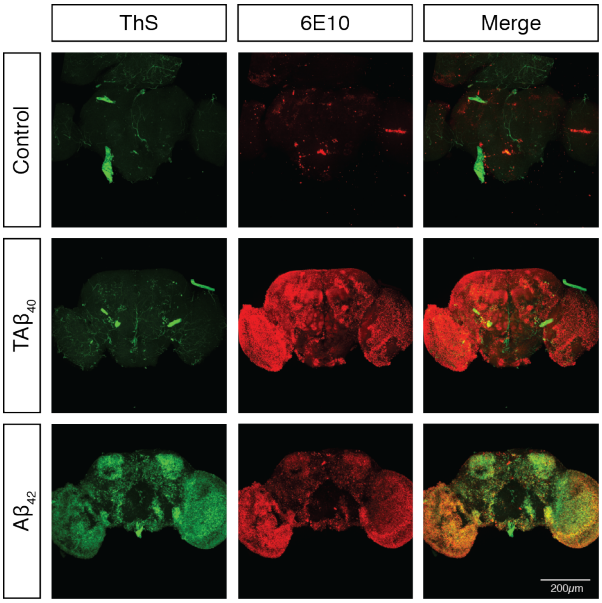

Figure 9: Amyloidogenic structures found in fly brains of $A\beta_{42}$ flies. Immunohistochemical analysis of 12-day old fly brains showed the strong deposition of Thioflavin S (green) positive amyloidogenic structures in $A\beta_{42}$ flies, but not in $TA\beta_{40}$ flies. Total Aβ was stained with 6E10 (red). All confocal microscopy images are maximum intensity projections. Scale bars: 200µm.

4.2 Analyzing the role of redox homeostasis and JNK stress response in *Drosophila* models of Aβ aggregation

4.2.1 Analyzing the changes in the redox homeostasis in *Drosophila* Aβ aggregation models.

Before validating the redox analysis with freshly dissected fly brains, a proof of principle experiment was performed to test whether the aggregation of a very toxic Tandem $A\beta_{42}$ ($TA\beta_{42}$) variant, a dimer consisting of two $A\beta_{42}$ peptides (Speretta et al. 2012), could lead to changes in the neuronal redox homeostasis in these flies. Therefore, the four different redox sensors (cyto-Grx1-roGFP2, mitoCOX8-roGFP2-Grx1, cyto-roGFP2-Orp1, mitoCOX8-roGFP2-Orp1) were expressed and $TA\beta_{42}$ was co-expressed under the control of the *elav*-Gal4 promoter in all neurons, using the UAS-Gal4 single expression system. All fly brains were dissected in NEM, a cell permeable alkylating agent, which is necessary to block the redox state of the sensors to protect from further oxidation. The fixed brains were imaged, processed and analyzed as described by (Barata & Dick 2013; Simone C. Albrecht et al. 2011). Redox analysis of 5-6 day old flies revealed that compared to control flies, flies expressing $TA\beta_{42}$ showed a significantly increased glutathione redox imbalance in the cytosol (Figure 10A, purple) and mitochondria (Figure 10A, red) of neurons, indicated by the increase in the fluorescent intensity ratio (405nm/488nm). No significant differences in cytosolic or mitochondrial H_2O_2 levels were detected between control flies and $TA\beta_{42}$ flies

(Figure 10A, blue and green). Additionally, fly brains were dissected 5-6 days after hatching and subsequently stained for total Aβ using the monoclonal antibody 6E10 (Figure 10B). This showed that compared to control flies in $TA\beta_{42}$ expressing flies a strong 6E10 staining was observed. This proof of principle experiment shows that redox analysis in the fly brain can detect changes in the redox homeostasis upon Aβ accumulation and furthermore identifies an increase in the fluorescence intensity of the cytosolic and mitochondrial glutathione redox sensor, but not in the H_2O_2 sensors, in flies expressing $TA\beta_{42}$ compared to control flies (Figure 10B).

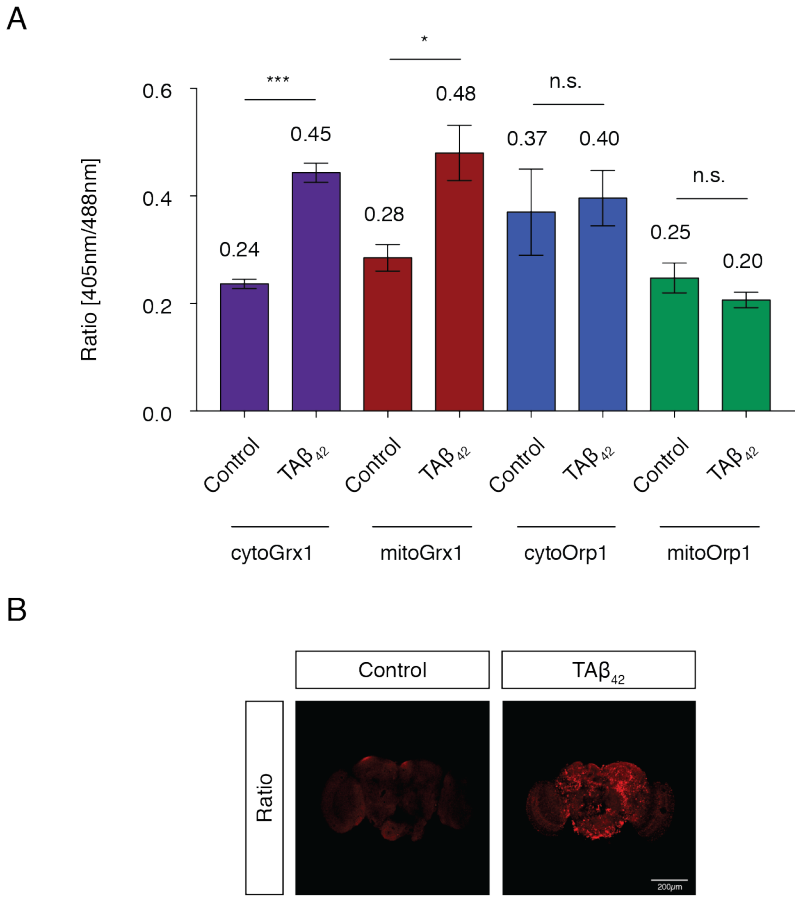

Figure 10: Changes in redox homeostasis can be studied in *Drosophila* Aβ aggregation models. (A) The *elav*-Gal4 driver was used to express different redox sensors (cyto-Grx1-roGFP2, mitoCOX8-roGFP2-Grx1, cyto-roGFP2-Orp1, mitoCOX8-roGFP2-Orp1) and co-express a very toxic and fast aggregating Tandem $A\beta_{42}$ ($TA\beta_{42}$) in neurons. The redox changes were analyzed in 5-6 day old flies (n=3-5 brains). All fluorescence intensity ratio (405nm/488nm) of the probe were plotted and normalized to respective DTT = 0.2 samples. All error bars indicate s.e.m. Statistical analysis was performed with one-way ANOVA, *p ≤ 0,05, ***p ≤ 0.001. (B) In addition fly brains were subsequently stained for Aβ using the monoclonal antibody 6E10 (red). Scale bar 200µm.

4.2.2 $A\beta_{42}$ deposition induces glutathione redox potential changes in neurons, but not in glia cells

In order to monitor H_2O_2 and glutathione redox changes during the onset and progression of Aβ accumulation in these Aβ fly models over time, detailed time course experiments with live imaging in freshly dissected fly brains were performed and the cytosolic E_{GSH} and H_2O_2 redox sensor were chosen. Due to the very strong toxicity and rapid death of flies expressing $TA\beta_{42}$ and to increase the time window for detailed time course analysis, the monomeric $A\beta_{42}$ variant was used. This $A\beta_{42}$ variant is also a fast aggregating and toxic variant, but less toxic than $TA\beta_{42}$. As in the previous experiments, the low toxic $TA\beta_{40}$ variant was used as negative control to exclude that protein accumulation per se is causing any redox stress. The intracellular H_2O_2 levels and glutathione redox potential (E_{GSH}) was monitored over time using the cyto-roGFP2-Orp1 and the cyto-Grx1-roGFP2 redox sensors, respectively (Simone C. Albrecht et al. 2011). First detailed time course experiments were performed, where dissected fly brains were analyzed (see Methods for details) at four different time points of neurodegeneration (day 3, 6, 9 and 12). Here, neither an increase in cytosolic (Figure 11A and A`) nor mitochondrial H_2O_2 levels (Figure 12) was observed in flies expressing either $TA\beta_{40}$ or $A\beta_{42}$. However, and most importantly, significant changes in the intracellular glutathione redox balance in neurons of $A\beta_{42}$ flies were detected, indicated by an increase in 405nm/488nm fluorescence intensity ratio (Figure 11B) and E_{GSH} (Table 15) using the cytoGrx1-roGFP2 redox sensor. The degree of probe oxidation (OxD) (Figure 21) and the corresponding intracellular E_{GSH} (Table 15) were calculated from the Nernst equation (Meyer & Dick 2010). This increase in E_{GSH} specifically observed in neurons was already detected at an early time point (day 6), and further increased over time in parallel to the deposition of insoluble $A\beta_{42}$ (Figure 7B). These changes in the E_{GSH} of $A\beta_{42}$ flies were not present in $TA\beta_{40}$ expressing flies (Figure 11B). With similar amounts of aggregated material in both Aβ fly lines, this finding suggest that the accumulation of protein deposits per se is not sufficient to evoke an increase in E_{GSH}. However, accumulation of amyloids of the $A\beta_{42}$ peptide is accompanied with significant changes in neuronal redox balance, as possible determinant of the consequently observed neurotoxicity and reduced fly survival (Figure 8). To further explore whether this effect is cell-type specific, this set of experiments were repeated in fly lines where Aβ expression is maintained by a neuronal driver (*nSyb*-Gal4), but where the redox sensors are specifically expressed in glia cells (*repo*-Gal4) (Figure 11). Because glia cells have shown to play an important role in the maintenance of brain homeostasis and in inflammatory processes, both in fly and human (Liddelow et al. 2017; Liu et al. 2015; Block et al. 2007), I was interested whether glia cells similarly respond to different Aβ accumulations. However, no changes in either H_2O_2 levels or E_{GSH} in glia cells were observed (Figure 11A` and B`), indicating that neurons are particularly sensitive to redox stress evoked by $A\beta_{42}$ deposition compared to glia cells. Taken together, the data show that changes in redox homeostasis are associated with $A\beta_{42}$-mediated neurotoxicity and most interestingly are amyloid-deposit-, E_{GSH}- and neuron-specific.

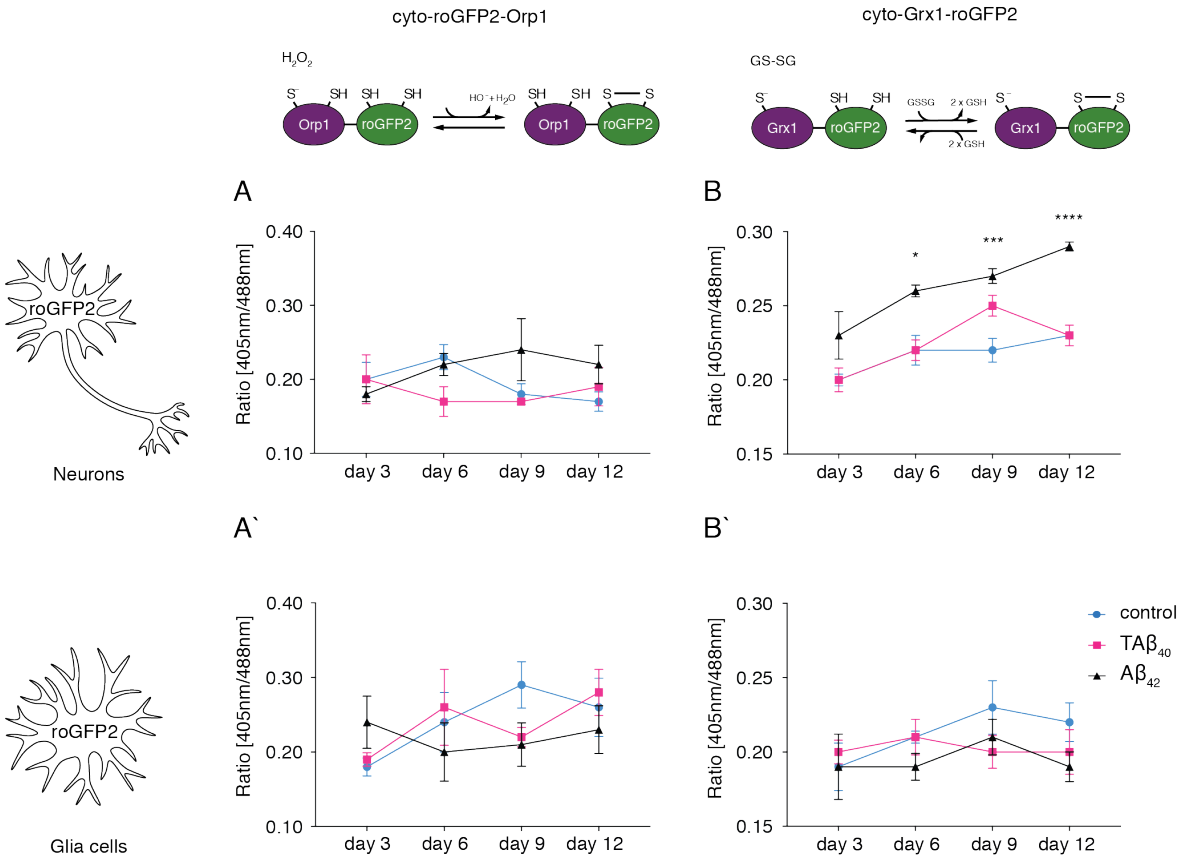

Figure 11: Quantitative redox analysis reveals glutathione redox changes only in neurons of $A\beta_{42}$ flies. Redox analysis with the H_2O_2 redox sensor cyto-roGFP2-Orp1 (A, A`) and the $E_{GSH}$ redox sensor cyto-Grx1-roGFP2 (B, B`) neurons (A, B) and glia cells (A`, B`) was performed in a time course (day 3, 6, 9, 12; n = 3-5 fly brains per time point and genotype). Flies expressing the less-toxic $TA\beta_{40}$ showed no redox changes whereas an intracellular glutathione redox imbalance could be detected in neurotoxic $A\beta_{42}$ expressing flies. An increase in cyto-Grx1-roGFP2 fluorescence intensity ratio in neurons but not in glia cells over time was observed (B, B`, respectively). No changes in $H_2O_2$ levels neither in neurons nor in glia cells could be detected (B, B`, respectively) upon Aβ accumulation. Depicted are the 405nm/488nm fluorescent intensity ratio of the probe normalized to DTT = 0.2. All error bars indicate s.e.m. Statistical analysis was performed with one-way ANOVA, *p ≤ 0,05, ***p ≤ 0.001, ****p ≤ 0.0001.

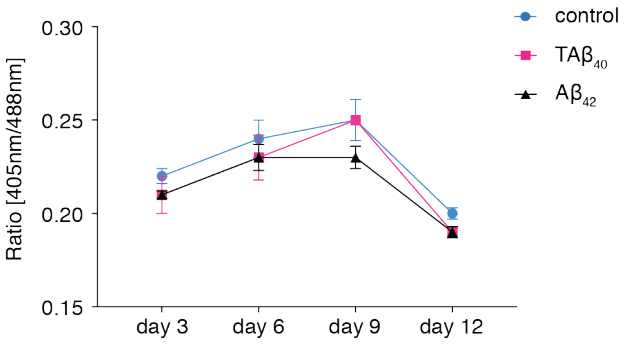

Figure 12: No changes in mitochondrial H_2O_2 levels upon Aβ deposition. Redox analysis with the mitochondrial H_2O_2 redox sensor mito-roGFP2-Orp1 in neurons, under the control of the *nSyb*-Gal4 promoter was performed in a time course (day 3, 6, 9, 12; n = 3-6 fly brains per time point and genotype). Graph representing the 405nm/488nm fluorescent intensity ratio of the probe normalized to DTT = 0.2. All error bars indicate s.e.m. Statistical analysis was performed with one-way ANOVA.

Table 15: Overview of the effects of Aβ accumulation on E_{GSH} (in mV) over time

Genotype	day 3	day 6	day 9	day 12
Control	– 340	– 313	– 315	– 310
$TA\beta_{40}$	– 344	– 314	– 304	– 311
$A\beta_{42}$	– 311	– 300	– 297	– 293

Using the dual expression system we co-expressed the cyto-Grx1-roGFP2 (under the control of the *nSyb*-Gal4 promoter) sensor and two different Aβ variants pan-neuronal (under the control of the *nSyb*-LexA promoter). Compared to control flies, flies expressing the non-toxic $TA\beta_{40}$ showed no changes in E_{GSH}, whereas flies expressing the neurotoxic $A\beta_{42}$ showed an increase in intracellular E_{GSH}, in neurons. The neuronal intracellular glutathione redox potentials (E_{GSH}) were calculated from the Nernst equation, as described previously (Meyer & Dick 2010). $E^{o\prime}_{roGFP2}$ has been determined as –280 mV (Dooley et al. 2004).

4.2.3 Accumulation of $A\beta_{42}$ leads to the activation of JNK stress response

Answering the question how changes in redox balance can be translated into a neuronal death-signaling cascade is of great importance. The JNK pathway is an important stress responsive pathway and has been linked to cell death in response to oxidative stress (Sclip et al. 2014; Tare et al. 2011; Marques et al. 2003; Jang & Surh 2002; Shoji et al. 2000) but also to stress tolerance (Liu et al. 2015; Wu et al. 2009; Wang et al. 2003). In the next step, the involvement of the JNK pathway and its connection to the observed glutathione redox imbalance in the Aβ aggregation models was analyzed. For this, the activation of the JNK pathway was monitored using a transgenic construct with stress inducible promoter elements fused to the DsRed fluorescent reporter (Chatterjee & Bohmann 2012). Here, JNK-mediated transcriptional stress response can be monitored in our Aβ *Drosophila* models by an increase in DsRed fluorescent intensity (Figure 13A). I observed that the JNK pathway is activated from day 6 onwards and was increased over

time in $A\beta_{42}$, but not in $TA\beta_{40}$ fly brains (Figure 13B). The quantification is depicted in Figure 13C. This finding mirrors our previously observed E_{GSH} changes (Figure 11B), illustrating that only the accumulation of amyloid deposits promotes stress responses. The progressive deposition of $A\beta_{42}$ induces an increase in E_{GSH} (Figure 11B) as well as the activation of the JNK pathway (Figure 13B, C), ultimately resulting in severe neurotoxicity (Figure 8). It is still under debate whether JNK activation contributes to neurotoxicity or acts as a neuroprotective factor in AD. The progressive increase in JNK activity, concomitant with $A\beta_{42}$ aggregation and glutathione redox imbalance over time supports the role for JNK in $A\beta_{42}$-mediated toxicity as suggested by previous studies (Tare et al. 2011). Importantly, our data additionally provide *in vivo* evidence for the selective cellular toxicity for different protein aggregate conformations, which is mediated by the different activation of cellular stress response pathways by β-sheet-rich $A\beta_{42}$ aggregates and less ordered $A\beta_{40}$ deposits.

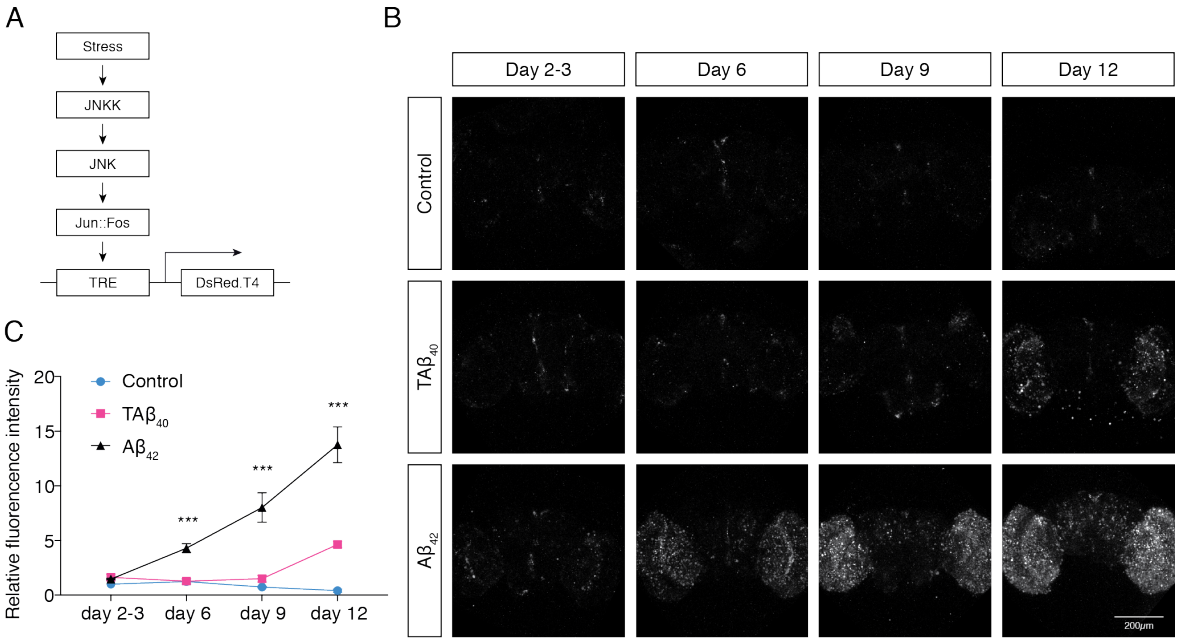

Figure 13: Deposition of $A\beta_{42}$ is associated with the activation of the JNK stress response. (A) Schematic overview of the stress-inducible promoter elements fused to the fluorescent reporter (TRE-DsRed-2R) (Chatterjee and Bohmann, 2012). (B) Time course analysis at day 3, 6, 9, 12 (n = 4 fly brains per time point and genotype) showed a JNK activation in $A\beta_{42}$ fly brains (black), which was further increasing over time, but no JNK activation in $TA\beta_{40}$ flies (pink). Freshly dissected fly brains were directly imaged via confocal microscopy. Confocal microscopy images are shown as maximum intensity projections. Scale bar: 200µm. (C) Quantification shows the relative fluorescent intensity of the whole confocal microscopy image. All error bars indicate s.e.m. Statistical analysis was performed with one-way ANOVA, ***$p \leq 0.001$.

4.3 Increased neuronal glutathione redox potential is linked to $A\beta_{42}$-mediated toxicity

4.3.1 Manipulation of the glutathione synthesis does not change JNK activation in $A\beta_{42}$ flies

To distinguish whether glutathione homeostasis is directly liked to neurotoxicity, or indirectly mediates this effect by activating the JNK stress-signaling pathway, I analyzed whether changes in glutathione synthesis influence the neurotoxic effect of $A\beta_{42}$. First, the impact of modulating glutathione metabolism on JNK activation was investigated, by specifically manipulating the glutathione synthesis genetically as well as pharmacologically. To modulate neuronal glutathione levels, the glutamate cysteine ligase catalytic subunit (Gclc), first rate-limiting enzyme of the glutathione synthesis (Orr et al. 2005)was targeted. Importantly, neither the pan-neuronal overexpression of Gclc (Gclc-OE) nor the reduction of Gclc via RNAi (GclcRNAi), under the control of the *nSyb*-Gal4 promoter, led to significant changes in JNK activation in $A\beta_{42}$ expressing flies 6 days post eclosion (Figure 14). The maximum intensity projections of confocal microscopy images are depicted in Figure 14A and the quantification of the relative DsRed fluorescent intensity is shown in Figure 14B. To confirm this disconnection between glutathione redox imbalance and JNK activation in $A\beta_{42}$ flies, glutathione levels were modulated pharmacologically by administering Buthionine Sulfoximine (BSO), an inhibitor of the γ-glutamylcysteine synthetase, the second rate-limiting enzyme of the glutathione synthesis. Interestingly, also the pharmacological manipulation of glutathione synthesis did not result in any changes of JNK activation in $A\beta_{42}$ flies (Figure 18A), confirming the observations from the genetic manipulation experiment. This demonstrates that JNK stress signaling is not directly associated with changes in glutathione synthesis.

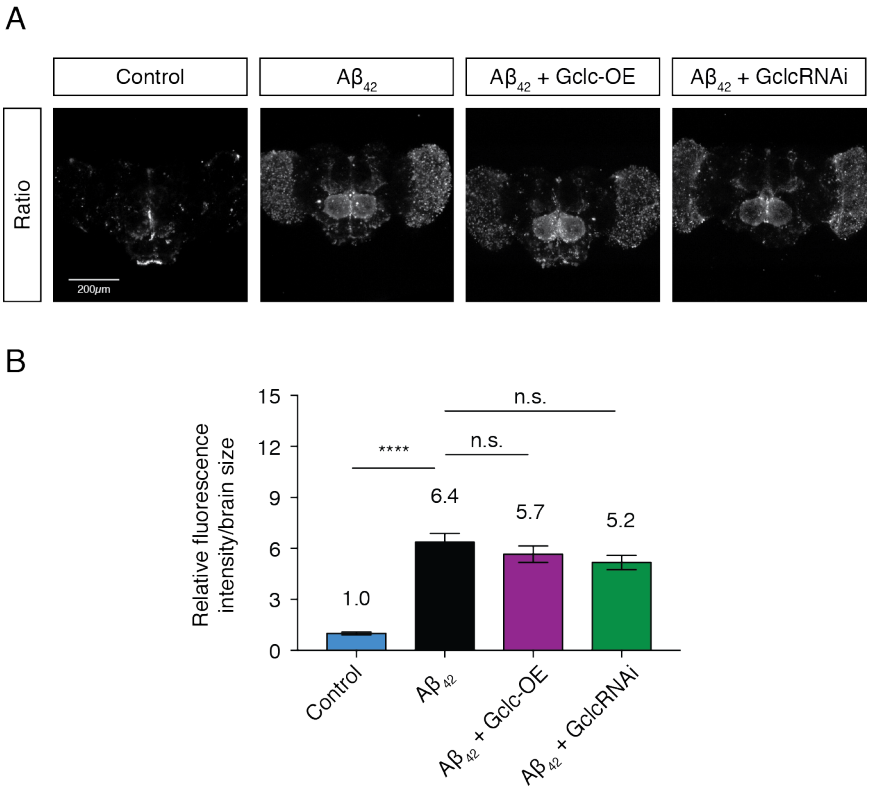

Figure 14: Genetic manipulation of the glutathione synthesis does not change JNK activation in 6-day old $A\beta_{42}$ flies. Genetic manipulation of glutathione synthesis in $A\beta_{42}$ flies by pan-neuronal up- (purple) or downregulation (green) of the glutamate-cysteine ligase catalytic subunit (Gclc), driven by the pan-neuronal *nSyb*-Gal4 promoter and its effect on JNK activation (A, B). Confocal microscopy images are depicted in (A) Quantification of the relative DsRed fluorescent intensity divided by brain size (n=15-18 fly brains per genotype) depicted in (B). All depicted confocal microscopy images are maximum intensity projections. Scale bar: 200µm. All error bars indicate s.e.m. Statistical analysis was performed with one-way ANOVA, ****p ≤ 0,0001.

4.3.2 Manipulation of the glutathione synthesis further increases glutathione redox imbalance in $A\beta_{42}$ flies

To next investigate how manipulation of glutathione metabolism influences the glutathione redox balance in $A\beta_{42}$ flies, redox analysis was performed in our $A\beta_{42}$ cyto-Grx1-roGFP2 fly line after overexpressing or downregulating Gclc (Figure 15). Here, for pan-neuronal overexpression of $A\beta_{42}$ and the redox sensor the UAS-Gal4 single expression system under the control of the *elav*-Gal4 driver was used. Redox analysis of 12-day old $A\beta_{42}$ flies +/- Gclc-OE revealed that Gclc-OE further increased the glutathione redox imbalance, indicated by the increased 405nm/488nm ratio of the cyto-Grx1-roGFP2 sensor (Figure 15B, purple) and a 22,7% increase in probe oxidation (Table 16), compared to $A\beta_{42}$ flies. The downregulation of Gclc function, either genetically by GclcRNAi or pharmacologically via BSO treatment did not result in significant changes in glutathione redox balance compared to $A\beta_{42}$ flies (Figure 15B, green and Figure

18B). These data indicate the increased glutathione synthesis does not buffer any effects mediated by $A\beta_{42}$ deposition, but in contrary exacerbates the effect and leads to increased OxD and E_{GSH} (Table 16).

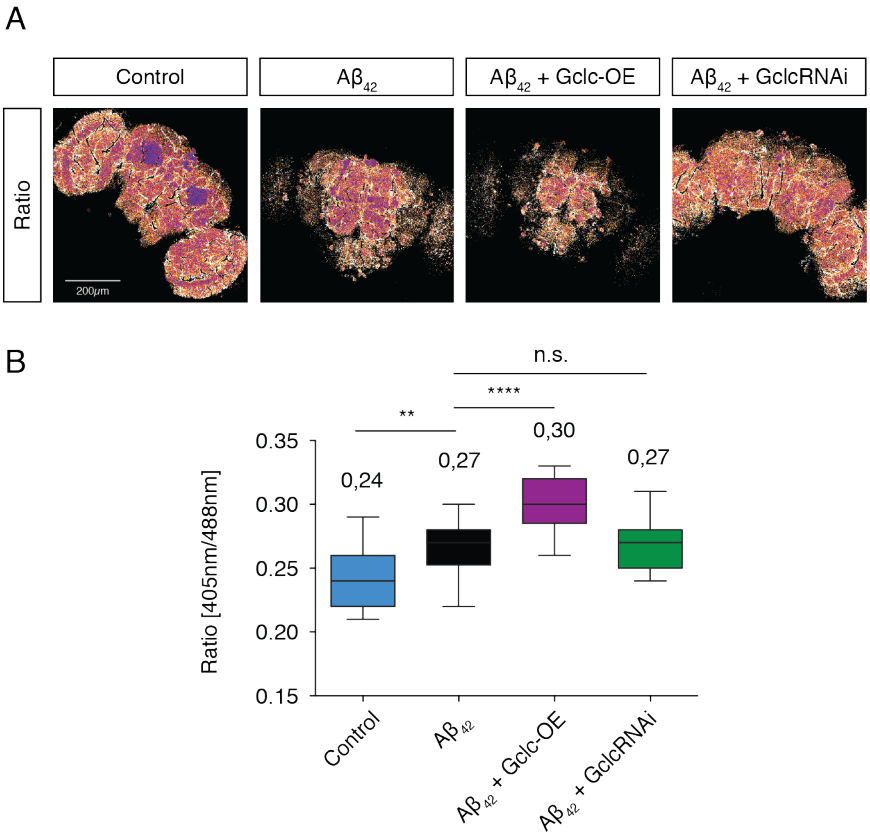

Figure 15: Increase in E_{GSH} upon Gclc-OE in $A\beta_{42}$ flies. Genetic manipulation of glutathione synthesis in $A\beta_{42}$ flies by pan-neuronal up- (purple) or downregulation (green) of the glutamate-cysteine ligase catalytic subunit (Gclc), driven by the pan-neuronal *elav*-Gal4 and its effect on glutathione redox potential. (A) Redox analysis of 12-day old $A\beta_{42}$ flies with Gclc-OE showed an increase in the cyto-roGFP-Grx1 fluorescent ratio (n=15-17 fly brains per genotype) compared to $A\beta_{42}$ flies without glutathione synthesis manipulation. Multiplicative J Gamma 7 and false color scale (fire) was applied to present 405/488nm ratio images. (B) The quantification is depicted in box plot, lower/upper quartile: whiskers, 5th/95th percentile. All depicted confocal microscopy images are maximum intensity projections. Scale bar: 200µm. All error bars indicate s.e.m. Statistical analysis was performed with one-way ANOVA, **p ≤ 0,01.

Table 16: Overview of the effects of genetic manipulation of GSH synthesis on E_{GSH} (in mV) and life span

Genotype	OxD_{roGFP2} [% roGFP2]	E_{GSH} [mV]	Median life span [days]
Control	33.1 ± 3.8	– 289	54.2 ± 1.2
$A\beta_{42}$	52.7 ± 5.2	– 279	16.5 ± 0.4
$A\beta_{42}$ + Gclc-OE	75,4 ± 5.4	– 266	11.5 ± 0.5
$A\beta_{42}$ + GclcRNAi	53.1 ± 2.9	– 278	19.8 ± 0.5

The degree of roGFP2 oxidation (OxD_{roGFP2}) and the corresponding intracellular glutathione redox potential (E_{GSH}) were calculated from the Nernst equation, as described previously (Meyer & Dick 2010). $E^{o\prime}_{roGFP2}$ has been determined as –280 mV (Dooley et al. 2004). Median life span of control and $A\beta_{42}$ flies with and without glutathione synthesis manipulation is represented in days. We conclude that a further increase in E_{GSH} is associated with decreased life span//increased $A\beta_{42}$ neurotoxicity.

4.3.3 Increased neuronal glutathione redox potential is linked to $A\beta_{42}$ neurotoxicity

Previous studies have shown beneficial effects of glutathione synthesis on life span of aging *Drosophila* (Orr et al. 2005). To investigate whether the modulation of the glutathione redox balance in $A\beta_{42}$ expressing flies also influences $A\beta_{42}$ neurotoxicity, longevity assays (Figure 16A`) were performed. Intriguingly, increasing glutathione synthesis by Gclc-OE in $A\beta_{42}$ flies resulted in a dramatically reduced life span of flies (Figure 16A, A` purple). In contrast, the life span of control flies remained unchanged by the manipulation of glutathione synthesis (Figure 17). Importantly, decreasing glutathione synthesis via GclcRNAi and BSO treatment was beneficial for fly survival and significantly prolonged life span of $A\beta_{42}$ flies (Figure 16A, A` green, Figure 18C, C` orange). These findings suggest that the neuronal E_{GSH} directly impacts the neurotoxic stress signaling mediated by $A\beta_{42}$ amyloid deposits.

To further determine whether this redox imbalance is not only coupled to cell survival, but also to the levels of accumulating $A\beta_{42}$, the levels of $A\beta_{42}$ were analyzed in these fly lines with modified glutathione synthesis. Using sensitive ELISA methods to measure total, soluble and insoluble Aβ levels of these flies (Figure 16B, B`, B``), I however did not observe significant changes in the levels that would correlate with the dramatic decrease in the life span of these flies (Figure 16A, A`). Similarly, levels of $A\beta_{42}$ were unchanged in flies treated with BSO (Figure 18D-D`) concluding that the observed changes in neurotoxicity are not solely based on changes in the level of $A\beta_{42}$ in these fly lines, but rather directly relate to the E_{GSH}. Taken together, these data suggest that an increase in the neuronal E_{GSH} is directly linked to the cellular impact of $A\beta_{42}$ deposition on neurons and is therefore a crucial regulator of $A\beta_{42}$-mediated neurotoxicity.

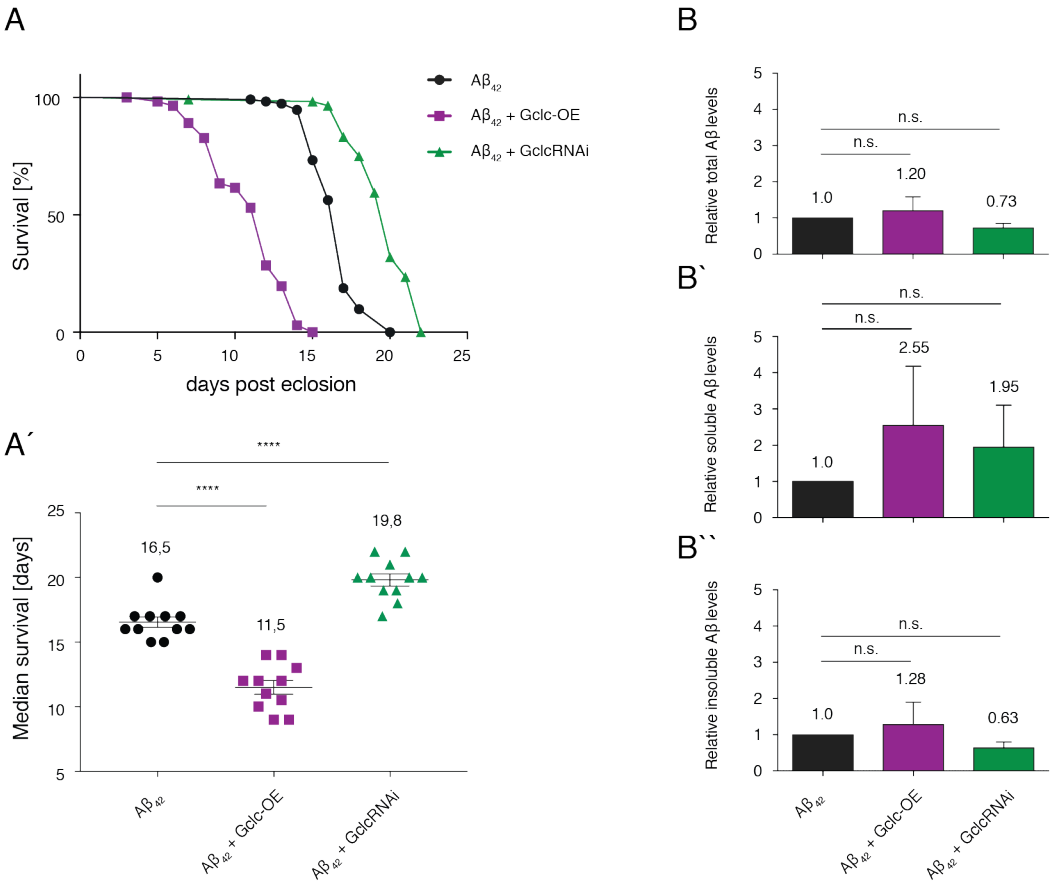

Figure 16: Increased neuronal E_{GSH} is associated with increased $A\beta_{42}$ neurotoxicity. (A, A`) Survival assays, here using the dual expression system under the control of the *nSyb*-Gal4 promoter, revealed that glutathione redox changes (Figure 15) of $A\beta_{42}$ flies with Gclc-OE were associated with a further decreased life span compared to $A\beta_{42}$ only flies. n≥100 flies per genotype were used. Gclc-RNAi increased life span of $A\beta_{42}$ flies (green), but did not change glutathione redox state (A, A`, green). ELISA assays of fly head extracts of 6-day old flies revealed that manipulation of the glutathione synthesis did not change total (B), soluble (B`) or insoluble (B``) Aβ levels. n=3 independent biological replicates. All error bars indicate s.e.m. Statistical analysis was performed with one-way ANOVA, ****p ≤ 0,0001.

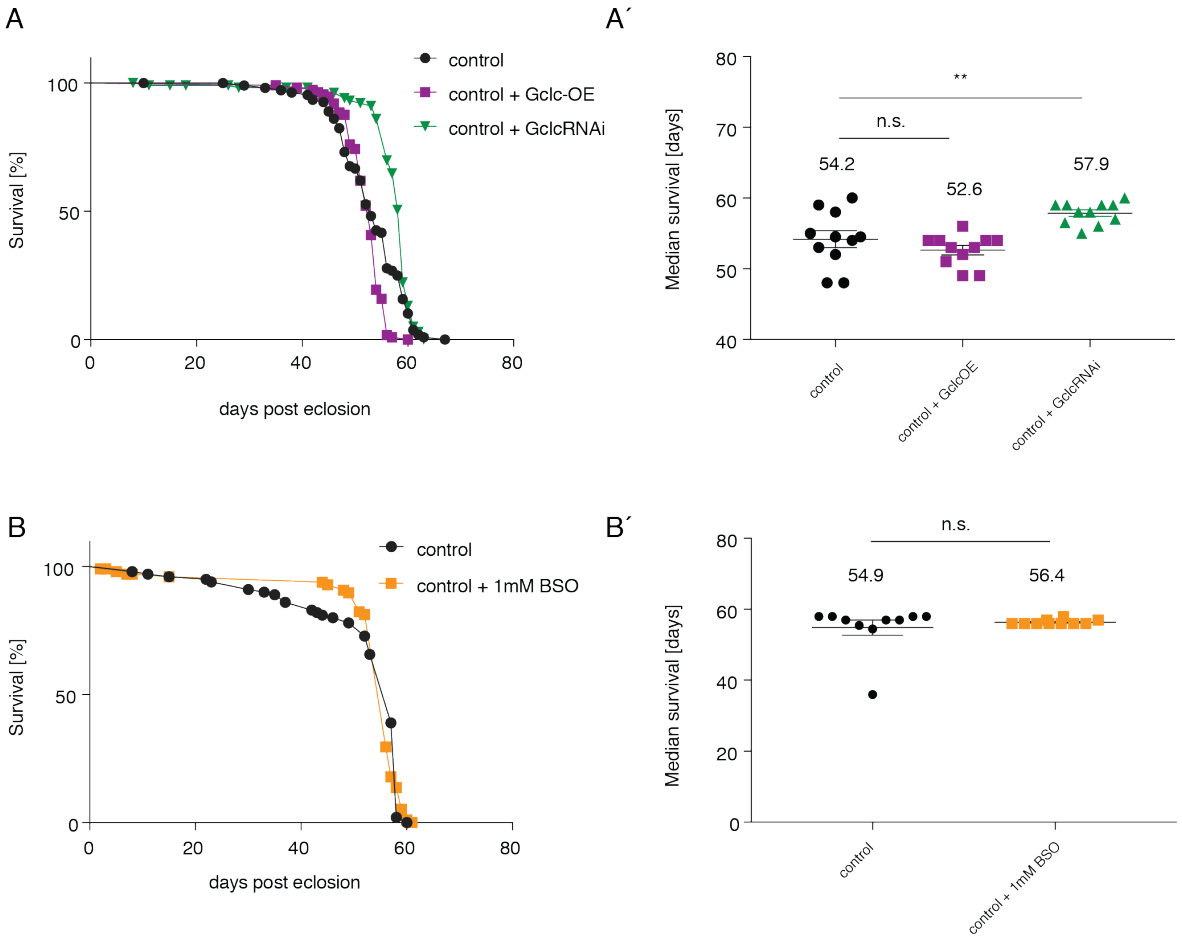

Figure 17: Genetically and pharmacologically manipulation of glutathione synthesis does not severely change life span of control flies. Genetically manipulation of glutathione synthesis with Gclc-OE or GclcRNAi in control flies. Gclc-OE does not change survivals of control flies, whereas GclcRNAi slightly increased survival of control flies. Survival curves are depicted in (A) and median survivals in (A`). Survival assays revealed that glutathione depletion with 1mM BSO did not change the life span of control flies. Flies treated with 1mM BSO are depicted in orange, control flies only in black. For survival assays n≥100 flies per genotype were used. All error bars indicate s.e.m. Statistical analysis was performed with one-way ANOVA,**p ≤ 0.01.

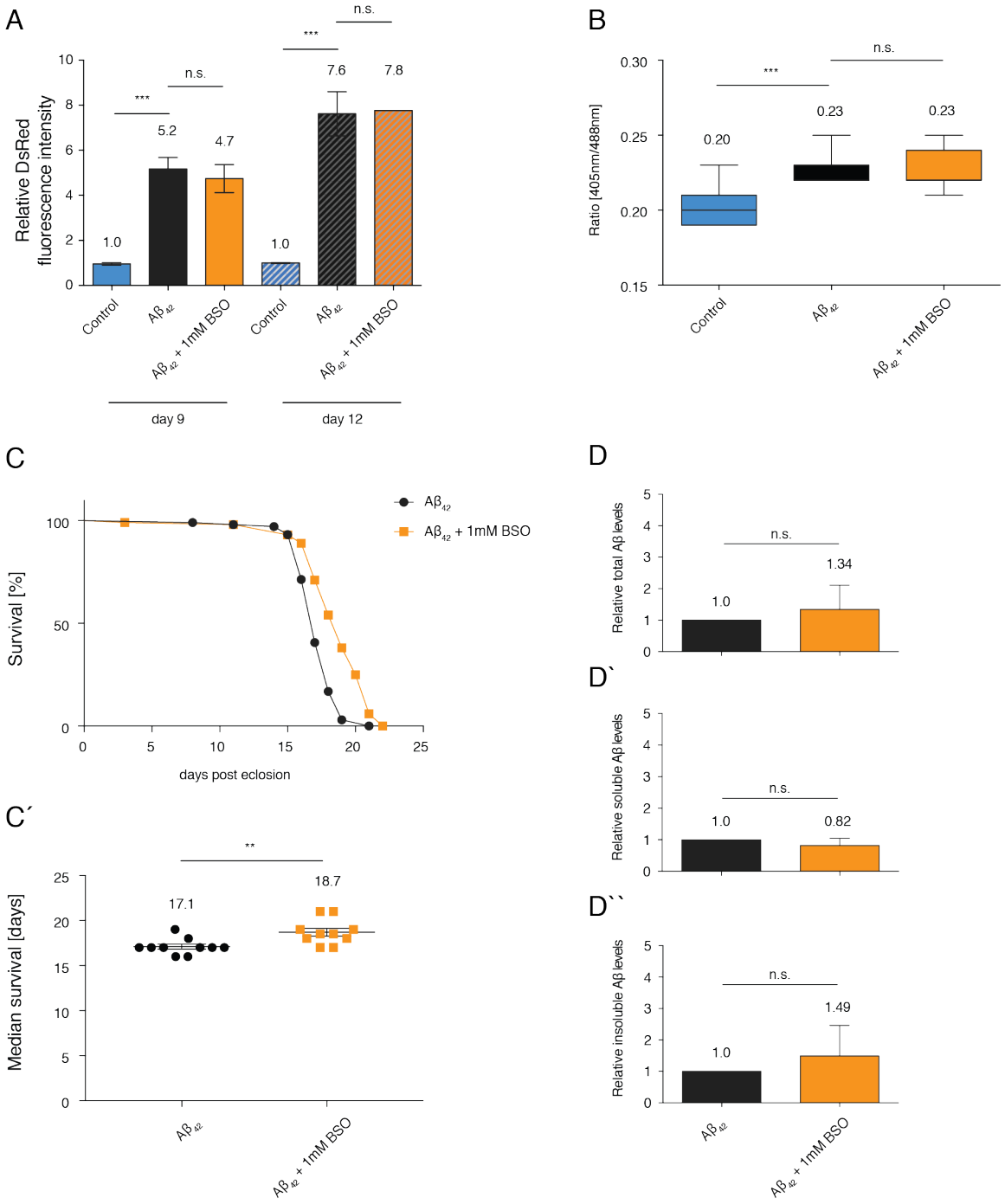

Figure 18: Pharmacological inhibition of glutathione synthesis in Aβ$_{42}$ flies and its effects on JNK activation, E$_{GSH}$, life span and Aβ levels. (A) No changes in JNK activation upon glutathione depletion with 1mM BSO in Aβ$_{42}$ flies. Glutathione depletion with 1mM BSO (orange) did not change JNK activation in Aβ$_{42}$ flies compared Aβ$_{42}$ flies alone (black). On each time point (day 9 and 12), freshly dissected fly brains (n=4) were directly imaged with confocal microscopy. Quantification shows the relative DsRed fluorescent intensity of the whole confocal microscopy image, normalized to control flies (blue). (B) BSO treatment did not change the E$_{GSH}$ of 12-day old Aβ$_{42}$ flies. Box plot representing the 405nm/488nm fluorescent intensity ratio of the cyto-Grx1-roGFP2 probe normalized to DTT = 0.2 (n=8-10 fly brains per condition, lower/upper quartile; whiskers, 5th/95th percentile). Survival assays revealed that treatment with BSO increased life span of Aβ$_{42}$ flies. Survival curves are depicted in (C) and median survival in (C`). For longevity assays n≥100 flies per genotype were used. ELISA assays of fly head extracts of 12-day old flies revealed that glutathione depletion with 1mM BSO did not change total (D), soluble (D`) and insoluble (D``) Aβ levels. n=3 independent biological replicates. All error bars indicate s.e.m. Statistical analysis was performed with one-way ANOVA, **p ≤ 0.01, ***p ≤ 0.001.

4.4 Preliminary data of drug and genetic screenings for potential modifiers of $A\beta_{42}$-induced neurotoxicity

The here established *Drosophila* models could be used for large-scale drug and genetic screening platform to investigate potential mechanistic processes involved in the observed redox imbalance in $A\beta_{42}$ flies (Figure 11) for future studies. In this last chapter, a small-scale screening was performed where different non-enzymatic, enzymatic antioxidants and other important players involved in redox homeostasis were tested and their potential influence on neurotoxicity was examined in $A\beta_{42}$-expressing flies using longevity assays as readout. Preliminary data of candidate-based drug and genetic screenings are presented.

For the drug screen, different drugs were tested. Three different survival rounds were performed, which are shown in Table 17 to Table 20. Oxidative stressors, such as Paraquat and H_2O_2 decreased life span of $A\beta_{42}$-expressing flies. Unexpectedly, administration of well-known antioxidants such as NAC and α-tocopherol decreased the life span of flies $A\beta_{42}$. This worsening in $A\beta_{42}$ neurotoxicity was also observed after administration of an inducer of the Nrf2 antioxidant pathway, tBHQ. Other antioxidants, such as ascorbic acid, L-4 Thiazolidinecarboxylic acid (TCA) and Nordihydroguaiaretic acid (NDGA) had no influence on the life span of $A\beta_{42}$-expressing flies. The preliminary data of all tested conditions are listed in Table 17 to Table 20.

Table 17: Overview of median survival of the small-scale drug screening in control and $A\beta_{42}$-expressing flies: Part I

Name	Median Survival (days)	Significance
Experiment I:		
Holidic fly food		
0_control	44.1	
a_control + EtOH_2% (v/v)	48.0	^{0} n.s.
1_$A\beta_{42}$	19.5	^{0} ****
2_$A\beta_{42}$ + Paraquat_1mM	16.0 ↓	^{1} ****
3_$A\beta_{42}$ + NAC_10mg/ml	15.7 ↓	^{1} *
4_$A\beta_{42}$ + α-tocopherol_13.29mM	8.1 ↓	^{1} ****
5_$A\beta_{42}$ + ascorbic acid_0.36mM	19.0	^{1} n.s.
6_$A\beta_{42}$ + reduced GSH_0.22mM	19.0	^{1} n.s.
7_$A\beta_{42}$ + TCA_0.5% (w/v) [L-4 Thiazolidinecarboxylic acid]	19.7	^{1} n.s.
8_$A\beta_{42}$ + NDGA_16.54mM [Nordihydroguaiaretic acid]	18.5	^{1} n.s.
9_$A\beta_{42}$ + Propyl gallate_0.1mM	17.3 ↓	^{1} *
Standard fly food		
b_control	52.3	^{0} **
c_$A\beta_{42}$	16.1	^{y} ****
c_$A\beta_{42}$ + C18 10% (w/v)	20.3 ↑	^{x} ****

For each survival assay approximately 100 female flies were used (n ≥ 100). All significances are compared to [1]$A\beta_{42}$ flies and [2]$A\beta_{42}$ + EtOH 2% on holidic fly food or [x]$A\beta_{42}$ flies on standard fly food (one-way ANOVA Dunnett´s test). All significances are compared to [0]control flies on holidic fly food or significance compared to [y]control flies on standard fly food. Statistical analysis was performed using one-way ANOVA and Dunnett´s multiple comparisons test. Significantly increased life span (🡅) or decreased life span (🡇) compared to respective $A\beta_{42}$-expressing flies.

Table 18: Overview of median survival of the small-scale drug screening in control and $A\beta_{42}$-expressing flies: Part II

Name	Median Survival (days)	Significance
Experiment II:		
Holidic fly food		
Control	49.3	
Control + C18_10% (w/v)	39.5 ∨	[0] **
Control + α-tocopherol_13.29mM	19.9 ∨	[0] ****
$A\beta_{42}$	20.8	[0] ****
$A\beta_{42}$ + EtOH_2% (v/v)	20.3	[1] n.s.
$A\beta_{42}$ + DMSO_0.2% (v/v)	19.7	[1] n.s.
$A\beta_{42}$ + α-tocopherol_13.29mM (wdh)	10.6 🡇	[2] ***
$A\beta_{42}$ + α-tocopherol_6.7mM	9.4 🡇	[2] ****
$A\beta_{42}$ + C18_10% (w/v)	21.4	[1] n.s.
$A\beta_{42}$ + tBHQ_0.15 % (w/v)	11.9 🡇	[1] **

All significances are compared to each [0] to control flies, [1]$A\beta_{42}$ flies, [2]$A\beta_{42}$ + EtOH 2%, [3]$A\beta_{42}$ + DMSO 0.2%. Significantly increased life span (🡅) or decreased life span (🡇) compared to respective $A\beta_{42}$-expressing flies. Significantly increased life span (∧) or decreased life span (∨) compared to respective control flies. Statistical analysis was performed using one-way ANOVA. For each survival assay approximately 100 female flies were used (n ≥ 100).

Table 19: Overview of median survival of the small-scale drug screening in $A\beta_{42}$-expressing flies: Part III

Name	Median Survival (days)	Significance
Experiment III.a:		
Standard fly food		
$A\beta_{42}$	17.1	
$A\beta_{42}$ + EtOH-1_0.175% (v/v)	19.8 🡅	[1] **
$A\beta_{42}$ + EtOH-2_0.026% (v/v)	20.7 🡅	[1] ****
$A\beta_{42}$ + α-tocopherol_1.1mM	19.0 🡇	[7] **
$A\beta_{42}$ + α-tocopherol_6.7mM (wdh)	18.0 🡇	[6] ***
$A\beta_{42}$ + C18_10% (w/v)	19.2 🡅	[1] *
$A\beta_{42}$ + tBHQ_0.15% (w/v)	6.7 🡇	[1] ****
$A\beta_{42}$ + tBHQ_0.1% (w/v)	11.0 🡇	[1] ****
$A\beta_{42}$ + H_2O_2_88mM	11.2 🡇	[1] ****

All significances are compared to [0]control flies, [1]$A\beta_{42}$ flies, [6]$A\beta_{42}$ + EtOH-1 0.175%, [7]$A\beta_{42}$ + EtOH-2 0.026%, [8]$A\beta_{42}$ + EtOH-3 0.7%. Significantly increased life span (🡅) or decreased life span (🡇) compared to respective $A\beta_{42}$-expressing flies. For each survival assay approximately 100 female flies were used (n ≥ 100). For statistical analysis one-way ANOVA was used.

Table 20: Overview of median survival of the small-scale drug screening in control flies: Part IV

Name	Median Survival (days)	Significance
Experiment III.b:		
Standard fly food		
Control	54.9	
Control + EtOH_0.175% (v/v)	56.5	^{0} n.s.
Control + α-tocopherol_1.1mM	54.3	^{i} n.s.
Control + α-tocopherol_6.7mM	54.4	^{i} n.s.
Control + C18_10% (w/v)	54.8	^{0} n.s.
Control + tBHQ_0.15% (w/v)	7.3 ∨	^{0} ****
Control + tBHQ_0.1% (w/v)	10.4 ∨	^{0} ****
Control + H_2O_2_88mM	10.1 ∨	^{0} ****

For each survival assay approximately 100 female flies were used (n ≥ 100). All significances are compared to ^{0}control flies and ^{i}control flies + EtOH-1 0.175%. Significantly increased life span (∧) or decreased life span (∨) compared to respective control flies. Statistical analysis was performed using one-way ANOVA.

For the genetic screen, downregulation (DsRNA, TRiP and RNAi lines) and overexpression (OE lines) of various important players of the redox system was performed in the background of $A\beta_{42}$-expessing flies (Figure 19). For a better presentation all tested candidate genes were grouped in seven different subgroups (Table 21) 1) Antioxidant enzymes important for the detoxification of hydrogen peroxide from cells and organisms 2) Enzymes of the thioredoxin and peroxiredoxin antioxidant system 3) Glutathione dependent antioxidant enzymes 4) Enzyme of the glutathione synthesis, 5) Enzyme of the pentose phosphate pathway (major source for NADPH) 6) Components of the Nrf2 antioxidant response pathway 7) Glutamate transporter. Each of the longevity assay rounds is depicted Figure 19 A-G. Among the 31 tested fly lines in the background of $A\beta_{42}$ expression, 9 fly lines showed a significant increase in life span and in 9 fly lines a decrease in life span of $A\beta_{42}$ flies was detected. All these lines, superoxide dismutase 1 RNAi line 1 (24750), superoxide dismutase 2 DsRNA (24489), catalase overexpression (24621) but also catalase TRiP line 1 (43197), deadhead TRiP line (41857), and the cap-n-collar TRiP lines 1 and 2 (25984 and 40854) prolonged the life span of $A\beta_{42}$ flies. Candidates that reduced the life span of $A\beta_{42}$ flies were the second peroxiredoxin-5 overexpression line (W.Orr), the first thioredoxin reductase TRiP line (53883), the glutathione S-transferase D1 TRiP line (36818), the first glucose-6-phosphate dehydrogenase overexpression line (W.Orr), the transcription factor MafS (40853) and the excitatory amino acid transporter 1 overexpression line (8202). The overview of all preliminary survival results of all candidates and fly lines are listed in Table 21.

Decrypting the complexity of the preliminary results of both small-scale screenings will be the task of future work. These datasets only provided a rough overview of the complex processes of redox homeostasis and their impact on the neurotoxicity of $A\beta_{42}$. However, the here established models provide a suitable

screening platform to perform redox analysis and to analyze the activation of stress signaling pathways, such as the JNK pathway, for the future.

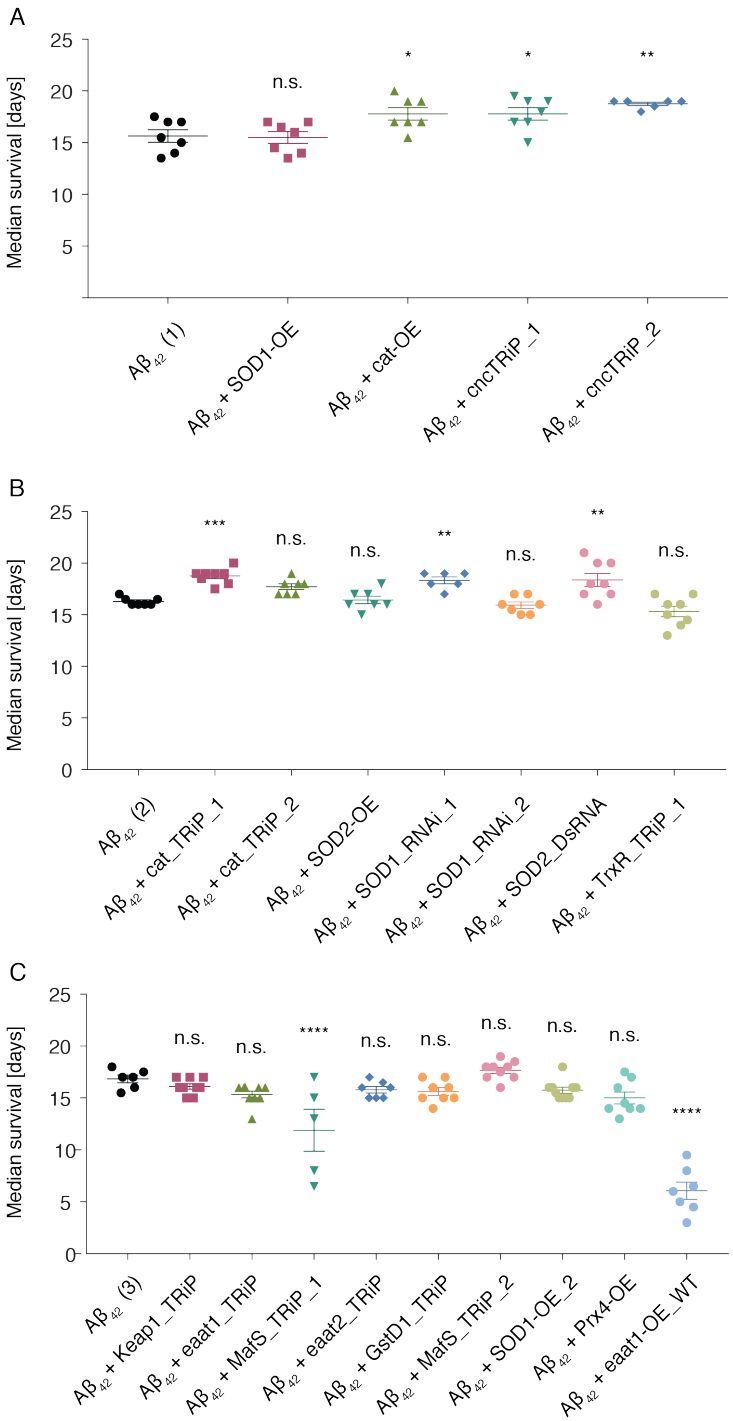

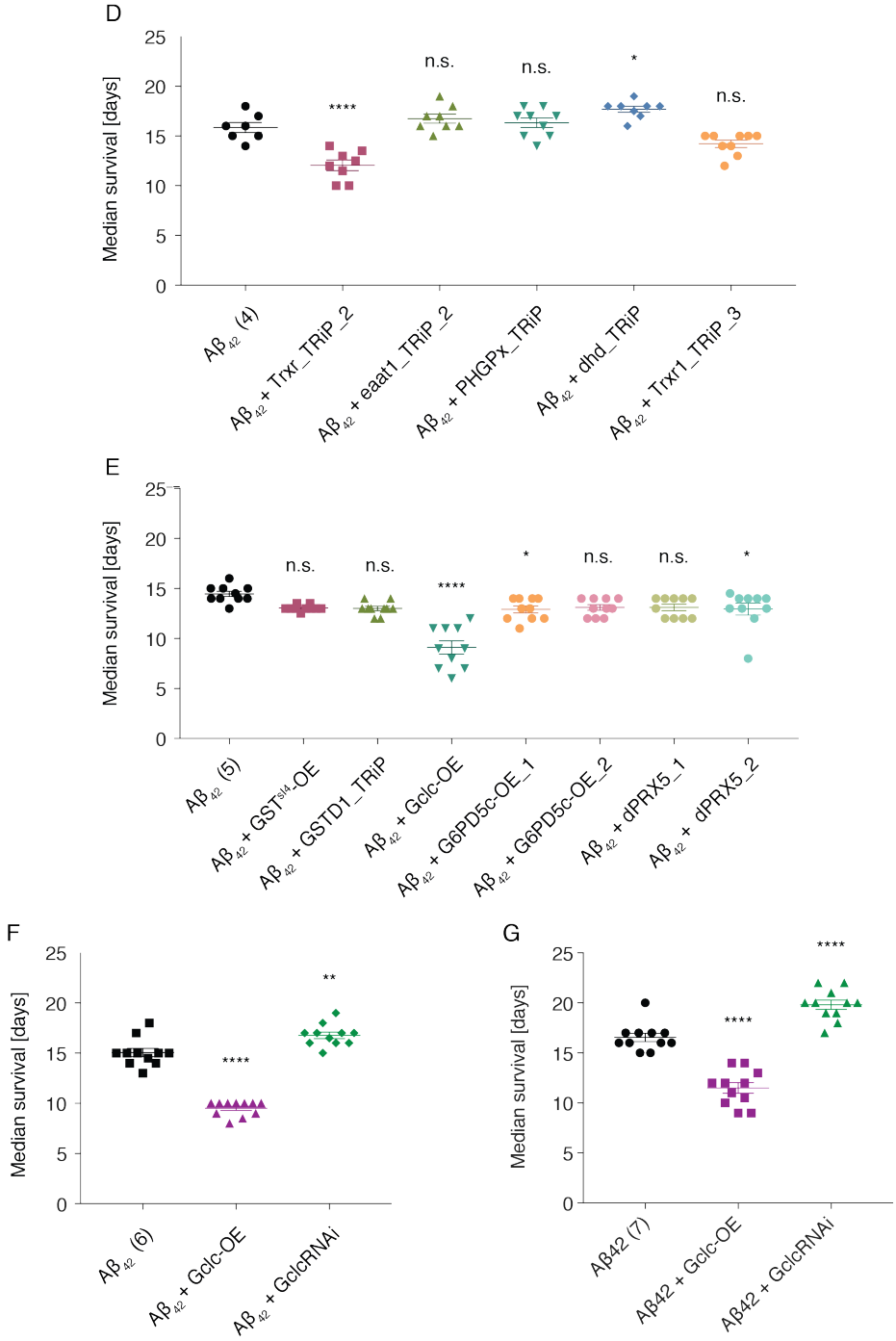

Figure 19: Overview of all seven redox survivals for the genetic screening for potential modifiers of redox-related $A\beta_{42}$ neurotoxicity. Longevity assays were performed in the background of $A\beta_{42}$ with overexpression (OE) or downregulation (TRiP or RNAi) of various redox proteins. (A) Redox survival I (B) Redox survival II (C) Redox survival III (D) Redox survival IV (E) Redox survival V (F) Redox survival VI (G) Redox survival VI

Table 21: Overview of the survival data of the genetic screening in $A\beta_{42}$-expressing flies

Name	Median Survival (days)	Significance	n-number	Identification
All $A\beta_{42}$ from all seven survival rounds				
[1]$A\beta_{42}$ (Redox survival I)	15.6	-	66	-
[2]$A\beta_{42}$ (Redox survival II)	16.3	-	63	-
[3]$A\beta_{42}$ (Redox survival III)	16.8	-	47	-
[4]$A\beta_{42}$ (Redox survival IV)	15.9	-	61	-
[5]$A\beta_{42}$ (Redox survival V)	14.5	-	102	-
[6]$A\beta_{42}$ (Redox survival VI)	15.0	-	112	-
[7]$A\beta_{42}$ (Redox survival VII)	16.5	-	112	-
1) Antioxidant enzymes important for the detoxification of hydrogen peroxide from cells and organisms				
$A\beta_{42}$ + SOD1-OE_1	15.5	[1] n.s.	64	24754
$A\beta_{42}$ + SOD1-OE_2	15.8	[3] n.s.	62	24750
$A\beta_{42}$ + SOD1_RNAi_1	18.3 ↑	[2] **	62	24493
$A\beta_{42}$ + SOD1_RNAi_2	15.9	[2] n.s.	59	24491
$A\beta_{42}$ + SOD2-OE	16.4	[2] n.s.	58	24494
$A\beta_{42}$ + SOD2_DsRNA	18.4 ↑	[2] **	65	24489
$A\beta_{42}$ + cat-OE	17.8 ↑	[1] *	59	24621
$A\beta_{42}$ + cat_TRiP_1	18.8 ↑	[2] ***	60	43197
$A\beta_{42}$ + cat_TRiP_2	17.7	[2] n.s.	62	31894
$A\beta_{42}$ + PHGPx_TRiP	16.3	[4] n.s.	64	41879
2) Enzymes of the thioredoxin and peroxiredoxin antioxidant system:				
$A\beta_{42}$ + Prx4-OE	15.0	[3] n.s.	64	18489
$A\beta_{42}$ + dPRX5-OE_1	13.1	[5] n.s.	95	W. Orr
$A\beta_{42}$ + PRX5-OE_2	13.0 ↓	[5] *	102	W. Orr
$A\beta_{42}$ + TrxR_TRiP_1	15.3	[2] n.s.	63	36805
$A\beta_{42}$ + Trxr1_TRiP_2	12.1 ↓	[4] ****	63	53883
$A\beta_{42}$ + Trxr1_TRiP_3	14.2	[4] n.s.	63	32984
$A\beta_{42}$ + dhd_TRiP	17.7 ↑	[4] *	56	41857
3) Glutathione dependent antioxidant enzymes:				
$A\beta_{42}$ + GstD1_TRiP	15.6	[3] n.s.	59	36818
$A\beta_{42}$ + GSTD1_TRiP (repeated)	13.0 ↓	[5] *	100	36818
$A\beta_{42}$ + GST^{sl4}-OE	13.1	[5] n.s.	98	A.J. Whitworth
4) Enzyme of the glutathione synthesis:				
$A\beta_{42}$ + Gclc-OE	9.1 ↓	[5] ****	103	W. Orr
$A\beta_{42}$ + Gclc-OE (repeated)	9.5 ↓	[6] ****	113	W. Orr
$A\beta_{42}$ + Gclc-OE (repeated)	11.5 ↓	[7] ****	105	W. Orr
$A\beta_{42}$ + GclcRNAi	16.8 ↑	[6] **	111	W. Orr
$A\beta_{42}$ + GclcRNAi (repeated)	19.8 ↑	[7] ****	109	W. Orr

5) Enzyme of the pentose phosphate pathway (major source for NADPH)				
$A\beta_{42}$ + G6PD5c-OE_1	12.9 ↓	[5] *	99	W. Orr
$A\beta_{42}$ + G6PD5c-OE_2	13.1	[5] n.s.	103	W. Orr
6) Components of the Nrf2 antioxidant response pathway:				
$A\beta_{42}$ + cncTRiP_1	17.8 ↑	[1] *	57	25984
$A\beta_{42}$ + cncTRiP_2	18.8 ↑	[1] **	64	40854
$A\beta_{42}$ + Keap1_TRiP	16.1	[3] n.s.	73	57801
$A\beta_{42}$ + MafS_TRiP_1	11.9 ↓	[3] ****	8	40853
$A\beta_{42}$ + MafS_TRiP _2	17.7	[3] n.s.	84	25986
7) Glutamate transporter				
$A\beta_{42}$ + eaat1-OE_WT	6.1 ↓	[3] ****	15	8202
$A\beta_{42}$ + eaat1_TRiP	15.3	[3] n.s.	67	43287
$A\beta_{42}$ + eaat1_TRiP (repeated)	16.8	[4] n.s.	61	43287
$A\beta_{42}$ + eaat2_TRiP	15.8	[3] n.s.	40	40832

All significances are compared to [1]$A\beta_{42}$ flies from Redox Survival I, [2]$A\beta_{42}$ flies from Redox Survival II, [3]$A\beta_{42}$ flies from Redox Survival III, [4]$A\beta_{42}$ flies from Redox Survival IV, [5]$A\beta_{42}$ flies from Redox Survival V, [6]$A\beta_{42}$ flies from Redox Survival VI, [7]$A\beta_{42}$ flies from Redox Survival VII. Statistical analysis was performed using one-way ANOVA and Dunnett´s multiple comparisons test. Significantly increased life span (↑) or decreased life span (↓) of $A\beta_{42}$-expressing flies.

5. Discussion

5.1 Glutathione redox imbalance is an early event in AD pathology

Numerous studies suggest that oxidative stress is connected to AD pathology (von Bernhardi & Eugenín 2012; Cai et al. 2011). It is still not clear to what extend changes in the redox homeostasis contribute to the onset and progression of AD and whether there is a direct link between changes in redox balance and Aβ neurotoxicity. The discrimination of the oxidants and redox systems that are involved in Aβ neurotoxicity is crucial to better understand which pathways might be affected in AD pathology and therefore could be targeted for potential therapies against AD. Here, I present a versatile *in vivo Drosophila* model to address this question by combining cell-type-specific redox analysis, using genetically encoded glutathione and H_2O_2 redox sensors, with an AD neurodegeneration model based on the aggregation of the human $A\beta_{42}$ peptide. A main finding of this study is the relevance of an increased cytosolic glutathione redox potential, which was already observed at an early time point of $A\beta_{42}$ deposition (Figure 11B). This data indicates that glutathione redox imbalance is an early process in AD pathogenesis. This is consistent with previous studies, suggesting that oxidative damage in neurons is an early event occurring in AD pathology (Stephan et al. 2012; Mangialasche et al. 2009; Bermejo et al. 2008; Butterfield et al. 2007; Keller et al. 2005). In these studies, increased levels of protein carbonylation and lipid peroxidation were detected in early stage AD patients and in mild cognitive impairment (MCI) patients, who have a higher risk of developing AD. Furthermore, it has been reported that glutathione depletion is an early event already detectable in MCI and in mild AD patients (Mandal et al. 2015; Ansari & Scheff 2010; Bermejo et al. 2008), which supports and might provide an explanation for the increase in glutathione redox potential that was observed in our $A\beta_{42}$ fly model. Whether this pro-oxidant shift in cytosolic glutathione redox potential results from a depletion of the total glutathione pool, an increase in oxidized glutathione (GSSG), or a combination of both, needs to be elucidated in future studies.

Furthermore, one of the most intriguing question, whether oxidative stress has a causative role in AD pathogenesis or is a consequence of Aβ accumulation is still highly debated in the literature (Andersen 2004). Several studies suggest that oxidative stress has a causal role in AD pathology and precedes Aβ plaque formation (Lin & Beal 2006; Praticò et al. 2001), whereas other work shows that Aβ aggregation precedes oxidative stress which is therefore a consequence of AD pathology (Xie et al. 2013). I tried to shed light on this intriguing question by performing a detailed time course redox analysis dissecting Aβ-expressing fly brains at early and later stages of disease progression. This data showed, that the glutathione redox imbalance was already detectable at an early time point of $A\beta_{42}$ aggregate formation (at day 6), but occurred after I observed the first depositions of $A\beta_{42}$ aggregates in the fly brain from day 3 on. This supports redox changes may be a consequence of $A\beta_{42}$ aggregation. More detailed time course analysis of young flies and employing temperature sensitive expression systems to switch Aβ expression on and off in

combination with monitoring the deposition of amyloidogenic structures using amyloid-specific polymer probes like p-FTAA or ThS stainings (Berg et al. 2010; Åslund et al. 2009; LeVine 1999) in more detail might give more insights into surely answering this question.

5.2 Changes in glutathione redox potential, but not in H_2O_2 concentration, are linked to $A\beta_{42}$-induced neurotoxicity

There is accumulating evidence that mitochondrial dysfunction and its resulting ROS overproduction is correlated with AD pathology (Verri et al. 2012; von Bernhardi & Eugenín 2012; Lin & Beal 2006). Previous *in vitro* studies have shown, that H_2O_2 is generated during early stages of Aβ aggregation and can mediate Aβ protein toxicity (Tabner et al. 2005; Behl et al. 1994). In this thesis, I did not measure any changes in cytosolic or mitochondrial H_2O_2 levels, neither in neurons (Figure 11A, Figure 12), nor in glia cells (Figure 11A`). The lack of datable changes in H_2O_2 concentration in this *in vivo* model, strongly suggest that H_2O_2 levels are not the major factor in neurons or glia cells for the $A\beta_{42}$-mediated neurotoxicity. Whether an accumulation of other ROS species or reactive nitrogen species (RNS) are involved in $A\beta_{42}$-mediated neurotoxicity in this model, needs further investigation. As for example, nitric oxide (NO) has already been linked to AD pathogenesis as an important mediator of Aβ-induced neuronal cell death (Vodovotz et al. 1996; Hashimoto et al. 2002; Kadowaki et al. 2005). Thereby, using other ROS and NO detection methods, like Mitosox or DCFDA (Eruslanov & Kusmartsev 2010; Robinson et al. 2008) and DAF-2 DA or genetically encoded NO• probes (geNOps) (Kojima et al. 1998; Eroglu et al. 2016), could help to shed light on this open question in more detail. Furthermore, I cannot exclude that any other forms of mitochondrial dysfunction occur in this model, e.g. morphological changes or disruption of functional mitochondria including mitochondrial fragmentation, which has been published by Knott et al (Knott et al. 2008). The limitation of the H_2O_2 redox sensor (Orp1-roGFP2) used in this study is that it cannot measure H_2O_2 changes in the nano- or picomolar ranges. Peroxiredoxin-based redox sensors which posses higher sensitivity would need to be validated in the background of our Aβ aggregation models to address this question (Fujikawa et al. 2016; Sobotta et al. 2014). There could be small changes in H_2O_2 concentration that I cannot detect. Still it would need to be elucidated whether and to what extent potential nano- or picomolar H_2O_2 changes could contribute to the neurotoxicity mediated by $A\beta_{42}$.

5.3 $A\beta_{42}$ deposition induces glutathione redox potential changes in neurons but not in glia cells

Interestingly, expression of $A\beta_{42}$ in neurons and co-expression of the redox sensors in neurons or glia cells, revealed that the glutathione redox imbalance observed in the fly brain, which occurs in parallel to the deposition of $A\beta_{42}$, is mainly observed in neurons, but not in glia cells (Figure 11B and Figure 11B`, respectively). It has been reported that neurons maintain their glutathione levels by the uptake of cysteine or precursors provided by glia cells (Sagara et al. 1993; Dringen, Pfeiffer, et al. 1999). Neurons with their relatively low levels of antioxidants are more sensitive and vulnerable to oxidative stress compared to glia cells which contain higher amounts of glutathione and have a more efficient peroxide detoxification system (Dringen, Kussmaul, et al. 1999; Iwata-Ichikawa et al. 1999; Dringen 2000; Yu et al. 2016). This increased resistance to redox stress of glia cells, could be an explanation why I did not observe any cytosolic glutathione redox imbalance or H_2O_2 level changes those cells. Whether this is due to their higher levels of glutathione (Sagara et al. 1993), their up-regulation of glutathione synthesis upon stress (Iwata-Ichikawa et al. 1999), or shutting down the supply of cysteine to neurons or because of an increased release of more oxidized glutathione (Hirrlinger et al. 2001; Morgan 2012; Ye et al. 2015) needs to be elucidated. The fact that in this fly model glia cells do not respond to the accumulation of $A\beta_{42}$ with redox changes does not mean, that glia cells do not react or contribute to the neurotoxic effect of $A\beta_{42}$ at all. I do not exclude, that glial dysfunction and inflammatory processes are initiated, including the release of pro-inflammatory cytokines, potentially leading to the activation of other stress response pathways, which could increase neuronal vulnerability to $A\beta_{42}$ and therefore could be involved in $A\beta_{42}$-induced toxicity (Wyss-Coray & Rogers 2012; Wyss-Coray & Mucke 2002). The exact mechanism, which mediates the crosstalk between neurons and glia cells remain a very important open question for future studies.

5.4 Accumulation of $A\beta_{42}$ results in the activation of the JNK stress response

The literature is not consistent concerning the role of JNK signaling in AD. On the one hand it has been reported that the activation of JNK contributes to cell death in response to oxidative stress (Sclip et al. 2014; Tare et al. 2011; Marques et al. 2003; Jang & Surh 2002; Shoji et al. 2000) and on the other hand that it can also protect against it since it is involved in stress tolerance (Liu et al. 2015; Wu et al. 2009; Wang et al. 2003). In the presented work, I observed an increase in JNK activation in $A\beta_{42}$ flies over time (Figure 13), which supports its role in neuronal stress signaling upon $A\beta_{42}$ deposition and confirms the activation of JNK signaling in the progression of AD pathology. However, I did not observe a further

increase in JNK activation in $A\beta_{42}$ flies with increased glutathione synthesis by pan-neuronal Gclc-OE (Figure 14) with accompanied elevated toxicity (Figure 16A), suggesting that JNK activation is not directly associated with glutathione-mediated toxicity in this Aβ aggregation model. In this study, I did not observe a further increase of JNK activation upon glutathione depletion (via GclcRNAi or BSO treatment), which has been reported to trigger JNK activation (Fratelli et al. 2005; Yue et al. 2006; Franco et al. 2007; Circu & Aw 2012). Whether other factors are involved in glutathione-mediated $A\beta_{42}$ toxicity, such as glutathione-S-transferase pi (GST-π), which catalyzes the conjugation of glutathione to electrophilic substances and is known to regulate JNK activation in cancer (Adler et al. 1999; Laborde 2010) would be very interesting for further analysis. Looking at the involvement of other important stress pathways, such as the NF-E2-related factor-2 (Nrf2) pathway or the activation of death receptors like TNF-alpha, might also be of interest for future studies (Le Gal et al. 2015; Sayin et al. 2014; DeNicola et al. 2011). Manipulation of glutathione synthesis (via Gclc overexpression or GclcRNAi and BSO) did not influence JNK activation and neuronal E_{GSH}, suggesting JNK pathway activation happens in parallel to changes in the overall redox balance. But gaining a comprehensive understanding of the relationship between glutathione synthesis and JNK activation in the background of AD could be highly interesting.

5.5 Changes in glutathione redox imbalance is linked to $A\beta_{42}$-mediated neurotoxicity

Most importantly, this study suggests a link between glutathione redox potential and $A\beta_{42}$-mediated neurotoxicity. Intriguingly, an increase in neuronal glutathione levels in $A\beta_{42}$ flies via pan-neuronal Gclc-OE further exacerbates $A\beta_{42}$ neurotoxicity, as life span was even more decreased (Figure 16A and Figure 16A`) compared to $A\beta_{42}$-expressing flies without glutathione synthesis manipulation. This was accompanied with a further increase in glutathione redox potential (Figure 15), indicating a direct mechanism for glutathione-synthesis manipulation-induced neurotoxicity, as ELISA assays did not reveal significant changes in the levels of $A\beta_{42}$ in flies overexpressing Gclc (Figure 16B-B``).

Moreover, the data indicate glutathione redox homeostasis is playing an important role in the cellular vulnerability to proteotoxic stress and might represent the missing factor that might explain to the fact that the Aβ plaque load in the brain does not directly correlate with the clinical symptoms of AD patients (Perez-Nievas et al. 2013; Sloane et al. 1997). Even though it has been reported that an increase in glutathione levels can be protective against ROS, increase cell viability (Luchak et al. 2007; Orr et al. 2005) and overexpression of Gclc extends life span in wild-type *Drosophila* flies (Orr et al. 2005), in the context of the here presented Aβ aggregation model opposing effects were observed. There is only limited data on the function of glutathione available besides being a generic antioxidant there. Interestingly, in the

context of neurodegeneration Duffy et al. (2014) have also linked an increase in glutathione levels with cognitive impairment in MCI patients. They observed high levels of glutathione in MCI patients compared to control patients, and that these higher levels of glutathione were associated with worsened neuropsychological performance, including verbal memory consolidation (Duffy et al. 2014). They suggested the increased levels of glutathione as an initially compensatory mechanism to adapt and respond to a subsequent injury (e.g. coping with increased oxidative stress), which is then followed by a decline in antioxidant levels. Furthermore, it has been shown in cultured cells that NAC treatment or overexpression of Gclc, resulting in higher levels of glutathione, caused glutathione-dependent reductive stress that triggered mitochondrial oxidation and caused in cytotoxicity (H. Zhang et al. 2012). Recently, reductive stress has been described to be a compensatory effect to oxidative stress, and has been reported to play a role in AD (Lloret et al. 2016; Badía et al. 2013; Russell et al. 1999). Whether reductive stress and subsequent mitochondrial oxidation are the cause for our observed enhanced toxicity in $A\beta_{42}$ flies with Gclc-OE needs further investigation. Additional supporting evidence that an increase in antioxidants can also evoke negative effects was described in the context of cancer. Previous studies show, that increasing the levels of antioxidants or over-activating antioxidant pathways can result in increased tumorigenesis, tumor growth and invasiveness (Le Gal et al. 2015; Sayin et al. 2014; DeNicola et al. 2011). Additionally, clinical trials administrating antioxidants as potential treatment for AD at this point have not been successful in slowing down AD progression (Mecocci & Polidori 2012; Galasko et al. 2012; Kryscio et al. 2017).

The exact molecular mechanism of glutathione-synthesis manipulation-induced neurotoxicity in our $A\beta_{42}$ fly model could not be elucidated in this study, but our observations provided stimulating incitements into redox-associated mechanisms and specifically identified glutathione metabolism as a promising therapeutic target for the treatment of AD. The protein glutathionylation status of the proteome is an important post-translational modification cysteine residues by addition of glutathione to protect proteins from oxidative damage (Dalle-Donne et al. 2009), plays an important role in regulating redox homeostasis and has been described to be a critical regulator of apoptosis (Dalle-Donne et al. 2009; Franco & Cidlowski 2009). Investigating the protein glutathionylation status might give rise to more detailed mechanistic information. Previous studies have identified an increase in S-glutathionylated proteins in AD patients compared to age-matched controls (Newman et al. 2007). Another study, using mice brains and blood samples, suggested that the protein glutathionylation status can be used as a biomarker of AD progression and for early stage screening indicating its important role in AD (C. Zhang et al. 2012). Therefore, it would be very interesting to test whether the glutathionylation status of directly influences the glutathione redox potential of the cell.

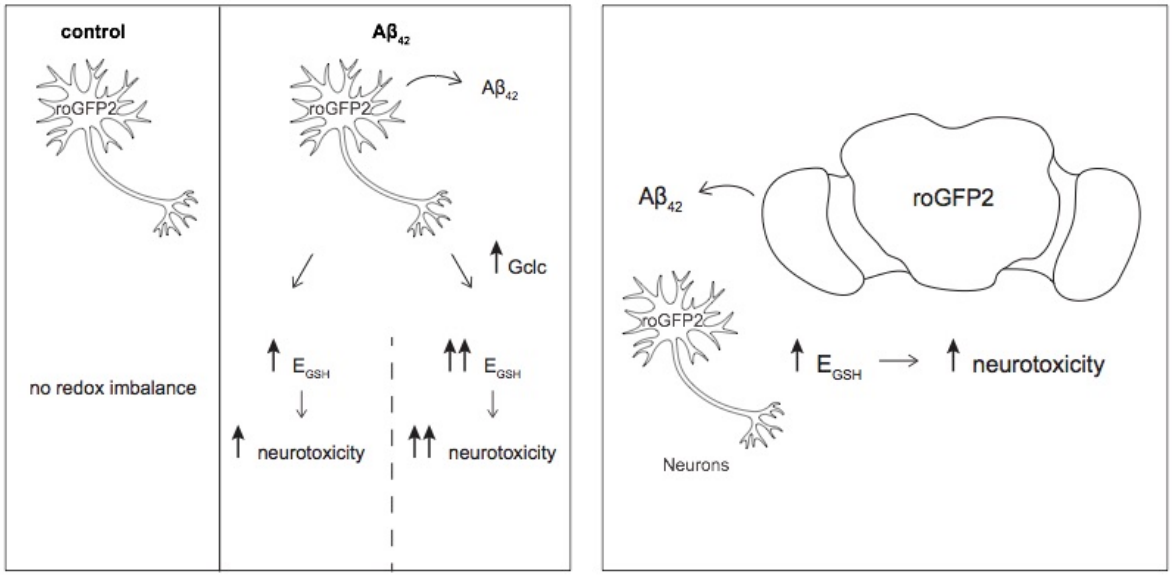

Figure 20: Schematic graphic of main findings of this thesis, describing that changes in glutathione redox imbalance are linked to $A\beta_{42}$ neurotoxicity. Pan-neuronal expression of $A\beta_{42}$ caused a decrease in life span, which was accompanied with an increase in E_{GSH}. An increase in glutathione synthesis worsened this phenotype. This study proposes additional roles of glutathione beyond the generic neuroprotective antioxidant and being involved in the $A\beta_{42}$-induced neurotoxicity.

5.6 Established *Drosophila* models provide screening platform for redox-related and non-redox-related potential modifiers of $A\beta_{42}$ neurotoxicity

To investigate potential mechanistic processes behind our observations, preliminary drug (Table 17 - Table 20) and genetic (Table 21 and Figure 19) screenings were performed and longevity assays were used as read out. Due to the complexity of the preliminary results of the screening, I only describe a few candidates that might stimulate interest for future research projects. In both screenings some reflective but interesting preliminary results were observed that might be of interest for upcoming research studies and might give another perspective on how changing the redox homeostasis can influence the neurotoxic effects of $A\beta_{42}$. One interesting preliminary result hinted towards the potential importance of the Nrf2 pathway, a widespread transcriptional antioxidant response pathway (Le Gal et al. 2015; Sayin et al. 2014; DeNicola et al. 2011). Administration of an Nrf2 activator, *tert*-Butylhydroquinone, reduced life span of $A\beta_{42}$-expressing flies (Table 18, Table 19) while downregulation of cap-n-collar (cnc), the *Drosophila* Nrf2 ortholog (Sykiotis & Bohmann 2008; Lacher et al. 2016), via cnc_TRiP increased their life span of flies expressing $A\beta_{42}$ (Table 21). As Nrf2 activation via tBHQ feeding also compromised the life span of control flies (Table 20) future studies should test lower concentrations of this Nrf2 inducer to confirm my preliminary observations and to exclude potential unspecific effects, which are not related to $A\beta_{42}$. But the spark for future investigations is still given, because the Nrf2 pathway is connected to glutathione

metabolism, as it has been shown that Nrf2 activation leads to increased glutathione levels and Gcl mRNA levels (Steele et al. 2013). Interestingly, recent studies also showed the negative aspect of increased tumor invasiveness and tumor growth due to Nrf2 over-activation in (Le Gal et al. 2015; Sayin et al. 2014; DeNicola et al. 2011). Therefore, it might be very interesting to further investigate the interconnection between Nrf2 and glutathione synthesis manipulation-induced neurotoxicity in $A\beta_{42}$ flies, which might help to decipher the exact mechanism behind our observations.

Another interesting observation was detected after the administration of α-tocopherol and NAC, both well-known and often applied antioxidants (Miquel et al. 1982; Sung et al. 2004; Di Domenico et al. 2015). Furthermore, it has been observed that the administration of Vitamin E improved cognitive dysfunction or slowing down clinical progression (Sano et al. 1997; Dysken et al. 2014). However, our in model $A\beta_{42}$ aggregation did not confirm these previous studies since the feeding of α-tocopherol and NAC decreased the life span of $A\beta_{42}$-expressing flies (Table 17 - Table 20). Control flies showed no changes in life span in the case of α-tocopherol. Whether NAC has the same effect on control flies without $A\beta_{42}$ expression, must be tested in upcoming studies. To be mentioned again that these are only preliminary data and need to be confirmed in future studies.

A limitation of this screenings was that almost no titration of the drugs was performed. Our model overexpresses human $A\beta_{42}$ fused to a secretion signal, which limits our model to the aggregation of $A\beta_{42}$ in the extracellular space. But how the treatment of these different compounds influence $A\beta_{42}$ generation, release or degradation might be interesting to investigate for future studies. On the first glance, these single preliminary results seem to be non-intuitive, but looking at the whole picture, this data are also very exciting, because the antioxidant NAC, and the activation of the prominent antioxidant pathway Nrf2 via tBHQ also caused a severe worsening of the life span of $A\beta_{42}$-expressing flies. These data indicate that the overall notion that pro-antioxidant conditions are only neuroprotective could be critically questioned. I hypothesize that messing around with the redox system in the background of pathological conditions might be detrimental in both ways, having too much pro-oxidant or pro-antioxidant conditions. The data of this screening must be seen very critically, because the point of criticism of these small-scale screenings was, that also control flies showed unexpected decrease in life span in some of these cases. To decipher, whether the negative effects on survival rate of these compounds can be confirmed, lower concentrations of these drugs must be administered, where the effect on control flies are not significantly changing to make sure that the observed life span changes are in fact $A\beta_{42}$-dependent. Additionally, the time point of drug administration might be crucial. Another limitation of the drug screenings was that the glutathione redox potential could not be reduced with any drug treatment (preliminary data not shown). For future studies, I suggest the genetic approach might be more promising. This might give more information of what is happening with fewer side effects and more and targeted manipulations. The preliminary data of the genetic screening showed that downregulation of cnc, SOD1, SOD2 and catalase (using following

$A\beta_{42}$-expressing fly lines with cnc_TRiP_1, cnc_TRiP_2, cat_TRiP_1, SOD1_RNAi_1 and SOD2_DsRNA) increased in life span of $A\beta_{42}$-expressing flies (Table 21 and Figure 19). This does not confirm previous studies showing that downregulation of these candidates worsen AD pathology (Murakami et al. 2011; Li et al. 2004; Gsell et al. 1995). Knockdown of antioxidant enzymes, such as the cytosolic and mitochondrial superoxide dismutase (*SOD1* and *SOD2*, respectively) and catalase (*Cat*) have been shown to increase amyloid plaque load and worsen cognitive functions in AD transgenic mouse models (Murakami et al. 2011; Li et al. 2004; Gsell et al. 1995). Interestingly, in our model downregulation of SOD1 ($A\beta_{42}$ + SOD1_RNAi_1) and SOD2 ($A\beta_{42}$ + SOD2 DsRNA) resulted in a prolonged life span of flies expressing $A\beta_{42}$ or in no difference in life span (Table 21, Figure 19B). Paradoxically both, overexpression and downregulation of catalase showed an increase or no significant changes in the life span of $A\beta_{42}$-expressing flies.

Testing higher number of RNAi and overexpression lines of each candidate, maybe with and without the combination of antioxidants and oxidants treatment, and then measuring the glutathione redox potential and H_2O_2 concentrations of these flies in the background of $A\beta_{42}$ deposition might be very interesting. For upcoming studies, also control survivals must be performed, to identify the $A\beta_{42}$-dependent changes. Finding out how a decrease in the glutathione redox balance can be achieved in the background of $A\beta_{42}$ accumulation and whether this is directly translated into a further increase in life span, might give some more insights into the mechanistic processes and could be followed up in future studies.

In summary, preliminary data of both small-scale screenings in some cases showed non-consistent and contra-intuitive results. They emphasized the complexity of redox homeostasis and its mechanisms, seeming not easily to be unraveled and calling upon more critical thinking on the application of antioxidants. Nevertheless, the screenings provided a few potential and promising targets to look into in following studies. Even though this thesis could not provide detailed mechanistic processes that are involved in the observed redox imbalance the $A\beta_{42}$-aggregation model, it provided a suitable screening platform with a few potential and promising targets giving spark for future investigations.

6. Outlook & Conclusion

This study provides new evidence for the relevance of redox signaling events in the onset and progression of AD. The development of versatile models, which are presented in this study, that combine redox analysis with *Drosophila* models of Aβ aggregation, will help deciphering these complex mechanisms and present a significant advance to the field of redox biology and neurodegeneration research. The main contribution of this study was to identify the direct link between glutathione redox potential and $A\beta_{42}$ neurotoxicity *in vivo* (Figure 20), which opened exciting insights into its involvement in $A\beta_{42}$-mediated neurotoxicity. In contrast to the common view of "oxidative stress", this thesis suggests additional roles of glutathione in addition to a generic antioxidant and proposes that the increase in neuronal glutathione redox potential is not just a byproduct of Aβ-mediated redox stress but might be an important regulator of $A\beta_{42}$ neurotoxicity. Furthermore, this study also points out that the regulation of redox homeostasis and its impact on diverse diseases like AD is very complex, sometimes even paradoxical and needs more critical examination (Table 17 - Table 20) (Le Gal et al. 2015; DeNicola et al. 2011). Taken together these data also demonstrate that we need to be cautious with manipulations of the antioxidant system in AD disease background without knowing all side effects emerging from changing the redox balance. Especially since clinical trials administrating antioxidants as potential treatment for AD at this point have not been very promising in slowing down AD progression (Mecocci & Polidori 2012; Galasko et al. 2012; Kryscio et al. 2017) and other studies link increased glutathione levels in MCI patients with increased cognitive impairment (Duffy et al. 2014). It might be very interesting to look at the cellular protein glutathionylation status, which has been reported to act protective against oxidative damage (Dalle-Donne et al. 2009) and found to be increased in AD patients (Newman et al. 2007). This might give more information about the exact mechanisms involved in glutathione-related $A\beta_{42}$ neurotoxicity (Dalle-Donne et al. 2009; Franco & Cidlowski 2009). The death receptor RAGE is a neuronal and glial cell-surface receptor for advanced glycation end products (AEGs) and has been shown to be involved in promoting the perturbation of cellular functions that result in oxidative stress and cytotoxicity (Yan et al. 1996). Investigating how death receptors could be involved in this might be an additional interesting aspect. Another approach might be the examination of the oxidation status of $A\beta_{42}$ in this model. Previous studies have shown that the oxidation of Aβ on Methionine 35 (Met^{OX}) on the one hand can prevent the formation of Aβ aggregates by reducing hydrophobic and electrostatic associations, which leads to changes in structure during the initial stages of aggregation (Hou et al. 2004) and on the other hand can decrease the amount and length of $A\beta_{40}$ and $A\beta_{42}$ fibers *in vitro* (Gu & Viles 2016). I observed an increased life span of $A\beta_{42}$ flies, when glutathione synthesis was decreased by downregulating Gclc via GclcRNAi (Figure 16A and A`). Maybe the lower levels of glutathione could result in more oxidation of $A\beta_{42}$, which might lead to a decreased amount of $A\beta_{42}$ fibers, which does not automatically must lead to less

neurotoxicity, but which could be an explanation of the observed increased life span of $A\beta_{42}$ flies. Performing detailed structural analysis of $A\beta_{42}$ in this model might be interesting for future studies. Whether an oxidative modification of Met35 in $A\beta_{42}$ could positively affect the outcome of disease progression in AD or could have a beneficial effect on $A\beta_{42}$ neurotoxicity *in vivo*, might also of interest in the future.

One limitation of this study is that the neuronal glutathione redox potential could not be decreased significantly by any genetic or pharmacologic manipulation tested here. This could hint to a very tight control of this pathway in neurons and point out its important relevance. But this information might give us insights whether a decrease in glutathione redox potential could further increase survival or improve cognitive functions such as learning or memory, respectively. Additional investigation could also include the analysis of any cognitive decline in $A\beta_{42}$ flies with and without Gclc-OE in order to test for a potential link between glutathione redox imbalance and redox-related cognitive dysfunction which would be very interesting to prospectively compare this with patient data. Deciphering the exact mechanism how the cell senses redox stress and translates it into downstream signaling events will be very exciting and of high importance to help combat AD. The developed models in this thesis offers the required *in vivo* tools to examine the link between glutathione redox potential and $A\beta_{42}$ neurotoxicity in more detailed and provides stimulating insights into the relevance of redox signaling processes associated with neurodegeneration that will hopefully give spark for follow up studies. Importantly, this model provides a suitable platform to help finding strategies for therapeutic approaches and therefore can be used for clinical applications including drug screenings or screenings for genetic modifiers involved in redox-associated mechanisms in AD.

7. Abbrevations

Aβ	Amyloid-beta
AD	Alzheimer´s Disease
AICD	APP intracellular domain
APP	amyloid precursor protein
BBB	blood brain barrier
BDSC	Bloomington *Drosophila* Stock Center
BSA	Bovine Serum Albumin
BSO	Buthionine Sulfoximine
DA	Diamide
DEM	Diethyl maleate
DMSO	Dimethyl sulfoxide
DR	dynamic range
DTT	Dithiothreitol
EDTA	Ethylenediaminetetraacetic acid
E_{GSH}	glutathione redox potential
ELISA	enzyme-linked immunosorbent assay
FBS	Fetal bovine serum
FTD	Frontotemporal dementia
Gclc	glutamate cysteine ligase catalytic subunit
GdnHCl	Guanidine hydrochloride
GFP	green fluorescent protein
Grx1	glutaredoxin 1
GSH	reduced glutathione
GSSG	oxidized glutathione
JNK	c-Jun N-terminal Kinase
LSM	Laser Scanning Microscope
MCI	mild cognitive impairment
NAC	N-acetyl-L-cysteine
NaN	not a number
NDGA	Nordihydroguaiaretic acid
NEM	N-ethyl maleimide
NFTs	neurofibrillary tangles

Nrf2	NF-E2-related factor-2
dNTPs	Nucleoside triphosphate
n.s.	not significant
OE	overexpression
Orp1	oxidant receptor peroxidase 1
OxD	degree of oxidation
PBS	Phosphate buffered saline
PCR	Polymerase chain reaction
p-FTAA	pentamer formyl thiophene acetic acid
RNAi	RNA interference
roGFP	reduction-oxidation sensitive green fluorescent protein
RT	room temperature
SDS	Sodium dodecyl sulfate
s.e.m.	standard error of the mean
SOD1/2	Superoxide dismutase 1/2
TAβ	Tandem Amyloid-beta
tBHQ	*tert*-Butylhydroquinone
TCA	L-4-Thiazolidinecarboxylic acid
ThS	Thioflavin S
UAS	Upstream Activating Sequence
VDRC	Vienna *Drosophila* Resource Center
v/v	volume/volume
w/v	weight/volume

8. List of Figures

9. References

Adler, V. et al., 1999. Regulation of JNK signaling by GSTp. *The EMBO journal*, 18(5), pp.1321–34.

Aguzzi, A. & O'Connor, T., 2010. Protein aggregation diseases: pathogenicity and therapeutic perspectives. *Nature reviews. Drug discovery*, 9(3), pp.237–248.

Albrecht, S.C. et al., 2011. In vivo mapping of hydrogen peroxide and oxidized glutathione reveals chemical and regional specificity of redox homeostasis. *Cell Metabolism*, 14(6), pp.819–829.

Alzheimer, A., 1907. Uber eine eigenartige Erkrankung der Hirnrinde. *Allg Zeitschr f Psychiatrie u Psych-Gerichtl Med*, 64(64), pp.146–8.

Andersen, J.K., 2004. Oxidative stress in neurodegeneration: cause or consequence? *Nature Medicine*, 10 Suppl(July), pp.S18–25.

Ansari, M.A. & Scheff, S.W., 2010. Oxidative stress in the progression of Alzheimer disease in the frontal cortex. *Journal of neuropathology and experimental neurology*, 69(2), pp.155–67.

Apelt, J. et al., 2004. Aging-related increase in oxidative stress correlates with developmental pattern of beta-secretase activity and beta-amyloid plaque formation in transgenic Tg2576 mice with Alzheimer-like pathology. *International Journal of Developmental Neuroscience*, 22(7), pp.475–484.

Aquilano, K., Baldelli, S. & Ciriolo, M.R., 2014. Glutathione: New roles in redox signalling for an old antioxidant. *Frontiers in Pharmacology*, 5 AUG(August), pp.1–12.

Åslund, A. et al., 2009. Novel pentameric thiophene derivatives for in vitro and in vivo optical imaging of a plethora of protein aggregates in cerebral amyloidoses. *ACS Chemical Biology*, 4(8), pp.673–684.

Atwood, C.S. et al., 2003. Amyloid-β: A chameleon walking in two worlds: A review of the trophic and toxic properties of amyloid-β. *Brain Research Reviews*, 43(1), pp.1–16.

Badía, M.-C. et al., 2013. Reductive stress in young healthy individuals at risk of Alzheimer disease. *Free radical biology & medicine*, 63(34), pp.274–9.

Barata, A.G. & Dick, T.P., 2013. *In vivo imaging of H2O2 production in Drosophila* 1st ed., Copyright © 2013 Elsevier, Inc. All rights reserved.

Behl, C. et al., 1994. Hydrogen peroxide mediates amyloid beta protein toxicity. *Cell*, 77(6), pp.817–827.

Bellen, H.J., Tong, C. & Tsuda, H., 2010. 100 years of Drosophila research and its impact on vertebrate neuroscience: a history lesson for the future. *Nature reviews. Neuroscience*, 11(7), pp.514–22.

Berg, I. et al., 2010. Efficient imaging of amyloid deposits in Drosophila models of human amyloidoses. *Nature protocols*, 5(5), pp.935–944.

Bermejo, P. et al., 2008. Peripheral levels of glutathione and protein oxidation as markers in the development of Alzheimer's disease from Mild Cognitive Impairment. *Free radical research*, 42(2), pp.162–170.

von Bernhardi, R. & Eugenín, J., 2012. Alzheimer's disease: redox dysregulation as a common denominator for diverse pathogenic mechanisms. *Antioxidants & redox signaling*, 16(9), pp.974–1031.

Bischof, J. et al., 2007. An optimized transgenesis system for Drosophila using germ-line-specific phiC31 integrases. *Proceedings of the National Academy of Sciences of the United States of America*, 104(9), pp.3312–7.

Bitan, G. et al., 2003. Amyloid beta -protein (Abeta) assembly: Abeta 40 and Abeta 42 oligomerize through distinct pathways. *Proceedings of the National Academy of Sciences of the United States of America*, 100(1), pp.330–5.

Biteau, B. et al., 2011. Regulation of Drosophila lifespan by JNK signaling. *Experimental Gerontology*, 46(5), pp.349–354.

Blennow, K., de Leon, M.J. & Zetterberg, H., 2006. Alzheimer's disease. *Lancet*, 368(9533), pp.387–403.

Block, M.L., Zecca, L. & Hong, J.S., 2007. Microglia-mediated neurotoxicity: uncovering the molecular mechanisms. *Nat Rev Neurosci*, 8(1), pp.57–69.

Boulianne, G.L. et al., 1997. Cloning and characterization of the Drosophila presenilin homologue. *Neuroreport*, 8(4), pp.1025–9.

Brand, A.H. & Dormand, E.L., 1995. The GAL4 system as a tool for unravelling the mysteries of the Drosophila nervous system. *Current opinion in neurobiology*, 5(5), pp.572–8.

Van Broeckhoven, C. et al., 1990. Amyloid beta protein precursor gene and hereditary cerebral hemorrhage with amyloidosis (Dutch). *Science (New York, N.Y.)*, 248(4959), pp.1120–2.

Burnouf, S. et al., 2015. Aβ43 is neurotoxic and primes aggregation of Aβ40 in vivo. *Acta neuropathologica*, 130(1), pp.35–47.

Butterfield, D.A. et al., 2001. Evidence of oxidative damage in Alzheimer ' s disease brain : central role for amyloid β -peptide. *Trends in Molecular Medicine*, 7(12), pp.548–554.

Butterfield, D.A. et al., 2007. Roles of amyloid ??-peptide-associated oxidative stress and brain protein modifications in the pathogenesis of Alzheimer's disease and mild cognitive impairment. *Free Radical Biology and Medicine*, 43(5), pp.658–677.

Cai, Z., Zhao, B. & Ratka, A., 2011. Oxidative stress and ??-amyloid protein in Alzheimer's disease. *NeuroMolecular Medicine*, 13(4), pp.223–250.

Cao, W. et al., 2008. Identification of novel genes that modify phenotypes induced by Alzheimer's β-amyloid overexpression in Drosophila. *Genetics*, 178(3), pp.1457–1471.

Chan, H.Y.E. & Bonini, N.M., 2000. Drosophila models of human neurodegenerative disease. *Cell Death & Differentiation*, 7(11), pp.1075–1080.

Chartier-Harlin, M.C. et al., 1991. Early-onset Alzheimer's disease caused by mutations at codon 717 of the beta-amyloid precursor protein gene. *Nature*, 353(6347), pp.844–846.

Chatterjee, N. & Bohmann, D., 2012. A versatile φC31 based reporter system for measuring AP-1 and NRF2 signaling in Drosophila and in tissue culture. *PLoS ONE*, 7(4).

Chen, T.S., Richie Jr., J.P. & Lang, C.A., 1989. The effect of aging on glutathione and cysteine levels in different regions of the mouse brain. *Proc Soc Exp Biol Med*, 190(4), pp.399–402.

Chen, Y.-R. & Glabe, C.G., 2006. Distinct Early Folding and Aggregation Properties of Alzheimer Amyloid-β Peptides Aβ40 and Aβ42. *Journal of Biological Chemistry*, 281(34), pp.24414–24422.

Chételat, G. et al., 2010. Relationship between atrophy and beta-amyloid deposition in Alzheimer disease. *Annals of neurology*, 67(3), pp.317–24.

Circu, M.L. & Aw, T.Y., 2012. Glutathione and modulation of cell apoptosis. *Biochimica et biophysica acta*, 1823(10), pp.1767–77.

Coffey, E.T., 2014. Nuclear and cytosolic JNK signalling in neurons. *Nature reviews. Neuroscience*, 15(5), pp.285–99.

Crowther, D.C. et al., 2005. Intraneuronal Aβ, non-amyloid aggregates and neurodegeneration in a Drosophila model of Alzheimer's disease. *Neuroscience*, 132(1), pp.123–135.

Currais, A. & Maher, P., 2013. Functional consequences of age-dependent changes in glutathione status in the brain. *Antioxidants & redox signaling*, 19(8), pp.813–22.

Dalle-Donne, I. et al., 2009. Protein S-glutathionylation: a regulatory device from bacteria to humans. *Trends in Biochemical Sciences*, 34(2), pp.85–96.

Dawson, H.N. et al., 2010. Loss of tau elicits axonal degeneration in a mouse model of Alzheimer's disease. *Neuroscience*, 169(1), pp.516–531.

DeNicola, G.M. et al., 2011. Oncogene-induced Nrf2 transcription promotes ROS detoxification and tumorigenesis. *Nature*, 475(7354), pp.106–9.

Dietzl, G. et al., 2007. ARTICLES A genome-wide transgenic RNAi library for conditional gene

inactivation in Drosophila. , 448(July).

Di Domenico, F. et al., 2015. Strategy to reduce free radical species in Alzheimer's disease: an update of selected antioxidants. *Expert Review of Neurotherapeutics*, 15(1), pp.19–40.

Dooley, C.T. et al., 2004. Imaging dynamic redox changes in mammalian cells with green fluorescent protein indicators. *Journal of Biological Chemistry*, 279(21), pp.22284–22293.

Dringen, R., 2000. Metabolism and functions of glutathion in brain. *Progress in Neurobiology*, 62, pp.33–57.

Dringen, R., Kussmaul, L., et al., 1999. The glutathione system of peroxide detoxification is less efficient in neurons than in astroglial cells. *Journal of Neurochemistry*, 72(6), pp.2523–2530.

Dringen, R., Pfeiffer, B. & Hamprecht, B., 1999. Synthesis of the Antioxidant Glutathione in Neurons: Supply by Astrocytes of CysGly as Precursor for Neuronal Glutathione. *The Journal of Neuroscience*, 19(2), pp.562–569.

Duce, J.A. et al., 2010. Iron-Export Ferroxidase Activity of β-Amyloid Precursor Protein is Inhibited by Zinc in Alzheimer's Disease. *Cell*, 142(6), pp.857–867.

Duffy, S.L. et al., 2014. Glutathione relates to neuropsychological functioning in mild cognitive impairment. *Alzheimer's and Dementia*, 10(1), pp.67–75.

Dumont, M. et al., 2009. Reduction of oxidative stress, amyloid deposition, and memory deficit by manganese superoxide dismutase overexpression in a transgenic mouse model of Alzheimer's disease. *The FASEB Journal*, 23(8), pp.2459–2466.

Dysken, M.W. et al., 2014. A Randomized, Clinical Trial of Vitamin E and Memantine in Alzheimer's Disease (TEAM-AD). *Jama*, 311(1), pp.33–44.

Eroglu, E. et al., 2016. Development of novel FP-based probes for live-cell imaging of nitric oxide dynamics. *Nature Communications*, 7, p.10623.

Eruslanov, E. & Kusmartsev, S., 2010. Identification of ROS using oxidized DCFDA and flow-cytometry. *Methods in molecular biology (Clifton, N.J.)*, 594, pp.57–72.

Ferrer, I. et al., 2001. Phosphorylated mitogen-activated protein kinase (MAPK/ERK-P), protein kinase of 38kDa (p38-P), stress-activated protein kinase (SAPK/JNK-P), and calcium/calmodulin-dependent kinase II (CaM kinase II) are differentially expressed in tau deposits in neurons. *Journal of Neural Transmission*, 108(12), pp.1397–1415.

Finelli, A. et al., 2004. A model for studying Alzheimer's Abeta42-induced toxicity in Drosophila melanogaster. *Molecular and cellular neurosciences*, 26(3), pp.365–75.

Finkel, T., 1998. Oxygen radicals and signaling. *Current Opinion in Cell Biology*, 10(2), pp.248–253.

Finkel, T. & Holbrook, N.J., 2000. Oxidants, oxidative stress and the biology of ageing. *Nature*, 408(6809), pp.239–247.

Franco, R. & Cidlowski, J. a, 2009. Apoptosis and glutathione: beyond an antioxidant. *Cell death and differentiation*, 16(10), pp.1303–1314.

Franco, R., Panayiotidis, M.I. & Cidlowski, J.A., 2007. Glutathione depletion is necessary for apoptosis in lymphoid cells independent of reactive oxygen species formation. *The Journal of biological chemistry*, 282(42), pp.30452–65.

Fratelli, M. et al., 2005. Gene expression profiling reveals a signaling role of glutathione in redox regulation. *Proc Natl Acad Sci U S A*, 102(39), pp.13998–14003.

Fujikawa, Y. et al., 2016. Mouse redox histology using genetically encoded probes. *Science Signaling*, 9(419 rs1), pp.1–10.

Furuta, A. et al., 1995. Localization of superoxide dismutases in Alzheimer's disease and Down's syndrome neocortex and hippocampus. *The American journal of pathology*, 146(2), pp.357–67.

Le Gal, K. et al., 2015. Antioxidants can increase melanoma metastasis in mice. *Science Translational*

Medicine, 7(308), pp.308re8–308re8.

Galasko, D.R. et al., 2012. Antioxidants for Alzheimer disease: a randomized clinical trial with cerebrospinal fluid biomarker measures. *Arch Neurol*, 69(7), pp.836–841.

Gella, A. & Durany, N., 2009. Oxidative stress in Alzheimer disease. *Cell adhesion & migration*, 3(1), pp.88–93.

Goate, A., 2006. Segregation of a missense mutation in the amyloid beta-protein precursor gene with familial Alzheimer's disease. *Journal of Alzheimer's disease : JAD*, 9(3 Suppl), pp.341–347.

Goedert, M., 2009. Oskar Fischer and the study of dementia. *Brain*, 132(4), pp.1102–1111.

Goedert, M., Sisodia, S.S. & Price, D.L., 1991. Neurofibrillary tangles and beta-amyloid deposits in Alzheimer's disease. *Current opinion in neurobiology*, 1(3), pp.441–7.

Goedert, M. & Spillantini, M.G., 2000. Tau mutations in frontotemporal dementia FTDP-17 and their relevance for Alzheimer's disease. *Biochimica et Biophysica Acta - Molecular Basis of Disease*, 1502(1), pp.110–121.

Götz, J. & Ittner, L.M., 2008. Animal models of Alzheimer's disease and frontotemporal dementia. *Nature Reviews Neuroscience*, 9(7), pp.532–544.

Gough, D.R. & Cotter, T.G., 2011. Hydrogen peroxide: a Jekyll and Hyde signalling molecule. *Cell death & disease*, 2(10), p.e213.

Greene, J.C. et al., 2005. Genetic and genomic studies of Drosophila parkin mutants implicate oxidative stress and innate immune responses in pathogenesis. *Human Molecular Genetics*, 14(6), pp.799–811.

Grundke-Iqbal, I. et al., 1987. Abnormal phosphorylation of the microtubule-associated protein? (tau) in Alzheimer cytoskeletal pathology. *Alzheimer Disease & Associated Disorders*, 1(3), p.202.

Gsell, W. et al., 1995. Decreased catalase activity but unchanged superoxide dismutase activity in brains of patients with dementia of Alzheimer type. *Journal of neurochemistry*, 64(3), pp.1216–1223.

Gu, M. & Viles, J.H., 2016. Methionine oxidation reduces lag-times for amyloid-??(1???40) fiber formation but generates highly fragmented fibers. *Biochimica et Biophysica Acta - Proteins and Proteomics*, 1864(9), pp.1260–1269.

Guan, L. & Kaback, H.R., 2007. Site-directed alkylation of cysteine to test solvent accessibility of membrane proteins. *Nature protocols*, 2(8), pp.2012–2017.

Gutscher, M. et al., 2013. Real-time imaging of the intracellular glutathione redox potential. *Chemosphere*, 35(6), pp.461–473.

Haass, C. & Selkoe, D.J., 2007. Soluble protein oligomers in neurodegeneration: Lessons from the Alzheimer's amyloid β-peptide. *Nature Reviews Molecular Cell Biology*, 8(2), pp.101–112.

Hamanaka, R.B. & Chandel, N.S., 2010. Mitochondrial reactive oxygen species regulate cellular signaling and dictate biological outcomes. *Trends in Biochemical Sciences*, 35(9), pp.505–513.

Hardy, J., 1997. Amyloid, the presenilins and Alzheimer's disease. *Trends in neurosciences*, 20(4), pp.154–9.

Hardy, J. et al., 1998. Genetic dissection of Alzheimer's disease and related dementias: amyloid and its relationship to tau. *Nature neuroscience*, pp.355–8.

Hardy, J., 2002. The Amyloid Hypothesis of Alzheimer's Disease: Progress and Problems on the Road to Therapeutics. *Science*, 297(5580), pp.353–356.

Hardy, J. & Allsop, D., 1991. Amyloid deposition as the central event in the aetiology of Alzheimer's disease. *Trends in Pharmacological Sciences*, 12(C), pp.383–388.

Hardy, J. & Allsop, D., 1991. Amyloid Deposition As the Central Event in the Etiology of Alzheimers-Disease. *Trends in Pharmacological Sciences*, 12(10), pp.383–388.

Hardy, J. & Selkoe, D.J., 2002. The Amyloid Hypothesis of Alzheimer's Disease: Progress and Problems on the Road to Therapeutics. *Science*, 297(5580), pp.353–356.

Harman, D., 1956. Aging: A Theory Based on Free Radical and Radiation Chemistry. *Journal of Gerontology*, 11(3), pp.298–300.

HARMAN, D., 1972. The Biologic Clock: The Mitochondria? *Journal of the American Geriatrics Society*, 20(4), pp.145–147.

Harris, M.E. et al., 1995. Direct evidence of oxidative injury produced by the Alzheimer's β-Amyloid peptide (1–40) in cultured hippocampal neurons. *Experimental Neurology*, 131(2), pp.193–202.

Harzer, H. et al., 2013. FACS purification of Drosophila larval neuroblasts for next-generation sequencing. *Nature protocols*, 8(6), pp.1088–99.

Hashimoto, Y. et al., 2002. Neurotoxic mechanisms triggered by Alzheimer's disease-linked mutant M146L presenilin 1: Involvement of NO synthase via a novel pertussis toxin target. *Journal of Neurochemistry*, 80(3), pp.426–437.

Heneka, M.T., Kummer, M.P. & Latz, E., 2014. Innate immune activation in neurodegenerative disease. *Nat. Rev. Immunol.*, 14(7), pp.463–477.

Hirrlinger, J. et al., 2001. The multidrug resistance protein MRP1 mediates the release of glutathione disul®de from rat astrocytes during oxidative stress. *International Society for Neurochemistry Journal of Neurochemistry 627±636 Journal of Neurochemistry J. Neurochem*, 76(76), pp.627–636.

Holtzman, D.M., Morris, J.C. & Goate, A.M., 2011. Alzheimer ' s Disease : The Challenge of the Second Century. *Science Translational Medicine*, 3(77), pp.1–35.

Hong, C.S. & Koo, E.H., 1997. Isolation and characterization of Drosophila presenilin homolog. *Neuroreport*, 8(3), pp.665–8.

Hou, L. et al., 2004. Solution NMR Studies of the A??(1-40) and A??(1-42) Peptides Establish that the Met35 Oxidation State Affects the Mechanism of Amyloid Formation. *Journal of the American Chemical Society*, 126(7), pp.1992–2005.

Hutton, M. et al., 1998. Association of missense and 5'-splice-site mutations in tau with the inherited dementia FTDP-17. *Nature*, 393(6686), pp.702–704.

Iijima, K. et al., 2004. Dissecting the pathological effects of human A beta 40 and A beta 42 in Drosophila: A potential model for Alzheimer's disease. *Proceedings of the National Academy of Sciences of the United States of America*, 101(17), pp.6623–6628.

Iwata-Ichikawa, E. et al., 1999. Glial cells protect neurons against oxidative stress via transcriptional up-regulation of the glutathione synthesis. *Journal of Neurochemistry*, 72(6), pp.2334–2344.

Jang, J.H. & Surh, Y.J., 2002. beta-Amyloid induces oxidative DNA damage and cell death through activation of c-Jun N terminal kinase. *Ann N Y Acad Sci*, 973, pp.228–236.

Jucker, M. & Walker, L.C., 2013. Self-propagation of pathogenic protein aggregates in neurodegenerative diseases. *Nature*, 501(7465), pp.45–51.

Kadowaki, H. et al., 2005. Amyloid β induces neuronal cell death through ROS-mediated ASK1 activation. *Cell Death and Differentiation*, 12(1), pp.19–24.

Kang, D.E. et al., 2000. Modulation of amyloid β-protein clearance and Alzheimer's disease susceptibility by the LDL receptor-related protein pathway. *Journal of Clinical Investigation*, 106(9), pp.1159–1166.

Karran, E., Mercken, M. & De Strooper, B., 2011. The amyloid cascade hypothesis for Alzheimer's disease: an appraisal for the development of therapeutics. *Nature reviews. Drug discovery*, 10(9), pp.698–712.

Keller, J. et al., 2005. Evidence of increased oxidative damage in subjects with mild cognitive impairment. *Neurology*, 64(7), pp.1152–1156.

Kennedy, M.E. et al., 2016. The BACE1 inhibitor verubecestat (MK-8931) reduces CNS β-amyloid in animal models and in Alzheimer's disease patients. *Science translational medicine*, 8(363),

p.363ra150.

Knott, A.B. et al., 2008. Mitochondrial fragmentation in neurodegeneration. *Nature reviews. Neuroscience*, 9(7), pp.505–18.

Kojima, H. et al., 1998. Detection and imaging of nitric oxide with novel fluorescent indicators: diaminofluoresceins. *Anal. Chem.*, 70(13), pp.2446–2453.

Kryscio, R.J. et al., 2017. Association of Antioxidant Supplement Use and Dementia in the Prevention of Alzheimer's Disease by Vitamin E and Selenium Trial (PREADViSE). *JAMA Neurology*, 74(5), p.567.

Kuperstein, I. et al., 2010. Neurotoxicity of Alzheimer's disease Aβ peptides is induced by small changes in the Aβ42 to Aβ40 ratio. *The EMBO journal*, 29(19), pp.3408–20.

Laborde, E., 2010. Glutathione transferases as mediators of signaling pathways involved in cell proliferation and cell death. *Cell death and differentiation*, 17(9), pp.1373–1380.

Lacher, S.E. et al., 2016. network. , 88, pp.452–465.

Lai, S.-L. & Lee, T., 2006. Genetic mosaic with dual binary transcriptional systems in Drosophila. *Nature neuroscience*, 9(5), pp.703–9.

Lambert, M.P. et al., 1998. Diffusible, nonfibrillar ligands derived from A 1-42 are potent central nervous system neurotoxins. *Proceedings of the National Academy of Sciences*, 95(11), pp.6448–6453.

Lessing, D. & Bonini, N.M., 2009. Maintaining the brain: insight into human neurodegeneration from Drosophila melanogaster mutants. *Nature reviews. Genetics*, 10(6), pp.359–370.

LeVine, H., 1999. Quantification of β-sheet amyloid fibril structures with thioflavin T. *Methods in Enzymology*, 309, pp.274–284.

Levy, E. et al., 1990. Mutation of the Alzheimer's disease amyloid gene in hereditary cerebral hemorrhage, Dutch type. *Science (New York, N.Y.)*, 248(4959), pp.1124–6.

Lewis, J. et al., 2001. Enhanced neurofibrillary degeneration in transgenic mice expressing mutant tau and APP. *Science*, 293(5534), pp.1487–1491.

Lewis, J. et al., 2001. Neurofibrillary Degeneration in Transgenic Mice Expressing Mutant. , 293(5534), pp.1487–1491.

Li, F. et al., 2004. Increased plaque burden in brains of APP mutant MnSOD heterozygous knockout mice. *Journal of Neurochemistry*, 89(5), pp.1308–1312.

Liddelow, S.A. et al., 2017. Neurotoxic reactive astrocytes are induced by activated microglia. *Nature*, 541(7638), pp.481–487.

Lin, M.T. & Beal, M.F., 2006. Mitochondrial dysfunction and oxidative stress in neurodegenerative diseases. *Nature*, 443(7113), pp.787–795.

Liu, J. & Lin, A., 2005. Role of JNK activation in apoptosis: a double-edged sword. *Cell research*, 15(1), pp.36–42.

Liu, L. et al., 2015. Glial lipid droplets and ROS induced by mitochondrial defects promote neurodegeneration. *Cell*, 160(1-2), pp.177–190.

Lloret, A. et al., 2016. Reductive Stress: A New Concept in Alzheimer's Disease. *Current Alzheimer research*, 13(2), pp.206–11.

Luchak, J.M. et al., 2007. Modulating longevity in Drosophila by over- and underexpression of glutamate-cysteine ligase. *Annals of the New York Academy of Sciences*, 1119(1), pp.260–273.

Luheshi, L.M. et al., 2007. Systematic in vivo analysis of the intrinsic determinants of amyloid β pathogenicity. *PLoS Biology*, 5(11), pp.2493–2500.

Mallik, A., Drzezga, A. & Minoshima, S., 2017. Clinical Amyloid Imaging. *Seminars in Nuclear Medicine*, 47(1), pp.31–43.

Mandal, P.K. et al., 2015. Brain glutathione levels--a novel biomarker for mild cognitive impairment and

Alzheimer's disease. *Biological psychiatry*, 78(10), pp.702–10.

Mandelkow, E.-M.M. and E., 2012. Biochemistry and cell biology of tau protein in neurofibrillart degeneration. *Cold Spring Harb Perspect Med*, 2(5), p.a006247.

Mangialasche, F. et al., 2009. Biomarkers of oxidative and nitrosative damage in Alzheimer's disease and mild cognitive impairment. *Ageing Research Reviews*, 8(4), pp.285–305.

Manning, A.M. & Davis, R.J., 2003. Targeting JNK for therapeutic benefit: from junk to gold? *Nat Rev Drug Discov*, 2(7), pp.554–565.

Marques, C.A. et al., 2003. Neurotoxic mechanisms caused by the alzheimer's disease-linked Swedish amyloid precursor protein. Mutation oxidative stress, caspases, and the JNK pathway. *Journal of Biological Chemistry*, 278(30), pp.28294–28302.

Matsuoka, Y. et al., 2001. Fibrillar beta-amyloid evokes oxidative damage in a transgenic mouse model of Alzheimer's disease. *NEUROSCIENCE*, 104(3), pp.609–613.

Mawuenyega, K.G. et al., 2010. Decreased Clearance of CNS -Amyloid in Alzheimer's Disease. *Science*, 330(6012), pp.1774–1774.

McGurk, L., Berson, A. & Bonini, N.M., 2015. Drosophila as an in vivo model for human neurodegenerative disease. *Genetics*, 201(2), pp.377–402.

McKhann, G. et al., 1984. Clinical diagnosis of Alzheimer's disease: Report of the NINCDS-ADRDA Work Group* under the auspices of Department of Health and Human Services Task Force on Alzheimer's Disease. *Neurology*, 34(7), pp.939–939.

Mecocci, P. & Polidori, M.C., 2012. Antioxidant clinical trials in mild cognitive impairment and Alzheimer's disease. *Biochimica et Biophysica Acta (BBA) - Molecular Basis of Disease*, 1822(5), pp.631–638.

Meyer-Luehmann, M. et al., 2008. Exogenous Induction of Cerebal beta-Amyloidogenesis is Governed by Agent and Host. *Science*, 313(September), pp.1781–1784.

Meyer, a J. & Dick, T.P., 2010. Fluorescent protein-based redox probes. *Antioxid Redox Signal*, 13(5), pp.621–650.

Miquel, J., Fleming, J. & Economos, A.C., 1982. Antioxidants, metabolic rate and aging in Drosophila. *Archives of Gerontology and Geriatrics*, 1(2), pp.159–165.

Mohmmad Abdul, H. et al., 2006. Mutations in amyloid precursor protein and presenilin-1 genes increase the basal oxidative stress in murine neuronal cells and lead to increased sensitivity to oxidative stress mediated by amyloid β-peptide (1-42), H2O2and kainic acid: Implications for Al. *Journal of Neurochemistry*, 96(5), pp.1322–1335.

Morgan, B., 2012. Multiple glutathione disulfide removal pathways mediate cytosolic redox homeostasis. , (deCeMBer).

Morgan, T.H., 1910. Sex Limited Inheritance in Drosophila. *Science*, 32(812), pp.120–122.

Morishima, Y. et al., 2001. Beta-amyloid induces neuronal apoptosis via a mechanism that involves the c-Jun N-terminal kinase pathway and the induction of Fas ligand. *The Journal of Neuroscience*, 21(19), pp.7551–7560.

Morris, G.P., Clark, I. a & Vissel, B., 2014. Inconsistencies and controversies surrounding the amyloid hypothesis of Alzheimer's disease. *Acta neuropathologica communications*, 2, p.135.

Murakami, K. et al., 2011. SOD1 (copper/zinc superoxide dismutase) deficiency drives amyloid β protein oligomerization and memory loss in mouse model of Alzheimer disease. *Journal of Biological Chemistry*, 286(52), pp.44557–44568.

Nalivaeva, N.N. & Turner, A.J., 2013. The amyloid precursor protein: A biochemical enigma in brain development, function and disease. *FEBS Letters*, 587(13), pp.2046–2054.

Naslund, J. et al., 2000. Correlation Between Elevated Levels of Amyloid β-Peptide in the Brain and

Cognitive Decline. *Jama*, 283(12), pp.1571–1577.

Newman, S.F. et al., 2007. An Increase in S-Glutathionylated Proteins in the Alzheimer ' s Disease Inferior Parietal Lobule , a Proteomics Approach. , 1514(March), pp.1506–1514.

Nunomura, A. et al., 2006. Involvement of oxidative stress in Alzheimer disease. *Journal of Neuropathology and Experimental Neurology*, 65(7), pp.631–641.

Oddo, S., Caccamo, A., Kitazawa, M., et al., 2003. Amyloid deposition precedes tangle formation in a triple transgenic model of Alzheimer's disease. *Neurobiology of Aging*, 24(8), pp.1063–1070.

Oddo, S., Caccamo, A., Shepherd, J.D., et al., 2003. Triple-transgenic model of Alzheimer's Disease with plaques and tangles: Intracellular Aβ and synaptic dysfunction. *Neuron*, 39(3), pp.409–421.

Omar, R. a. et al., 1999. Increased Expression but Reduced Activity of Antioxidant Enzymes in Alzheimer's Disease. *Journal of Alzheimer's disease : JAD*, 1(3), pp.139–145.

Orr, W.C. et al., 2005. Overexpression of glutamate-cysteine ligase extends life span in Drosophila melanogaster. *Journal of Biological Chemistry*, 280(45), pp.37331–37338.

Padurariu, M. et al., 2010. Changes of some oxidative stress markers in the serum of patients with mild cognitive impairment and Alzheimer's disease. *Neuroscience Letters*, 469(1), pp.6–10.

Pearson, H.A. & Peers, C., 2006. Physiological roles for amyloid β peptides. *The Journal of Physiology*, 575(1), pp.5–10.

Perez-Nievas, B.G. et al., 2013. Dissecting phenotypic traits linked to human resilience to Alzheimer's pathology. *Brain*, 136(8), pp.2510–2526.

Pfeiffer, B.D. et al., 2010. Refinement of tools for targeted gene expression in Drosophila. *Genetics*, 186(2), pp.735–755.

Piper, M.D.W. et al., 2014. Europe PMC Funders Group Europe PMC Funders Author Manuscripts A holidic medium for Drosophila melanogaster. , 11(1), pp.1–19.

Plaine, H.L., 1955. The Effect of Oxygen and of Hydrogen Peroxide on the Action of a Specific Gene and on Tumor Induction in Drosophila Melanogaster. *Genetics*, 40(2), pp.268–280.

Plant, L.D. et al., 2003. The production of amyloid beta peptide is a critical requirement for the viability of central neurons. *The Journal of neuroscience : the official journal of the Society for Neuroscience*, 23(13), pp.5531–5535.

Poorkaj, P. et al., 1998. Tau is a candidate gene for chromosome 17 frontotemporal dementia. *Annals of neurology*, 43(6), pp.815–825.

Praticò, D. et al., 2001. Increased Lipid Peroxidation Precedes Amyloid Plaque Formation in an Animal Model of Alzheimer Amyloidosis. *The Journal of Neuroscience*, 21(12), pp.4183–4187.

Priller, C. et al., 2006. Synapse Formation and Function Is Modulated by the Amyloid Precursor Protein. *Journal of Neuroscience*, 26(27), pp.7212–7221.

Rajendran, L. & Annaert, W., 2012. Membrane Trafficking Pathways in Alzheimer's Disease. *Traffic*, 13(6), pp.759–770.

Rebrin, I. et al., 2004. Free aminothiols, glutathione redox state and protein mixed disulphides in aging Drosophila melanogaster. *The Biochemical journal*, 382, pp.131–136.

Rival, T. et al., 2009. Fenton chemistry and oxidative stress mediate the toxicity of the -amyloid peptide in a Drosophila model of Alzheimer's disease. *European Journal of Neuroscience*, 29(7), pp.1335–1347.

Robinson, K.M., Janes, M.S. & Beckman, J.S., 2008. The selective detection of mitochondrial superoxide by live cell imaging. *Nature protocols*, 3(6), pp.941–947.

Rosén, C. et al., 2013. Fluid biomarkers in Alzheimer's disease – current concepts. *Molecular Neurodegeneration*, 8(1), p.20.

Rosen, D.R. et al., 1989. A Drosophila gene encoding a protein resembling the human beta-amyloid

protein precursor. *Proceedings of the National Academy of Sciences of the United States of America*, 86(7), pp.2478–82.

Russell, R.L. et al., 1999. Increased neuronal glucose-6-phosphate dehydrogenase and sulfhydryl levels indicate reductive compensation to oxidative stress in Alzheimer disease. *Archives of Biochemistry and Biophysics*, 370(2), pp.236–239.

Sagara, J., Miura, K. & Bannai, S., 1993. Maintenance of Neuronal Glutathione by Glial Cells. *Journal of Neurochemistry*, 61(5), pp.1672–1676.

Saido, T. & Leissring, M.A., 2012. Proteolytic degradation of amyloid ??-protein. *Cold Spring Harbor Perspectives in Medicine*, 2(6), pp.1–18.

Sang, T.-K. & Jackson, G.R., 2005. Drosophila models of neurodegenerative disease. *NeuroRx : the journal of the American Society for Experimental NeuroTherapeutics*, 2(3), pp.438–46.

Sano, M. et al., 1997. A Controlled Trial of Selegiline, Alpha-Tocopherol, or Both as Treatment for Alzheimer's Disease. *New England Journal of Medicine*, 336(17), pp.1216–1222.

Sayin, V.I. et al., 2014. Antioxidants accelerate lung cancer progression in mice. *Science translational medicine*, 6(221), p.221ra15.

Sayre, L.M. et al., 1997. 4-Hydroxynonenal-derived advanced lipid peroxidation end products are increased in Alzheimer's disease. *Journal of neurochemistry*, 68(5), pp.2092–2097.

Schindelin, J. et al., 2012. Fiji: an open-source platform for biological-image analysis. *Nature Methods*, 9(7), pp.676–682.

Sclip, A. et al., 2014. c-Jun N-terminal kinase has a key role in Alzheimer disease synaptic dysfunction in vivo. *Cell death & disease*, 5(1), p.e1019.

Selkoe, D.J. & Wolfe, M.S., 2007. Presenilin: Running with Scissors in the Membrane. *Cell*, 131(2), pp.215–221.

Sepp, K.J., Schulte, J. & Auld, V.J., 2001. Peripheral glia direct axon guidance across the CNS/PNS transition zone. *Developmental biology*, 238(1), pp.47–63.

Serrano-Pozo, A. et al., 2011. Neuropathological alterations in Alzheimer disease. *Cold Spring Harbor perspectives in medicine*, 1(1), pp.1–24.

Sherrington, R. et al., 1995. Cloning of a gene bearing missense mutations in early-onset familial Alzheimer's disease. *Nature*, 375(6534), pp.754–760.

Shoji, M. et al., 2000. JNK activation is associated with intracellular beta-amyloid accumulation. *Brain research. Molecular brain research*, 85(1-2), pp.221–233.

Shulman, J.M. & Feany, M.B., 2003. Genetic modifiers of tauopathy in Drosophila. *Genetics*, 165(3), pp.1233–42.

Sies, H., 2015. Oxidative stress: A concept in redox biology and medicine. *Redox Biology*, 4, pp.180–183.

Sies, H., 1997. Oxidative stress: oxidants and antioxidants. *Experimental Physiology*, 82(2), pp.291–295.

SIES, H., 1993. Strategies of antioxidant defense. *European Journal of Biochemistry*, 215(2), pp.213–219.

Sloane, J.A. et al., 1997. Lack of correlation between plaque burden and cognition in the aged monkey. *Acta Neuropathologica*, 94(5), pp.471–478.

Smith, I.F. et al., 2004. Hypoxic remodelling of Ca2+ mobilization in type I cortical astrocytes: involvement of ROS and pro-amyloidogenic APP processing. *J Neurochem*, 88(4), pp.869–877.

Smith, M. a et al., 1998. Amyloid-beta deposition in Alzheimer transgenic mice is associated with oxidative stress. *Journal of neurochemistry*, 70(5), pp.2212–2215.

Snyder, S.W. et al., 1994. Amyloid-beta aggregation: selective inhibition of aggregation in mixtures of amyloid with different chain lengths. *Biophysical journal*, 67(3), pp.1216–28.

Sobotta, M.C. et al., 2014. Peroxiredoxin-2 and STAT3 form a redox relay for H2O2 signaling. *Nature chemical biology*, 11(november), pp.1–16.

Sowade, R.F. & Jahn, T.R., Seed-induced acceleration of amyloid-β mediated neurotoxicity in vivo. *Nature Communications*, pp.1–12.

Speretta, E. et al., 2012. Expression in Drosophila of tandem amyloid β peptides provides insights into links between aggregation and neurotoxicity. *Journal of Biological Chemistry*, 287(24), pp.20748–20754.

Steele, M.L. et al., 2013. Effect of Nrf2 activators on release of glutathione, cysteinylglycine and homocysteine by human U373 astroglial cells. *Redox Biology*, 1(1), pp.441–445.

Stephan, B.C.M. et al., 2012. The neuropathological profile of mild cognitive impairment (MCI): a systematic review. *Molecular psychiatry*, 17(11), pp.1056–76.

Stover, K.R. et al., 2015. Early detection of cognitive deficits in the 3xTg-AD mouse model of Alzheimer's disease. *Behavioural Brain Research*, 289, pp.29–38.

De Strooper, B. & Karran, E., 2016. The Cellular Phase of Alzheimer's Disease. *Cell*, 164(4), pp.603–615.

Sultana, R., Perluigi, M., Allan Butterfield, D., 2013. Lipid peroxidation triggersneurodegeneration: a redox proteomics view into the Alzheimer disease brain. *Free Radic. Biol. Med.*, 62(157-169), pp.157–169.

Sung, S. et al., 2004. Early vitamin E supplementation in young but not aged mice reduces AB levels and amyloid deposition in a transgenic model of Alzheimer's disease. *Faseb*, 18(2), pp.323–325.

Sykiotis, G.P. & Bohmann, D., 2008. Keap1/Nrf2 Signaling Regulates Oxidative Stress Tolerance and Lifespan in Drosophila. *Developmental Cell*, 14(1), pp.76–85.

Tabner, B.J. et al., 2005. Hydrogen peroxide is generated during the very early stages of aggregation of the amyloid peptides implicated in Alzheimer disease and familial British dementia. *Journal of Biological Chemistry*, 280(43), pp.35789–35792.

Tare, M. et al., 2011. Activation of JNK signaling mediates amyloid-β-dependent cell death. *PLoS ONE*, 6(9), pp.1–12.

Thal, D.R. et al., 2002. Phases of A beta-deposition in the human brain and its relevance for the development of AD. *Neurology*, 58(12), pp.1791–800.

Turner, P.R. et al., 2003. *Roles of amyloid precursor protein and its fragments in regulating neural activity, plasticity and memory*,

del Valle Rodríguez, A., Didiano, D. & Desplan, C., 2011. Power tools for gene expression and clonal analysis in Drosophila. *Nature Methods*, 9(1), pp.47–55.

Veal, E.A., Day, A.M. & Morgan, B.A., 2007. Hydrogen Peroxide Sensing and Signaling. *Molecular Cell*, 26(1), pp.1–14.

Venken, K.J.T., Simpson, J.H. & Bellen, H.J., 2011. Genetic manipulation of genes and cells in the nervous system of the fruit fly. *Neuron*, 72(2), pp.202–230.

Verri, M. et al., 2012. Mitochondrial alterations, oxidative stress and neuroinflammation in Alzheimer's disease. *International Journal of Immunopathology and Pharmacology*, 25(2), pp.345–353.

Vodovotz, Y. et al., 1996. Inducible nitric oxide synthase in tangle-bearing neurons of patients with Alzheimer's disease. *The Journal of experimental medicine*, 184(4), pp.1425–33.

Walsh, D.M. et al., 2002. Naturally secreted oligomers of amyloid β protein potently inhibit hippocampal long-term potentiation in vivo. *Nature*, 416(6880), pp.535–539.

Wang, M.C., Bohmann, D. & Jasper, H., 2003. JNK signaling confers tolerance to oxidative stress and extends lifespan in Drosophila. *Developmental Cell*, 5(5), pp.811–816.

Weingarten, M.D. et al., 1975. A protein factor essential for microtubule assembly. *Proceedings of the National Academy of Sciences of the United States of America*, 72(5), pp.1858–62.

de Wilde, A. et al., 2017. Alzheimer's biomarkers in daily practice (ABIDE) project: Rationale and design.

Alzheimer's and Dementia: Diagnosis, Assessment and Disease Monitoring, 6, pp.143–151.

Wu, H., Wang, M.C. & Bohmann, D., 2009. JNK protects Drosophila from oxidative stress by trancriptionally activating autophagy. *Mechanisms of Development*, 126(8-9), pp.624–637.

Wu, J.S. & Luo, L., 2006. A protocol for dissecting Drosophila melanogaster brains for live imaging or immunostaining. *Nature protocols*, 1(4), pp.2110–2115.

Wyss-Coray, T. & Mucke, L., 2002. Inflammation in neurodegenerative disease - A double-edged sword. *Neuron*, 35(3), pp.419–432.

Wyss-Coray, T. & Rogers, J., 2012. Inflammation in Alzheimer disease-A brief review of the basic science and clinical literature. *Cold Spring Harbor Perspectives in Medicine*, 2(1).

Xie, H. et al., 2013. Rapid cell death is preceded by amyloid plaque-mediated oxidative stress. *Proc.Natl.Acad.Sci.U.S.A*, 110(1091-6490 (Electronic)), pp.7904–7909.

Yan, S.D. et al., 1996. RAGE and amyloid-beta peptide neurotoxicity in Alzheimer's disease. *Nature*, 382(6593), pp.685–91.

Yarza, R. et al., 2016. c-Jun N-terminal kinase (JNK) signaling as a therapeutic target for Alzheimer's disease. *Frontiers in Pharmacology*, 6(JAN), pp.1–12.

Ye, B. et al., 2015. Dual pathways mediate ??-amyloid stimulated glutathione release from astrocytes. *Glia*, 63(12), pp.2208–2219.

Yonas E. Geda, MD, Ms., 2012. Mild Cognitive Impairment in Older Adults. *Curr Psychiatry Rep.*, 14(4), pp.320–327.

Yu, B.P. & Yang, R., 1996. Critical evaluation of the free radical theory of aging a proposal for the oxidative stress hypothesis. *Ann N Y Acad Sci.*, 786, pp.1–11.

Yu, X. et al., 2016. Differences in vulnerability of neurons and astrocytes to heme oxygenase-1 modulation: Implications for mitochondrial ferritin. *Sci Rep*, 6(April), p.24200.

Yue, P. et al., 2006. Depletion of intracellular glutathione contributes to JNK-mediated death receptor 5 upregulation and apoptosis induction by the novel synthetic triterpenoid methyl-2-cyano-3, 12-dioxooleana-1, 9-dien-28-oate (CDDO-Me). *Cancer Biology and Therapy*, 5(5), pp.492–497.

Zhang, C. et al., 2012. Prediction of S-glutathionylated proteins progression in Alzheimer's transgenic mouse model using principle component analysis. *Journal of Alzheimer's disease : JAD*, 30(4), pp.919–34.

Zhang, H. et al., 2012. Glutathione-dependent reductive stress triggers mitochondrial oxidation and cytotoxicity. *Faseb J.*, 26, pp.1442–1451.

Zhao, Y. et al., 2013. Oxidative stress and the pathogenesis of Alzheimer's disease. *Oxidative medicine and cellular longevity*, 2013, p.316523.

Zhu, X. et al., 2001. Activation and redistribution of c-Jun N-terminal kinase/stress activated protein kinase in degenerating neurons in Alzheimer's disease. *Journal of Neurochemistry*, 76(2), pp.435–441.

Zou, K. et al., 2002. A novel function of monomeric amyloid β-protein serving as an antioxidant molecule against metal-induced oxidative damage. *The Journal of neuroscience : the official journal of the Society for Neuroscience*, 22(12), pp.4833–41.

10. Supplementary

10.1 The degree of probe oxidation in neurons upon Aβ accumulation

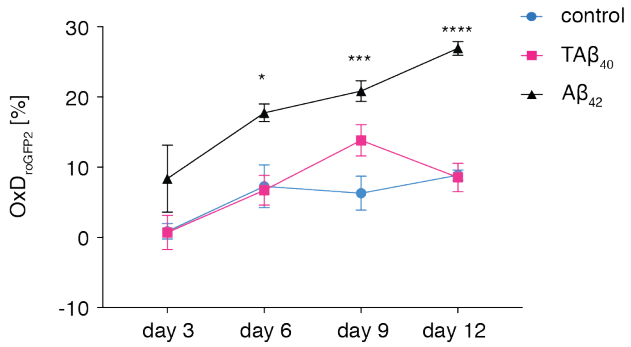

Figure 21: The degree of probe oxidation in neurons upon Aβ accumulation. Redox analysis with the cytosolic glutathione redox sensor (cyto-Grx1-roGFP2) in neurons, under the control of the *nSyb*-Gal4 promoter was performed in a time course (day 3, 6, 9, 12; n = 3-6 fly brains per time point and genotype). The graph represents the degree of probe oxidation of the cyto-Grx1-roGFP2 sensor. All error bars indicate s.e.m. Statistical analysis was performed with one-way ANOVA. *p ≤ 0,05, ***p ≤ 0.001, ****p ≤ 0.0001.

11. List of Publications

1. Yao V. Zhang, Shabab B. Hannan, **Zeenna A. Stapper**, Jeannine V. Kern, Thomas R. Jahn, Tobias M. Rasse. The *Drosophila* KIF1A Homolog unc-104 Is Important for Site-Specific Synapse Maturation. *Front. Cell. Neurosci. (2016) 10:207. Epub 2016 Sep 5.*

2. **Zeenna A. Stapper**, Thomas R. Jahn. Changes in glutathione redox potential are linked to $A\beta_{42}$-induced neurotoxicity. *Manuscript in revision in Cell Reports*

12. Acknowledgements

At this point I would like to thank all the people who supported me during my PhD. Especially, I want to thank Dr. Thomas R. Jahn. Thank you for bringing me into your team, giving me the opportunity to work on such an interesting topic and supporting me to become an independently working scientist, as I probably will call myself officially, when I hopefully pass my last PhD exam ;). I am thankful to my TAC members Prof. Dr. Bernd Bukau and PD Dr. Tobias P. Dick. Thank you for supporting my project through all this time, always giving me helpful feedback and advice through the challenging times. In particular, thank you for offering me a working place in your group after our lab closed. I highly appreciate your overall support and your comments on the manuscript. A big thank you to Dr. Björn Tews for hosting me in your lab for three months and supporting me to get a contract extension. Thank you to the Schaller Labs for keeping me store my bench equipment in your lab spaces as long as I needed it. Another big thank you to Prof. Dr. Aurelio Teleman for giving your feedback and support not only as deputy of our lab for the last year it officially existed but also as my referee for writing my reference letter. I would also like to thank Dr. Valéry Grinevich for joining the examination committee. Thank you to the Chica & Heinz Schaller Foundation, the DFKZ Heidelberg, and the Faculty of Biosciences at the University of Heidelberg for supporting my PhD. I strongly thank Lindsay Murrells and the Helmholtz International Graduate School for Cancer Research for your financial support in the last period of my PhD and for the excellent PhD program. A special thank you also to PD Tobias P. Dick, Prof. W.C. Orr, Dr. A. J. Whitworth, Prof. Dr. M. Boutros and Dr. D. Bohmann for providing reagents and fly lines. I also thank the University of Cambridge Department of Genetics Fly Facility and the Imaging Core Facility (DKFZ Heidelberg) for technical support. In addition I would like to thank Dr. Ana Barata for introducing me to the work with the redox sensors.

Thank you Fappy Lab aka Happy Lab. You all immediately welcomed me on the first day. Every one of you enriched my life in many different ways. I especially enjoyed our numerous valuable scientific and non-scientific discussions most memorable in the S1, fly room or at P11. I learned a lot from you and I am very happy that I met you. A special thank you also to my friends and my old high school crew, who supported me, distracted me and especially lightened my day whenever I needed it. I am happy to have you in my life, some for over 28 years and others for just a few, but more to come ☺ At the end, I want to thank you mum for all your positivity and optimism and for something that influenced my personality a lot: setting the example to always believe in the good.

Finally, I want to thank you Jan for all your love and support and of course for the preparation of the schematic drawings of the neurons and glia cells ;) Thank you for accompanying me through all my life. We went through a lot of challenges and strokes of fate. But together we were strong and have overcome them all. Jan, you are my love, my anchor, my best friend and my home. I am really looking forward to what´s to come ☺